University of Venda

School of Environmental Sciences

Department of Mining and Environmental Geology

Structural settings inferred from gravity, magnetic and seismic data for Durban Basin, east coast offshore of South Africa.

by

Nedzamba Iyani Bernard

Student no: 11552964

A Master's thesis submitted to the Department of Mining and Environmental Geology in the School of Environmental Sciences, University of Venda in fulfilment of the requirements for the degree of Master of Earth sciences in Mining and Environmental Geology.

Supervisor: Dr. M.O. Kataka

Co-supervisor: Prof. B. D. O. Odhiambo

April 2020

Declaration

I, Nedzamba Iyani Bernard, Student no 11552964, declare that this research thesis submitted for the Masters of Earth Sciences in Mining and Environmental Geology at the University of Venda, is my original work and has not been submitted by me at this or any other institution of higher learning for a degree and that all reference materials contained therein have been fully acknowledged.

Student's signature: ..... Date: .....

Abstract

The South African east coast offshore consists of two sedimentary basins namely, the Durban Basin and the Zululand Basin. The rift Mesozoic Durban Basin covers an area of about 10 000 km² between Port Shepstone Arch and the Zululand Basin. Structurally, it is complex with multiple fault systems and folds. Its development is a result of early extension of the East African plate, break-up of Godwana and initial movements of the AFFZ. The most prominent geological structures in the Durban Basin is the AFFZ, Tugela Cone, Tugela Canyon, Tugela Ridge and Naude Ridge. Only four wells have been drilled on the continental shelf of the Durban Basin i.e. Jc-A1, Jc-B1, Jc-C1 and Jc-D1. The structural setting of the Durban Basin for this study is inferred using gravity, magnetic and seismic data through an integrated approach of analyzing, processing and interpreting available gravity, magnetic and seismic 2D data. To properly map the basin extent, structures, estimate depth and thickness, pick horizons (basement, 1AT1, 17AT1, Oligocene/Miocene and seafloor), the followings were applied to gravity, magnetic and seismic 2D data to improve data interpretation: 1) Filters were applied to gravity and magnetic data i.e. reduced to the pole (RTP), 1st order horizontal derivative, 1st order vertical derivative, and power spectrum for depth estimation; 2) seismic well tie was applied to establish time-depth relationship of seismic data to pick formations and faults using well tops of Jc-C1 well and sonic log; 3) Velocity modeling using seismic stacking velocities to convert time to depth surfaces and estimate sedimentary cover thickness. The Durban Basin extent in the study area was mapped and subdivided into shallow and deep basin, occupying the southwestern, northern part and southeastern part of the study area respectively. The estimated thickness of the sedimentary cover is 2000 m-600m for the thinnest and > 2000 m-6000 m for the thickest part of the study area. The deepest and shallow part of the study area is the central to SW-SE and northern part. Structurally the study area is dissected by normal faults and graben structures with a S-N, W-E, SW-NE and SE-NW directional trends. These structures could be related to pre-rifting, rifting, AFFZ movements, compaction, abnormal gravitational load and contraction processes. The gas chimneys mapped could be evidence of an active petroleum system in the Durban Basin.

Keywords: Durban Basin, magnetic anomaly, gravity anomaly, seismic, power spectrum, tilt derivative, horizontal derivative, vertical derivative, grabens, basement, sediments, depth conversion, velocity modeling

Acknowledgements

My praise and worship is to the almighty God who gave me strength and wisdom to endure the learning process and accomplish the set-forth mission. I would like to thank Dr. Kataka and Prof. Odhiambo for their patience, support and guidance in writing and completing this research work. My gratitude to Petroleum Agency SA (PASA) for funding my research work and thanks to PASA staff members that directly and indirectly contributed to this research work. Datasets used for this research work was supplied by Compagnie Générale de Géophysique (CGG) and PASA, merci CGG. Special thanks to my wife Rachel Nedzamba, son Lebalela (Shalom) and daughter Princess Murendi. This research work is dedicated to my mother Mavhungu Nedzamba and my late father Lebalela Nedzamba for their endless love and faith in me.

Definition of key terms

Anomalies in geophysics are defined as an area where geophysical properties such as density or magnetism vary with the surrounding areas.

Bouguer anomaly is a gravity anomaly that is corrected for height at which is measured and the attraction of terrain.

Density is a volumetric mass of a material or rock.

Elasticity is the compressibility property of rocks.

Gravity method is an active geophysical method that defines the rocks based on density variation.

Magnetic method is an active geophysical method that characterizes subsurface rocks using magnetism or magnetic susceptibility.

Seismic method is a passive geophysical method that uses elasticity and density properties of rocks to characterize the subsurface rock.

Susceptibility is the degree of magnetism of a rock and it depends on the concentration of magnetic minerals in a rock.

Sedimentary basin is the low area in the earth's crust caused by long term subsidence which accumulated sediments.

Sedimentary rocks are rocks formed due to deposition and cementation processes within a water area or earth surface.

Acronyms and Abbreviations

AFFZ- Agulhas Falkland fracture zone

ASCII- American standard code for information interchange

CDP- Common depth point

CGG- Compagnie Générale de Géophysique

CRS- Coordinate reference system

et al.-many authors

FFT- Fast Fourie transform

g/cm^3- Gram per cubic centimetre

GPS- Geographical positioning system

GIS- Geographical information systems

Ha- Hectares

HD- Horizontal derivative

HP- High pass

LP- Low pass

Km- Kilometer

Km^2- Square kilometre

mGal- Miligal

mm- Milimeter

m- meter

n.d-No date

nT- nano tesla

PASA- Petroleum Agency South Africa

RTP- Reduced to the pole

Soekor- The Southern African oil exploration corporation

TMI- Total magnetic intensity

VD- Vertical derivative

UTM- Universal transverse mercator

WGS84- World geodetic system 1984

SEGY and SEGD- Society of exploration geophysics file for storing geophysical data

SI- Scientific unit

TWT- Two-way time

2D- Two dimension

°C- Degree Celsius

~ Estimated

> Greater than

< Less than

Table of Contents

List of Figures

List of tables

1. CHAPTER ONE: INTRODUCTION

1.0 Background

The South African east coast offshore consists of two sedimentary basins namely, the Durban Basin and the Zululand Basin. The basins are Mesozoic rift basins, but the Durban Basin is structurally complex with multiple fault systems and folds, and shallower than the Zululand Basin (Broad et al., 2006). Rift Mesozoic basins like the Durban Basin are known to be sources of economic resources such as petroleum, gas and uranium (Olsen et al., 1991; Schlische, 1993; Olsen et al., 1996). The Durban Basin covers an area of about 10 000 km² between Port Shepstone Arch and the Zululand Basin (Broad et al., 2006) (Figure 1.1). The mechanism of the Durban Basin formation is as a result of an early extension along the East African continental plate, the Gondwana break-up and initial movement of AFFZ (Broad and Mills, 1993; McMillian, 2003; Broad et al., 2006). These resulted in a series of geological structures in the basin (Broad et al., 2006).

The most prominent geological structures in the east coast of South Africa are the Agulhas Falkland Fractured Zone (AFFZ), Tugela Cone, Tugela Canyon and Naude Ridge within the continental shelf (Broad et al., 2006). Synrift sediments of Cretaceous Age, dominate the basin with their total thickness estimated to more than 4km as deduced by seismic refraction data (Broad et al., 2006). Geologically, the Durban Basin can be subdivided into four, ranging from oldest to youngest: Archaean basement, Table Mountain Supergroup, Karoo Supergroup and Cretaceous-Cenozoic sequence. It is dominated by Archaean granites, gneisses, schists, sandstones, and shales (Goodlad, 1986).

In terms of exploration, the area is under-explored with only four Jc series wells (Jc-A1, Jc-B1, Jc-C1 and Jc-D1) drilled in the shelf (Figure 1.1). Two of four wells intersected dolerite sills within the synrift section, indicative of Tertiary intrusive activity (Broad et al., 2006). Only Jc-D1 well revealed the presence of an active petroleum system because it intersected sandstone 1550 m and at 2200 m the well intersected shale with bitumen related to dry gas (Singh and McLachlan, 2003). Furthermore, Singh and McLachlan (2003) suggest that the four Jc-series wells were not optimally

positioned for drilling which resulted in negative drilling results, instead the target petroleum sources in the area should be of Upper Cretaceous and Lower Cretaceous-Turronian period.

Gravity and magnetic and seismic data are widely used in exploration and exploitation of oil and gas. Gravity method characterizes subsurface structures based on rock density while magnetic method on the other hand depends on rock magnetism. Onshore or offshore measurements of gravity and magnetic fields relies on the contributions from sources at both shallow and deep depths. Consequently, the source structures properties are defined and estimated using gravity and magnetic anomalies and indirectly delineating them as faults and folds because anomalies align themselves along definite preferable axes forming structural trends (Affleck, 1963; Selim, 2016). Magnetic anomalies are directly related to magnetization and ambient field i.e. angle of inclination. To remove the inclination effects, RTP calculations are applied to total magnetic data using inclination and declination (Fairfield, 2015)

Derivatives and filters are generally applied to gravity and magnetic data to improve interpretation of gravity and magnetic anomalies. The derivatives include vertical, horizontal and tilt derivative, these derivatives enhances structural interpretation by improving edge, contact and or boundaries of subsurface features (Fairfield, 2015). Power spectrum is applied to gravity and magnetic data to calculate and estimate depth of subsurface features. Power spectrum is a Fourier analysis of data where, spectral analysis is represented as log power versus wavelength graph. According to Spector and Grant (1970), different formations/horizons can be defined as linear sections on the power spectrum.

Seismic method is one of the active geophysical methods and triumph over other geophysical methods because of three factors; high accuracy, high resolution and great penetration capability (Telford et al., 1990). Its importance in petroleum exploration is such that no well location can be drilled without seismic data acquisition, processing and interpretation. This method is based on generating and detecting seismic waves. In oil exploration, a seismic source creates and sends sesimic waves through the subsurface geology and depending on the elasticity and density properties of subsurface geology, sesimic waves generated will be reflected and refracted to the

receiver (geophones/hydrophones) along the geological boundaries (Telford et al., 1990). The reflection of acoustic waves occurs along rock or sediments contacts due to variations in rock densities (Kearey et al., 2002). These variations are used for interpretations after a number of processes through standard procedures using commercial sofwares.

1.1 Problem statement

The Durban Basin, unlike other offshore South African basins, has seen limited petroleum exploration and research activities and in general, only four wells have been drilled on the continental shelf of the east coast of South Africa. Consequently, the structural setting and subsurface geology of the Durban Basin is poorly understood, the little available literature regard it as structurally complex. The lack of knowledge about the structural setting of the Durban Basin and its structural complexity has impacted negatively on the knowledge about the petroleum system within the Durban Basin.

1.2 Justification

The Durban Basin is a rift Mesozoic basin and these types of basins are regarded as potential sources of oil and gas. Durban Basin has seen limited exploration with only four wells having been drilled so far along the continental shelf. Both passive and active geophysical methods in the past have been used to delineate sedimentary basin and provided insight about subsurface geology and structural controls. This research work will improve the knowledge about the structural setting of the Durban Basin using seismic, gravity and magnetic data to determine basin extent, sedimentary cover thickness and structural framework of the Durban Basin through an integrative process approach.

1.3 Main and specific objective

1.3.1 Main objectives

The main objective of this research is to understand the structural setting of Durban Basin through the integration of seismic, gravity, and magnetic data.

1.3.2 Specific objectives

- To delineate Durban Basin extent in the study area.
- To map geological structures within the Basin.
- To conduct depth estimation and locate subsurface sources causing anomalies.
- To estimate sedimentary cover thickness of the study area.

1.4 Research hypothesis

- Durban Basin is structurally complex.
- Durban Basin is dissected by multiple fault system, which extends from the basement through the overlying sedimentary stratigraphic formations.
- Durban basin has potential for hydrocarbons based on the thick sediments cover and faulting system.
- This Mesozoic basin is dominated by grabens and half grabens that may be attributed to the Gondwana break up.

1.5 Study area

1.5.1 Location

The study area is located approximately 50-100 Km east of Durban on the east coastline of South Africa and covers an area of about 106340 hectares (Ha). The study area is part of the Durban Basin, which lies between Port Shepstone Arch and the Zululand Basin (Figure 1.1). According to Petroleum Agency South Africa (PASA), licensing and legal department's exploration rights and permits license the study area is referred as Block 236 and is represented by the L-shaped black polygon (Figure

1.1). The main reason for choosing this area was its potential for petroleum exploration and production. Jc-D1 well had traces of oil, which points to the existence of an active petroleum system in the basin.

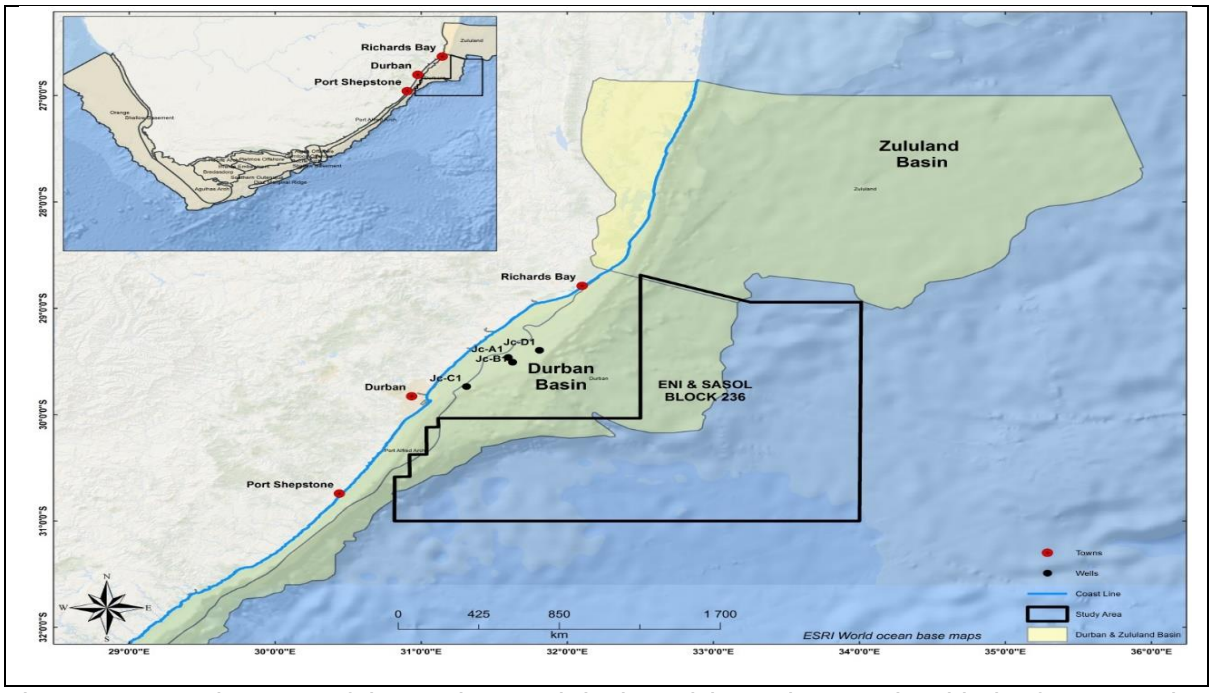

Figure 1.1 Location map of the study area (Block 236) in Durban Basin with the four Jc series wells drilled on the shelf (JC-A1, JC-B1, JC-C1, and JC-D1), offshore east coast South Africa.

1.5.2 Geology

The study area is part of the rift Mesozoic Durban Basin. The general morphology of the Durban basin is dominated by continental shelf and slope, Tugela Cone, deeply buried basement high Tugela Ridge, and Naude Ridge (Goodlad, 1986). Based on geochemical sampling, petrographic and seismic studies the Tugela Ridge consists of basaltic rocks while the Tugela Cone is covered with sediments of more than 4 Km thickness (Broad and Mills, 1993; Broad et al., 2006). Geologically, the basin is subdivided into Archaean basement, Table Mountain Supergroup, Karoo Supergroup and the Cretaceous-Cenozoic sequence (Broad et al, 2006 and Goodlad, 1986).

The Archaean basement rocks flooring the Durban Basin consist of Archaean crystalline granites, gneisses, and schists. The Table Mountain Supergroup is dominated by sandstones and shales overlying the Archaean basement (Figure 2.3).

The Karoo Supergroup unconformably overlies the Table Mountain Supergroup and outcrops onshore Zululand Basin of the Great Karoo Basin (Goodlad, 1986). The famous Karoo Supergroup consists of tillites of the Dwyka Group, sandstones and shales of the Ecca and Beaufort Group. The sandstones and shales onshore are capped by volcanic rocks forming the Drakensberg Mountain ranges.

The Creataceous-Cenozoic sequence forms the last geological sequence in the Durban Basin (Broad et al, 2006; Goodlad, 1986) (Figure 2.3). Aeolian, fluvial and marine sediments dominate this sequence, which outcrops along lowlands coastline.

1.5.3 Climate

Durban has humid subtropical climate with average summer and winter temperatures at about 24°C and 17°C respectively. It is generally hot and humid in summer with warm and dry winter. The area receives annual rainfall of about 1,009 mm (World meteorological Organization, 2013). Durban as a coastal city, offshore it is characterized with high and large sea swells related to the Agulhas current which is described as fast and deep, traced to about 2.5 km depth.

2. CHAPTER TWO: LITERATURE REVIEW

2.0 Introduction

This chapter presents a review of the available literature related to the rift Mesozoic Durban Basin, offshore east coast South Africa. A review is also presented on the geophysical methods used in this study i.e. gravity, magnetic and seismic methods. Literature review involved books, published and unpublished journals and reports related to the Durban Basin and its hydrocarbon potential.

2.1 Regional geological setting of the study area

The east coast offshore of South Africa is composed of Durban and Zululand Basin. The two basins have experienced limited exploration activities and because of the minimal petroleum explorations in the two basins, there is limited geological knowledge about the two basins (Broad and Mills, 1993; Soekor, 1994; Singh and Mclachlan, 2003). Broad and Mills (1993) indicated that; the Durban Basin is structurally more complex and deeper than the offshore Zululand Basin because of its close proximity to the continental spreading center and further identified the main feeder for sediments deposition in the Durban Basin as the Tugela River and Limpopo River thus contributing to the formation of the Tugela cone (Goodlad, 1986; Broad et al., 2006; PASA 2016).

The Durban basin regional geology consists of the Archaean granites and gneisses of the Kaapval Craton forming the basement rocks. The basin is predominated by siliclastic and marine sediments, which were deposited during Gondwana separation in the late Jurrassic to early Cretaceous followed by early Cretaceous to recent drift events (Goodlad, 1986; Broad and Mills, 1993; Broad et al., 2006; PASA, 2016).

2.2 Basin evolution

The rift Mesozoic Durban basin development evolution is poorly understood and documented due to lack of exploration work in the area (Hicks et al., 2014; McMillan, 2003; Du Toit and Leith, 1974). The Durban Basin covers an area of about10 000km^2

extending to 2500m isobaths (Broad et al., 2006) (Figure 2.1). The Durban Basin originated from the early extension of the East African continental plate that occurred before the Gondwana break-up and transformation which resulted in the formation of the new oceanic crust along the Agulhas Falkland Fracture Zone (AFFZ) (Broad et al., 2006). The dominant structural features in the Durban Basin is the Tugela cone, Agulhas Falkland Fracture Zone (AFFZ) and the paleo-basement high Naude Ridge, which separates the Durban Basin from the Zululand Basin (Goodlad et al., 1986) (Figure 2.1). The separation of the east and west Gondwana resulted into NE-SW synrift grabens (Dingle et al., 1983, and Broad et al., 2006 and PASA, 2016) (Figure 2.2).

Despite the Durban Basin's limited petroleum exploration activities, four wells have been drilled so far, i.e. JC series wells (JC-A1, JC-B1, JC-C1, and JC-D1) (Figure 1.1 and 2.1). All four wells intersected graben filled and synrift sediments and volcanics of late Jurassic to Valangian age but the wells did not penetrate the basement (McMillan, 2003 and Broad et al., 2006). It is only in the JC-D1 well, that traces of oil and bitumen were identified thus showing the presence of petroleum source rock and active petroleum system (PASA, 2016).

Structurally, the Durban and Zululand Basins are dominated by faults which extend from basement through stratigraphic column and folds are more prevalent in the Cretaceous and Cenozoic sedimentary packages (Figure 2.2). Structural trend of the faults within the Durban Basin is NW-SE and NE-SW predominantly normal faults system and a pre-rift normal fault trending from W-E direction (Figure 2.2). This faulting and folding system could be related to plate separation and drifting of the Gondwana (Broad et al, 2006; PASA, 2016). The basement development of the east coast of South Africa is uncertain as there are three different crustal occurrences recorded i.e. continental, transitional and oceanic crust (PASA, 2016).

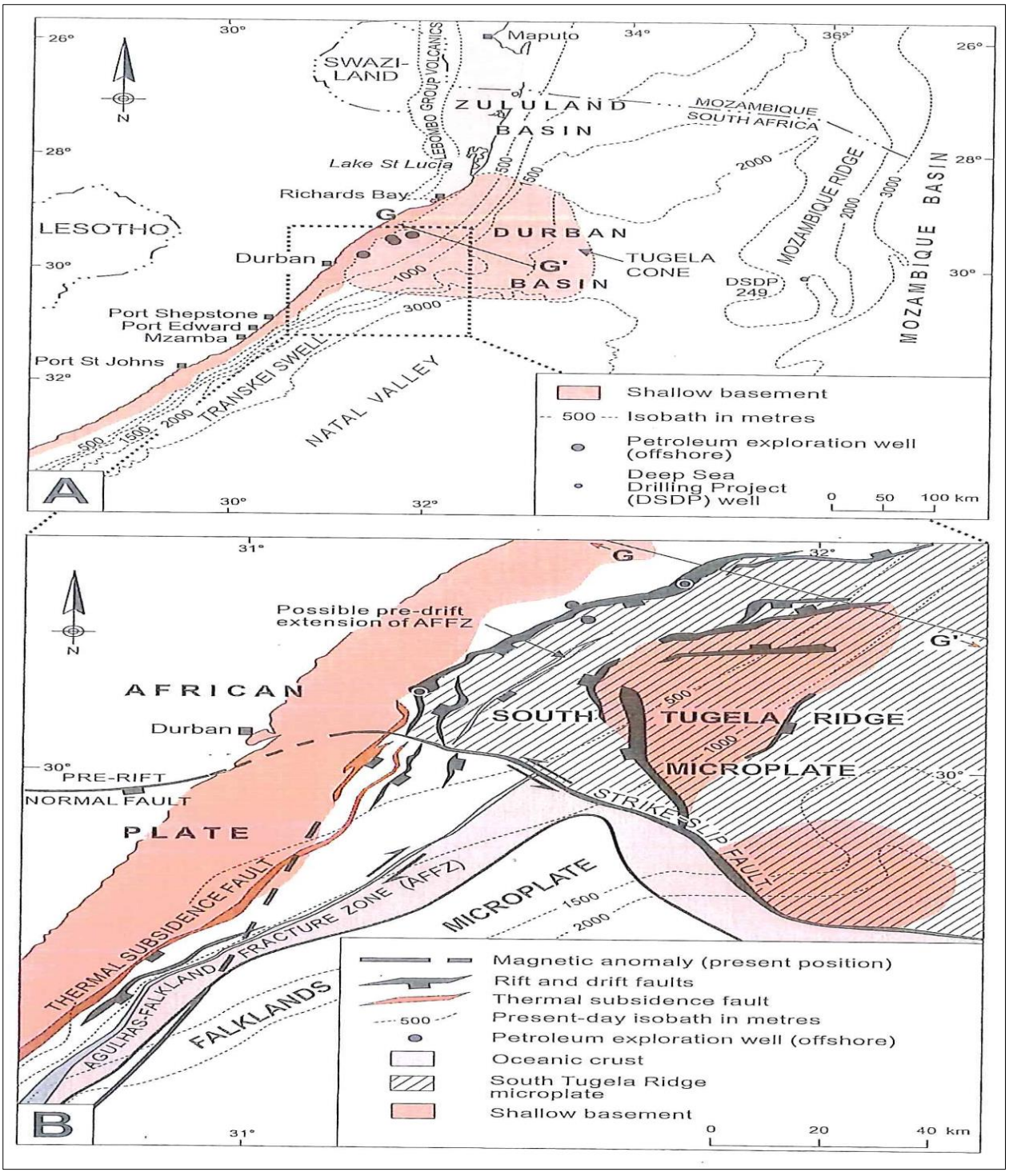

Figure 2.1. Map showing main geological features, major structural elements i.e. Tugela Cone, Tugela Ridge, AFFZ and Naude Ridge.

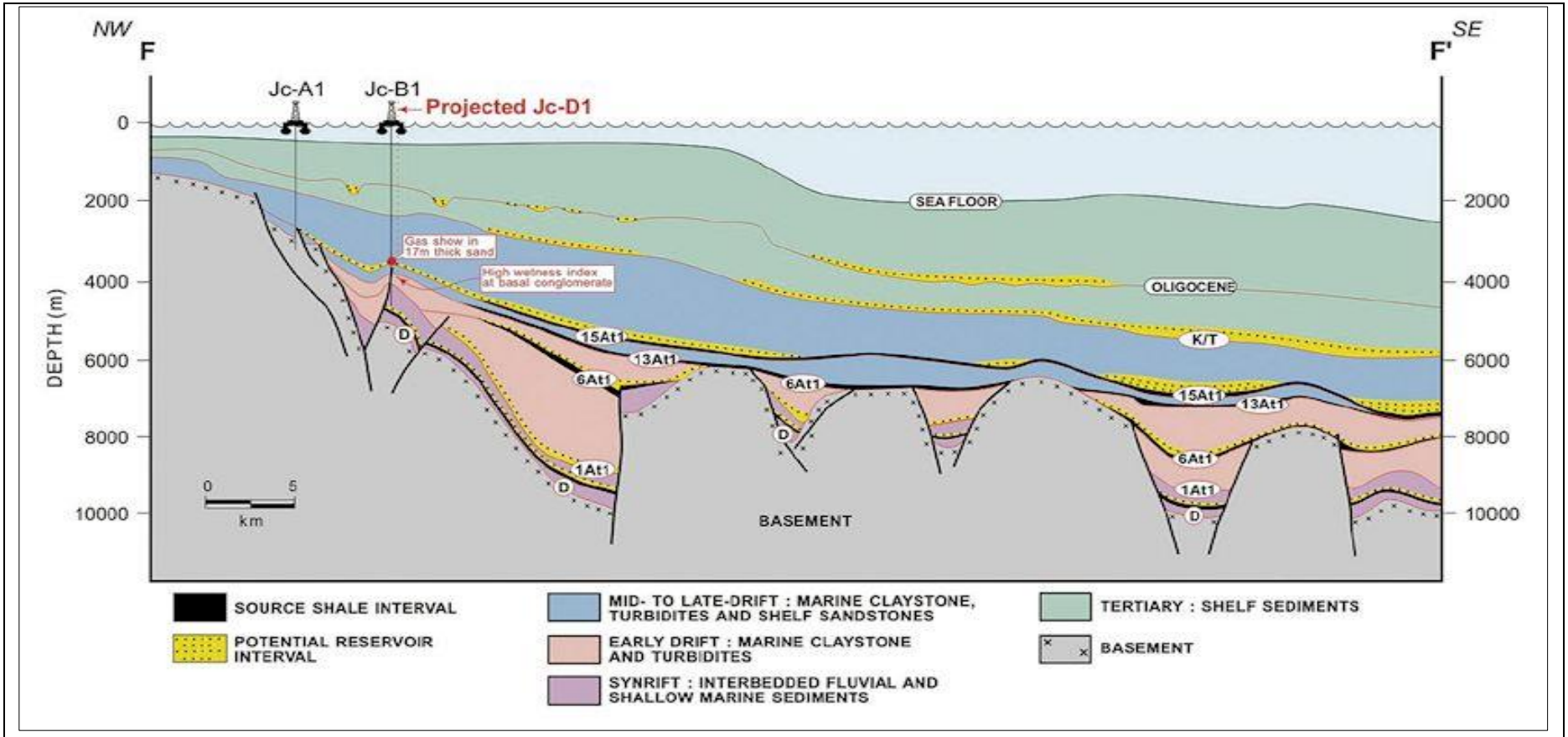

Figure 2.2 Durban Basin geological cross section (Profile F-F), based on seismic data interpretation and well data showing main structural features (synrift grabens) and stratigraphic subdivision (Broad and Mills, 1993; Soekor, 1994).

The synrift sedimentation started in the late Jurrassic to early-mid Cretaceous age resulting in the Durban Basin as depocentres and later became a single depocentre in the late Cretaceous (Broad et al., 2006). The basal synrift and synrift sediments are intruded by dolerite sills of late Cretaceous as recorded in the basal synrift units of JC-B1 well (Broad et al., 2006) (Figure 2.2).

The thickness of sedimentary package intersected and highlighted by seismic data interpretation is greater than 4km and are dated as of late Jurassic to early Cretaceous age (Broad and Mills, 1993; Broad et al., 2006) (Figure 2.2). Tertiary deep-water fan consisting of Cenozoic sandstones and claystones dominates the Tugela cone (Goodlad, 1986; PASA, 2016). Regional tectonics studies reveal multiple fault systems that could be due to regional transpression and transtensional events, trending in a NE-SW and E-W direction (PASA, 2016). Gravity and magnetic signature analyzed and interpreted by Leinweber and Jokat (2011) and Uenzelmann-Neben (2009), lean more to the oceanic crust flooring the northern Natal valley and Mozambique ridge i.e. Durban Basin.

According to Singh and McLachlan (2003), the structurally complex Durban Basin development resulted into normal faulting and right lateral strike-slip faults that hugely affected the geometry of the basement. Mapping by Kitchin (1995) and Ben Avraham et al. (1997), mapped shallow basement on the Tugela Ridge and on the southeastern side of the Durban Basin based on seismic and well data.

Based on seismic data interpretation by Bhattacharya and Duval (2016), the Durban Basin basement is characterized by rugged and eroded geometric appearance. Seismic data interpretation further revealed a variable depth to basement throughout the basin, with the deepest part of the basement on the south most of the basin and the shallowest north-to-north east of the basin (Bhattachrya and Duval, 2016). Volcanic rock units intersected by all four wells (JC-series) is supported by latest seismic data interpretation by Bhattacharya and Duval (2016) which noted two volcanic events in the Durban and Zululand Basin. It further revealed local volcanoes, sills and dykes intrusions. Structurally, the Durban Basin southwest part is highly affected by AFFZ, which resulted in basement listric faults.

2.3 Stratigraphic setting

The Durban Basin geological stratigraphy can be subdivided into four geological units (Figure 2.3); 1) ~3.1 Ga Archaean basement consisting of Archaean crystalline granites, gneisses and schists with the 2) Table Mountain Supergroup sandstones and shales overlying the Archaean granites. 3) Karoo Supergroup consisting of the Dwyka Group tillites and shales and sandstones of the Ecca and Beaufort Groups. 4) The final sequence is the Cretaceous-Cenozoic sediments consisting of Aeolian, fluvial and marine sediments deposited within grabens (Goodlad, 1986; Broad et al, 2006; PASA, 2016).

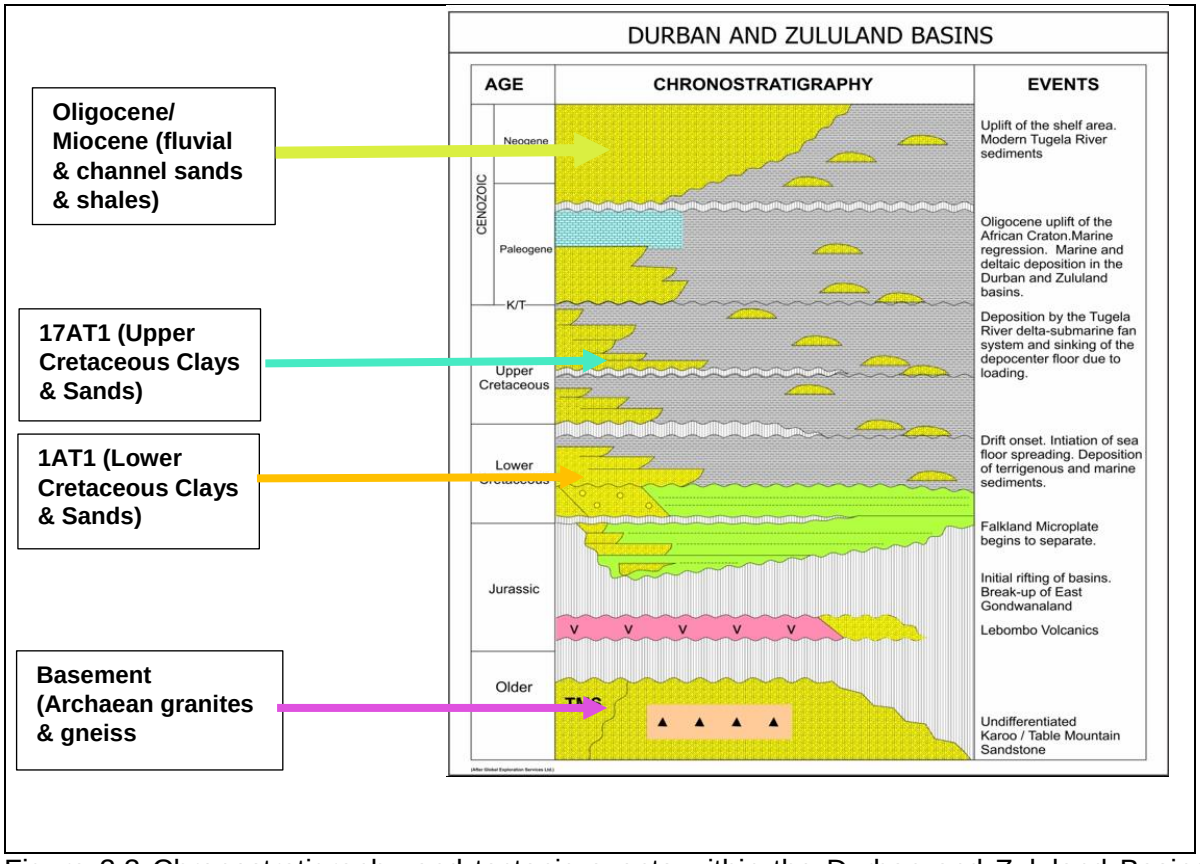

Figure 2.3 Chronostratigraphy and tectonic events within the Durban and Zululand Basins (after Kitchin, 1995; Ben Avraham et al., 1997; Global Exploration Services Ltd). Five horizons representing major geological events in the study area i.e. Basement (pink), 1AT (orange), 17AT1 (green), Oligocene/Miocene (yellow) and seafloor (blue).

2.4 Petroleum system

Only four wells have been drilled i.e. Jc-series wells Jc-A1, B1, C1 and D1 in the Durban Basin (Figure 1.1). Exploration work in the Durban Basin using seismic data

and core logging and sampling revealed the presence of an active mature petroleum system (Broad et al., 2006; PASA, 2016). Core logging and sampling of Jc-D1 extracted hydocarbons from a sandstone intersected at 1550m and bitumen stained shale associated with dry gas anomaly intersected at 2720 m (Singh and McLachlan, 2003; Broad et, al. 2006; PASA, 2016). Furthermore, Singh and McLachlan (2003) suggest that potential petroleum leads and plays developed in Upper Cretaceous and Cenomanian-Turonian period. This plays and leads are the fourway dip closures, turbidites slope fans, basin floor fans, channel sands and turbidites sands overlying basement features (Singh and McLachlan, 2003). Satellite gas seepage studies and seismic interpretation by Singh et al., (2005) revealed gas escape features that related to second and third order gas seepage slicks due to hydrocarbon expulsion.

2.5. Geophysical methods review

Geophysical methods have been applied in exploration of oil and gas since the 1920s mostly for structural and basement mapping. Geophysical techniques involves measuring reflectivity, magnetism, gravity and acoustic or elastic waves (Telford et al., 1976). Gravity and magnetic methods are very important in petroleum exploration but they do not replace seismic method rather complement it because of their low resolution compared to high resolution seismic method (Telford et al., 1976).

2.5.1 Gravity methods

Gravity method is a passive geophysical method that measures the earth's gravitational field caused by variations in the density of subsurface rocks (Telford et al., 1976). Since the twentieth century this method has been widely used in petroleum exploration mostly for structural investigation (Rivas, 2009). The basic theory of this method is Newton's Law of Gravitation and it states that objects attracts each other using the force (**F**). The force (**F**) is directly proportional to product of two objects masses ($\mathbf{m_1}$ and $\mathbf{m_2}$) and inversely proportional to the distance between their centers (**r**):

$$F = \frac{Gm_1m_2}{r^2} \qquad (2.1)$$

Gravity measurements does not reflect direct gravity measurements consequently, gravity measurements require gravity data reduction or corrections (Telford et al., 1976). This gravity data reduction includes drift, earth's tides, latitude, free-air, Bouguer and terrain corrections. The final product of these gravity measurements corrections is the Complete Bouguer Anomaly (CBA). Generally, the complete Bouguer anomaly show lateral variation of the density so that high density rocks such as basement rocks produces a positive gravity anomaly (Fairfield, 2015 and Telford et al., 1979).

2.5.2 Magnetic method

Magnetic method is a geophysical survey method that characterizes the subsurface geology based on variations in magnetic minerals stored in rocks (Adagunodo et al., 2015; Telford et al., 1976). This method is extensively applied in oil and gas exploration generally, for estimation of depth to basement, defining basin extent and structural mapping. The basic theory of magnetic method states that; "If two magnetic poles of strength m1 and m2 are separated by a distance r, a force, F, exists between them. If the poles are of the same polarity, the force will push the poles apart, and if they are of opposite polarity, the force is attractive and will draw the poles together" Telford et al., (1976). The equation for F is the following:

$$F = \frac{Gm_1m_2}{4\pi\mu^2} \qquad (2.2)$$

where μ is the magnetic permeability of the medium separating the poles; m1 and m2 are pole strengths and r the distance between them.

Magnetic measurements must be subjected to diurnal corrections, if the diurnal changes ranges from 15-20 gammas over a one-hour period (Telford et al., 1976; Dobrin and Savit, 1998; Kearey et al., 2002). The end product of magnetic reduction or corrections is the total magnetic intensity (TMI) anomaly.

According to Blakely et al., (1995), Magnetic anomalies are directly related to magnetization and ambient field i.e. angle of inclination. To remove the inclination effects and directly align the magnetic anomalies above the causative body the

Reduced to the pole (RTP) calculations should be applied to the total magnetic intensity (Fairfield, 2015). These calculations are achieved using the inclination, declination and elevation.

2.5.3 Gravity and magnetic data processing

Processing of gravity and magnetic data can be defined as conditioning of geophysical data to enhance effective quantitative interpretation process. Gravity and magnetic cannot be interpreted directly to identify and map structures and estimate depth of anomalies because their measurements are uncertain as such require application of filters to improve visualisation and interpretation of anomalies (Fairfield, 2015). A brief summary of filters that can be applied to gravity and magnetic data are presented below.

2.5.3.1 Vertical derivative (VD)

Application of derivatives is a norm in processing and interpreting gravity and magnetic anomaly data (Blakely et al., 1995). Transforming gravity and magnetic data into derivative map improves edge or boundaries detection by placing anomaly maxima at the point of the maximum horizontal gradient within the grid (Bronner et al., 2009). Vertical derivative (VD) filters when applied to gravity and magnetic data enhances shallow subsurface features, trends and resolution of subsurface features. Key assumptions when applying vertical derivatives to gravity and magnetic data are that:

- The potential field measured at the surface is the vertical component of the field (This assumption is true for gravity and RTP data)
- Contacts of subsurface rocks are abrupt, near vertical and isolated

2.5.3.2 Horizontal derivative (HD)

Horizontal derivative (HD) is defined as the result of gravity and magnetic anomaly changing horizontally (Rosid and Siregar, 2017). The application of horizontal derivative to gravity and magnetic data improves interpretation and mapping of subsurface rocks, faults (using first order derivative) and major basement or

sedimentary tectonics. The only limitation about horizontal derivative is that it tends to offset boundaries if boundaries are not near-vertical and close to each other (Graunch and Cordell, 1987; Gunn, 1997; Rosid and Siregar, 2017).

2.5.3.3 Tilt derivative (TDR)

Tilt derivative is a powerful filtering technique thus when applied to gravity and magnetic data it sharpens the edges and contacts, good for delineating subsurface shape and edge or lithological contact detections (Rosid and Siregar, 2017). TDR is a result of the ratio between first vertical derivative and horizontal derivative of gravity and magnetic anomaly (Miller and Singh, 1994; Verduzco et al., 2004; Cooper and Cowan, 2006).

2.5.3.4 Power spectrum

Depth of the causative body can be estimated from magnetic and gravity anomalies because they have rapid decay property with distance from the causative body (Spector and Grant, 1970). Magnetic and gravity anomalies from shallow sources have short-wavelengths compared to deep-seated sources (Kearey et al., 2002). Depth estimation from magnetic anomalies can be achieved by the use of power spectrum and this method, can also assist in determining the number of layers or horizons. This method provides direct depth estimation and is mostly used for regularly spaced field data (Kearey et al., 2002). Spector and Grant (1970) indicates that, for some sources the log-power spectrum has a linear gradient magnitude which is directly dependent on the depth of the causative body (details in 3.4.2).

2.5.4 Seismic method

Seismic method is one of the active geophysical methods and triumph over other geophysical methods because of three factors; high accuracy, high resolution and great penetration capability (Telford et al., 1990). Its importance in petroleum exploration is such that no well location can be drilled without seismic data acquisition, processing and interpretation. This method is based on generating and detecting seismic waves. In offshore oil exploration, a seismic source (air gun) creates and send

sound waves (shot) through the sea water and subsurface geology and depending on the elasticity and density properties of subsurface geology, sound waves generated will be reflected and refracted to the receiver (hydrophones) along the geological boundaries (Telford et al., 1990) (Figure 2.4). The reflection of acoustic waves occurs along rock or sediments contacts with variations in rock densities (Kearey et al., 2002).

Sensors or geophones placed on the surface measure the reflected acoustic energy, converting it into an electrical signal that is displayed as a seismic trace. The recorded seismic trace is a convolution ($*$) of the source signal (wavelet) and the reflectivity sequence of the Earth plus noise.

$$S = W * R + \text{Noises} \qquad (2.3)$$

where S is the recorded seismic trace, R is the reflectivity and W is the wavelet. A *wavelet* is a kind of mathematical function used to divide a given function into different frequency components and study each component with a resolution that matches its scale.

The end product of a 2D or 3D seismic data acquisition is raw field data in SEGD format. Seismic method is chiefly used to determine general geologic structures, sedimentary thickness cover and stratigraphy using seismic well tie and velocity modeling.

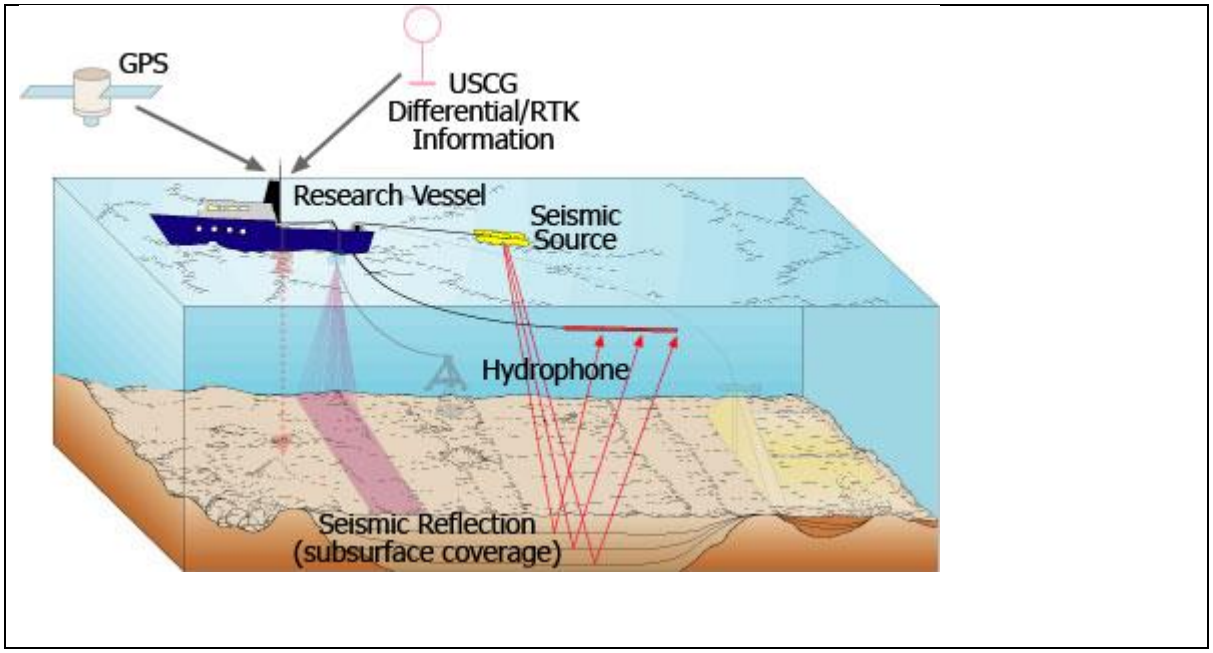

Figure 2.4 Basic equipment and configuration of marine seismic data acquisition; a vessel, equipped with navigation system (GPS), seismic source (Airgun) and receivers (Hydrophones), (After USCG, n.d.).

A number of steps are adopted during seismic data processing before the interpretation of the data. A flow chart in Figure 2.7 shows detailed steps followed during seismic data processing. The processing of seismic data generally follows a six-phased approach:

- **Phase 1: Data conditioning**

  This phase involves handling and loading raw field data to processing softwares, applying band-pass filters with corner frequency, setting sampling rate and sorting common depth point (CDP). The end product of phase is CDP file.

- **Phase 2: Parameter analysis**

  This phase uses the CDP file to apply parameter analysis and corrections. It is at this stage wherein shot delay effects are removed by applying static correction to the field data. Geometry setting for gathers and velocity analysis are conducted at this phase. The outputs of this phase is CDP and velocity files.

- **Phase 3: Data enhancement**

  The data enhancement phase uses velocities and CDP files to process raw data into time sections in SEGY file format by applying normal movement correction and static corrections.

- **Phase 4: Migration/Depth conversion**

  This phase mainly deals with migrating the time sections (SEGY) into stacks i.e. near, far, full and angle stacks and stacking velocities files. Furthermore, the stacking velocities are used to convert the time-domain sections into depth-domain seismic sections.

- **Phase 5: Modeling and interpretation**

  This phase involves tying wells to time seismic sections (SEGY) to establish time-depth relationship of depth-domain wells and time-domain seismic sections. The seismic well tie process enable accurate interpretation of faults and horizon picking to identify leads and plays for petroleum exploration and exploitation. Furthermore, this phase involves depth conversion by velocity modeling to estimate thickness of horizons and prospects.

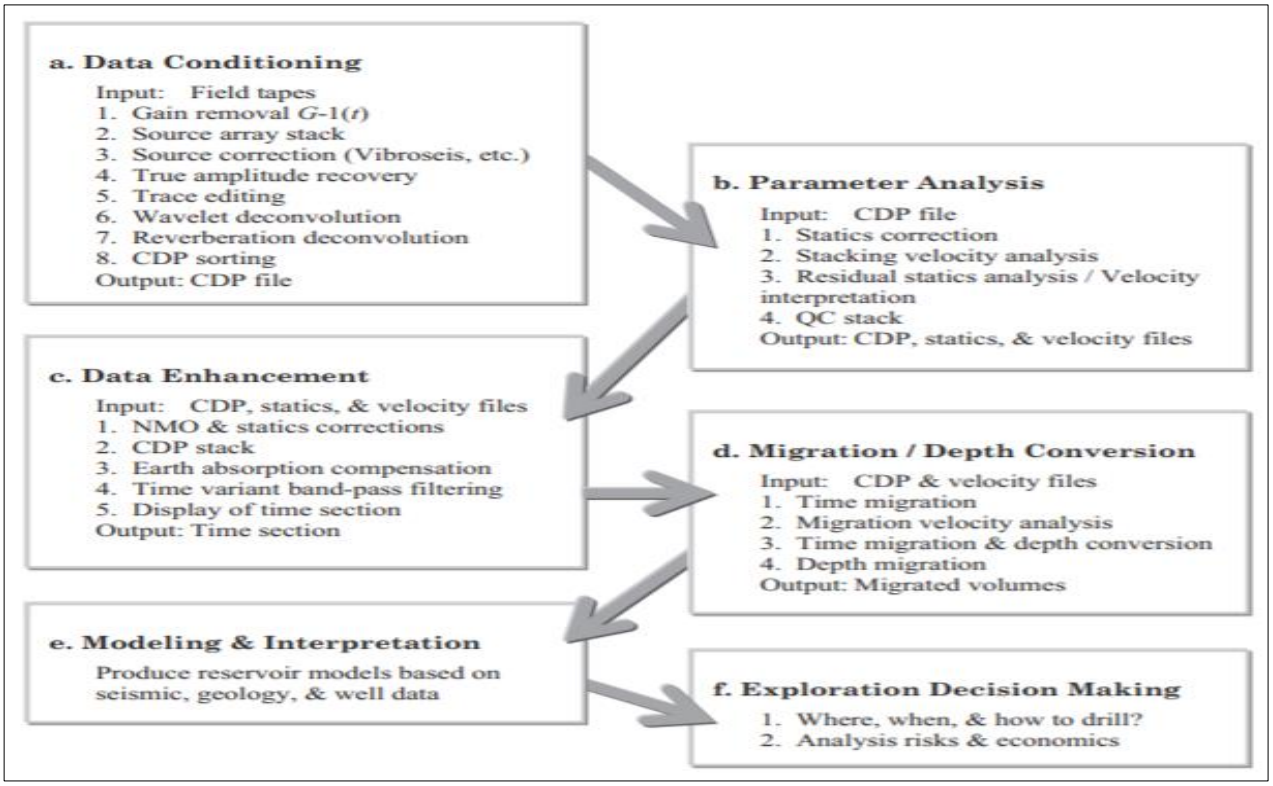

Figure 2.5 Simplified seismic data processing flow chart.

- **Phase 6: Exploration decision making**

  Phase 6 is decision making for exploration process, which involves volumetrics calculations, and drilling of identified and selected prospects in the study area.

Seismic well tie

To accurately pick the horizons or formation from seismic SEGY data and conduct time-depth conversion of picked time surfaces a seismic well tie and velocity model process is required and a very important process prior interpretation (White and Simms, 2003). The seismic well tie process uses well data such as well tops, check shots, sonic logs, density logs and seismic SEGY data to time-depth relationship because seismic data is time based while well data is depth based (Luton and Prieto, 2000). This process includes sonic log calibration, synthetic seismic generation and well tie. On the other hand, velocity modeling is achieved by well data in areas with drilled well(s) but in areas without any drilled well, seismic stacking velocities can be used.

According to Luton and Prieto (2000) sonic log and check shot data are accurate measure of vertical interval velocity. Sonic calibration is also known as well log calibration because it uses sonic log and checkshots to calibrate the timing of the sonic log for synthetic seismogram generation (White and Simm, 2003). Synthetic seismogram or seismic generation is defined as seismic trace created using sonic and density logs. The seismogram is used to compare seismic collected near the well location. According to White and Simm (2003), seismic well tie greatly improves seismic interpretation process thus enabling the picking of formations or horizon accurately from depth to time domain of well data and seismic data respectively.

The calibration site is needed as the velocity of that seismic wave is not same as the velocity that sonic logging to estimate. This is because of the basic theory of wave propagation in an attenuating medium which predicts that velocity must depend on frequency. The well log measurements are measured in depth and need to be converted to time to match the well synthetic with seismic data. This done by integrating the calibrated sonic values to create the time-depth relationship. The

reflection coefficients are calculated using the calibrated sonic and combined with the density to calculate the impedance (impedance =density x sonic) (Figure 2.8).
Once the synthetic seismogram has been generated from the calibrated sonic, the fnal wavelet can be estimated. Since phase of reflectivity is very complicated it is best that the final wavelet is estimated after all corrections so that the phase can be estimated with some accuracy. When estimating a wavelet, it is important that no asumptions are applied to the wavelet such as its appearance or timing, including phase (White and Simm, 2003). For wavelet estimation, there are several ways of estimating the amplitude spectra such as modelling it with a spline, polynomial or computing a more statistical amplitude spectrum such as method defined in White (1980).

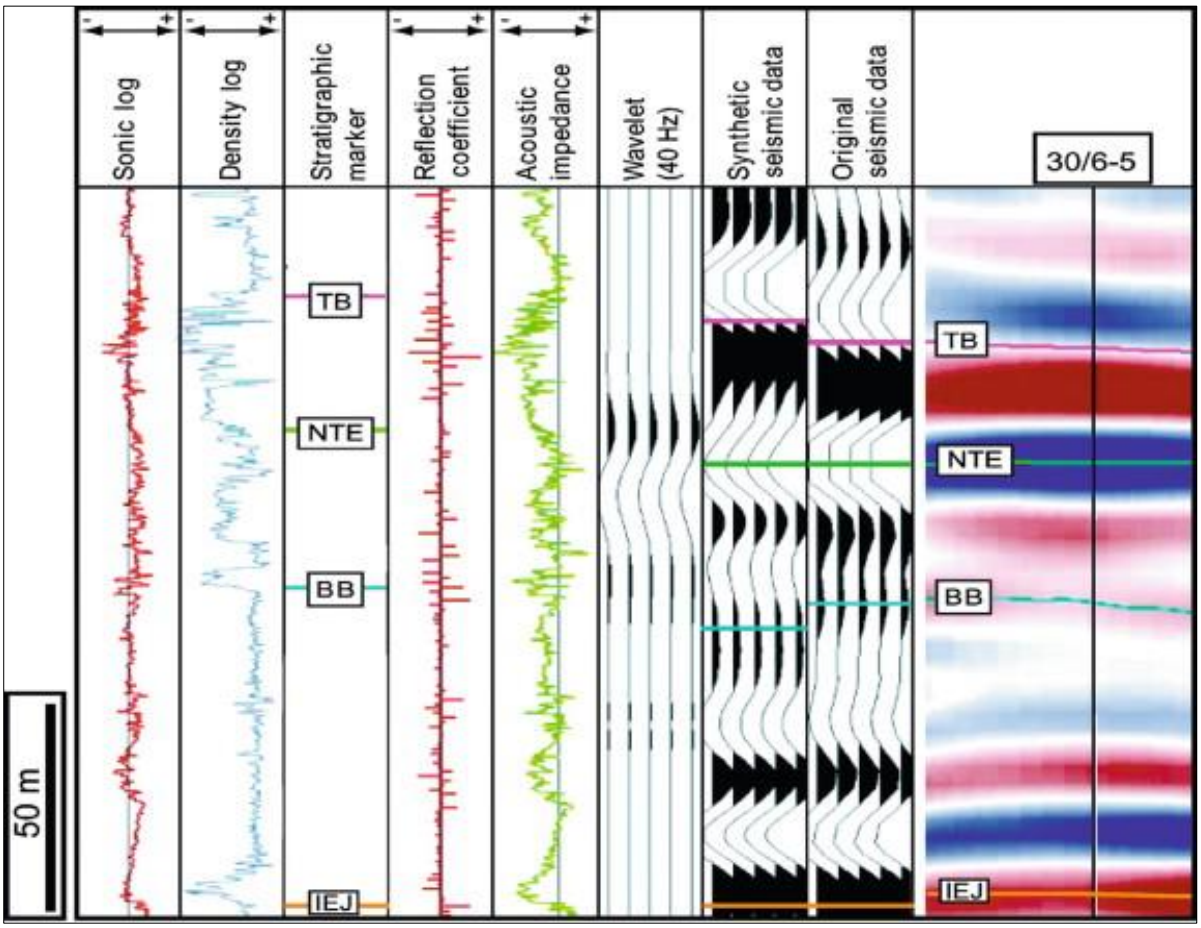

Figure 2.6 : Example of a generated synthetic seismogram. Density and Sonic inputs are used to obtain an acoustic impedance log and the results are multiplied with reflection coefficient to generate the synthetic seismogram for 3D seismic data (Anderson and Newric, 2008).

Velocity modeling

Velocity modelling according to White and Simms (2003) is used for depth conversion process. Time-depth conversions is an important step in seismic data interpretation for exploration study thus termed velocity modeling. Generally, time-depth conversion i.e. velocity modelling is achieved using well data (checkshots, well tops, sonic and density logs) but it is difficult to build a velocity model in an area with no well drilled. Depth conversion can be achieved using seismic well tie to convert all time surfaces into depth but incases wherein there is no well drilled in the area, velocity modelling can be achieved in using seismic stacking velocities (White and Simms, 2003).

From the parameters that are analysed and the interpretation that may be drawn from the analyses, a fourfold hierarchy of seismic interpretation can be achieved. These are: 1) seismic facies analysis (seismic profile provides information about the properties of sedimentary rocks); 2) seismic structural analysis (Interpreters can draw horizons and faults on inlines, cross-lines and arbitrary lines, as well as slices; 3) seismic attribute analysis (analysis may give an indication of the thickness and nature of the upper and lower contacts of a sand body (Selley, 1998); and 4) seismic sequence analysis (apart from structural and facies analysis, seismic signatures can be used to interpret the way the basin has been filled in). The most important parameters used for interpretation of seismic data are: Reflection amplitudes (the strength of the reflections is proportional to the energy reflected at the boundary between two beds which is a function of the difference in the acoustic impedances); Reflector spacing (the distance between the reflectors will indicate the thickness of the bed); Interval velocity (the interval velocity of a sequence can provide information about lithology and porosity); Reflector continuity (the continuity of reflectors will be a function of how continuous the sediment beds are, information which is essential for reconstructing the environment); Reflector configuration (the shape of the reflecting beds gives us a picture of the sedimentation surface as it was during deposition); and Instantaneous phase (the Instantaneous phase is a measure of the continuity of the events on a seismic section).

2.5.3 Interpretation of structures and Horizons

Structural interpretation may be thought of consisting of the following tasks: locating and interpretation of faults, tracking of uninterrupted horizon segments and correlating these segments across faults. The strong reflection events visible in seismic images are called horizons and indicate boundaries between rock formations and strata. This vertical displacement is called fault throw. Modern commercial softwares packages offer assistance for the intrerpretation of horizons and fault surfaces. The most commonly employed technique for horizon tracking is the so-called auto-tracking or auto-picking. These algorithms require manually selected seed points as initial control for the auto-tracking operations.

3. CHAPTER THREE: MATERIALS AND METHODS

3.0 Introduction

This chapter presents the methods and procedures that were used in this study to infer the structural setting of the Durban Basin. Figure 3.1 shows procedures and methods adopted in this study in the form of a flow chart. The study employed three phase approach: phase one was desktop studies followed by data collection in phase two and the last phase as data processing and interpretation.

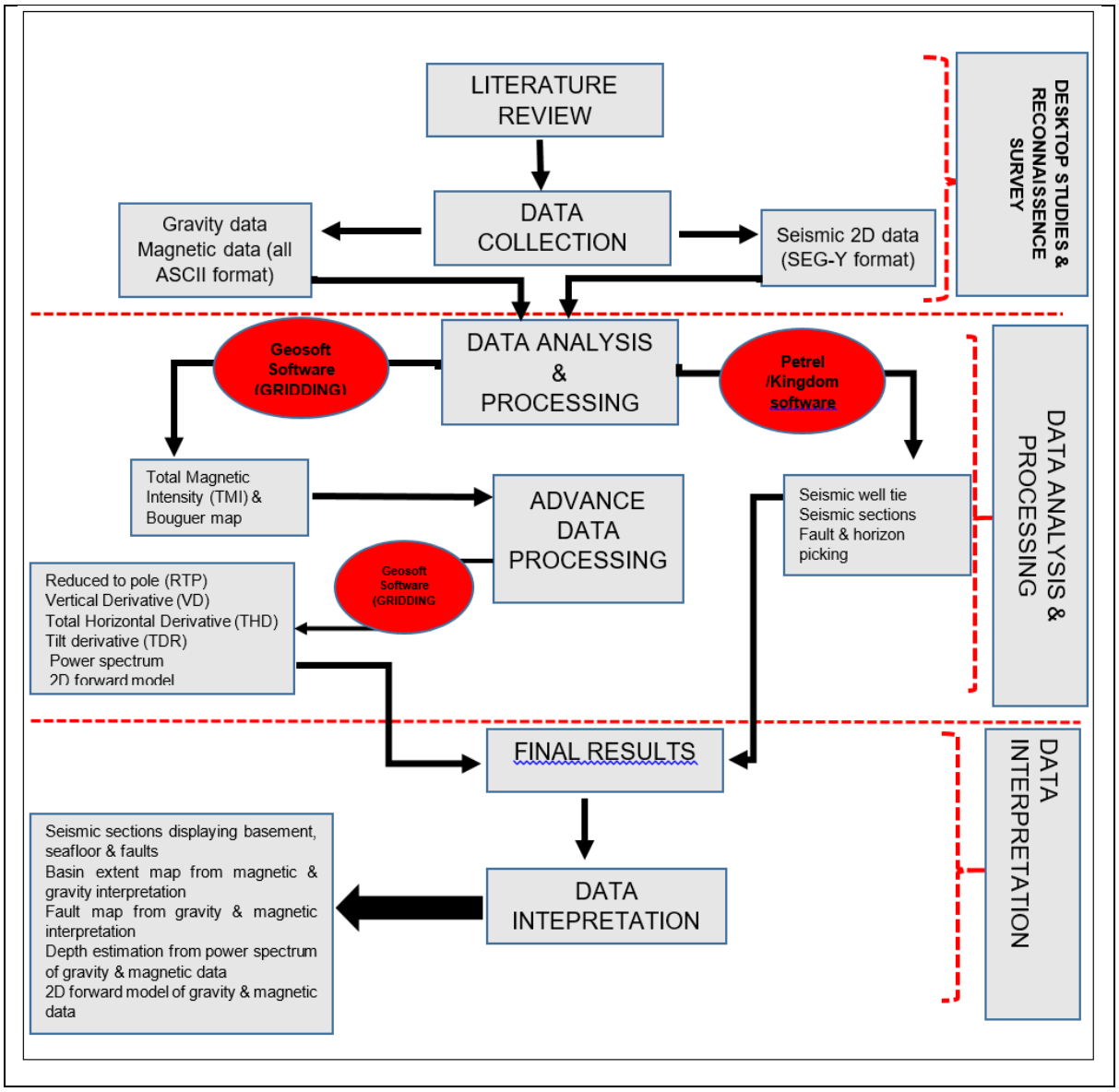

Figure 3.1 Methodology flow chart for this study.

3.1 Data collection and analysis

Data used in this study were gravity, magnetic and seismic 2D data. These data was supplied by Compagnie Générale de Géophysique (CGG), which was acquired through a multi-client agreement with PASA between year 2013 and 2014. The gravity and magnetic data were supplied in the ACSII file format while 2D seismic data was supplied as full migrated stack SEG-Y format. The auxiliary data used for this research work is well data for seismic well tie process and stacking velocities for velocity modeling to establish time-depth relation.

Gravity and magnetic methods are an essential part of oil exploration. They do not replace seismic. Rather, they add to it. Despite being comparatively low-resolution, they have some advantages. These geophysical methods passively measure natural variations in the earth's gravity and magnetic fields over a map area and then try to relate these variations to geologic features in the subsurface. Lacking a controlled source, makes such surveys to be subjected to noise.

3.2 Gravity data

A gravity anomaly is the difference between the observed gravity value and that predicted from a theoretical Earth model. A positive anomaly suggests the location is characterized by a higher gravity value than predicted, while a negative anomaly indicates a lower value than predicted (Heiskanen and Moritz, 1967).

The gravity data supplied consisted of Complete Bouguer Gravity Anomalies (CBA). Complete Bouguer Anomaly is refined gravity anomaly after latitude, elevation, terrain, Bouguer corrections etc. have been applied. The elevation or height correction alone defines a Free Air Anomaly (FAA) (Li and Götze, 2001). In this study, the gravity anomaly datasets were projected to UTM 36S in WGS 84 datum. The complete Bouguer gravity anomaly map is an excellent tool to perform pattern recognition and structural modeling (Blakley, 1996). The filtered Bouguer data was gridded and processed using Oasis Montaj Geosoft software to produce Bouguer, tilt derivative (TDR), horizontal derivative (HD) and vertical derivative (VD) anomaly maps. The

above-mentioned maps were used in both qualitative and quantitative interpretations to define the basin extent, map geological structures, and estimate sedimentary thickness cover and depth. Horizontal derivative map was used to map boundaries or contacts of subsurface geological features and deep-seated structures while VD was used to map small structures at shallow depths.

Gravity and magnetic data were digitally processed using Oasis Montaj Geosoft software. Minimum curvature gridding technique in Geosoft software was used to grid gravity and magnetic data. “Minimum curvature technique creates smooth surfaces of a given data. Minimum curvature first estimates grid values at the nodes of a coarse grid (usually 8 times the final grid cell). This estimate is based upon the inverse distance average of all data within a specified search radius. If there is no data within the radius, the average of all data points in the grid is used. An iterative method is then employed to adjust the grid to fit the actual points nearest the coarse grid nodes” Oasis Montaj (2014).

3.2.1 Gravity data processing

The gravity data was gridded and processed to create Bouguer anomaly map, using minimum curvature gridding technique in Geosoft software. The Bouguer anomaly map was contoured using 20 mGal contour interval. To enhance the gravity anomalies and improve gravity data interpretation, filtering techniques were applied to Bouguer anomaly map. These filters are computerized operations and grid-based.

Transforming gravity and magnetic data into derivative map improves edge or boundaries detection by placing anomaly maxima at the point of the maximum horizontal gradient within the grid (Bronner et al., 2009). Three filters (Vertical derivative, Horizontal derivative and Tilt derivative) were applied to the original Bouguer gravity anomaly data for analysis of the subsurface structure characteristics of the Durban Basin. 1st order horizontal derivative and 1st order vertical derivative were applied. The main aim of applying these filters was to improve edge, contacts or boundary detection to confidently identify and map subsurface structures or features, estimate depth of subsurface features and estimate sedimentary thickness cover.

3.3 Magnetic data

Magnetic data for this study was supplied by CGG in ACSII file format. A total of 6374 km of magnetic line data was acquired using a SeaSPY proton spin magnetometer which was located in the plastic towfish unit. The magnetometer was towed 130 m away from the vessel to eliminate effects introduced by the ship or vessel to the magnetic readings and 37.5 m shot spacing was maintained. The base station for magnetic diurnal reading was located in Gauteng, South Africa at 25.900^0 S , 27.700^0 E and elevation of 1555 m and these readings were used to correct diurnal effects.

Magnetic data consisted of adjusted filtered magnetic anomalies after applying diurinal corrections. The observed adjusted filtered magnetic anomalies were processed and gridded using Oasis Montaj Geosoft software to create Total Magnetic Intensity (TMI) anomaly map. The TMI anomaly were transformed to the poles using declination, inclination and local elevation to calculate Reduced to the pole (RTP), 1^{st} order vertical derivative (VD), 1^{st} order horizontal derivative (HD) and Tilt derivative (TDR) using Fourie transformation algorithms in Oasis Montaj Geosoft software were also applied. These calculated magnetic anomaly values were gridded to produce RTP, TDR, HD and VD anomaly maps that were used during qualitative and quantitative intepretations.

3.3.1 Magnetic data processing

Using minimum curvature technique in Geosoft, magnetic data was processed and gridded to create a total magnetic intensity (TMI) map and contoured with a 100 nT contour interval. Magnetic anomalies are directly related to magnetization and ambient field. Like the gravity field, magnetic field of the Earth is a vector field. A geometric vector is a mathematical quantity with both direction and magnitude (Blakely, 1996). In magnetics, the field directions vary from horizontal (magnetic equator) to vertical (magnetic poles), and remanent magnetism can often be strongly related to the induced component.

Telford (1990) and Fairfield (2015) indicates that if the induced magnetization and ambient field are not vertical, symmetrical magnetic body will create an asymmetrical anomaly thus distorting subsurface features. For this study, to remove these effects caused by inclination, TMI grid was transformed to the poles. The main aim for transforming magnetic data from TMI to reduce to the pole (RTP) was to align the magnetic anomalies directly above the subsurface or causative features. Thus, reduction to the pole (RTP) was employed to remove the effects of magnetic inclination.

The results of RTP calculation were analyzed and gridded to interpolate the point data to produce an RTP grid map. The following filtering methods were applied to RTP map, 1st order vertical derivative (VD), 1st order Horizontal derivative (HD), and Tilt derivative (TDR) to enhance edge, contact and or boundary detection during interpretation process. The gridded data was used to produce a VD, HD and Tilt derivative grid maps for both qualitative and quantitative interpretation, to define the basin extent, map major structures, and estimate sedimentary thickness cover and depth of the features.

3.4. Filters applied for this study

Processing of gravity and magnetic data in this study involved applying various filtering techniques to enhance shallow or certain features, edge and boundary detection that will improve interpretation of both gravity and magnetic data. Brief description of the filters or derivatives applied to Bouguer and TMI;

3.4.1 Reduced to the pole (RTP)

Magnetic anomalies are directly related to magnetization and ambient field. Magnetization and ambient field are not vertical thus, symmetrical magnetic body creates asymmetrical anomaly thus distorting subsurface features. For this study, to remove these effects caused by inclination, TMI grid was transformed to the poles because the study area is in the poles not the equator. The main aim for transforming magnetic data from TMI to reduce to the pole (RTP) was to align the magnetic anomalies directly above the subsurface or causative features. The RTP calculation

were done using -61 Inclination (I), and -22 declination (D) using the Fourie Transform option in Geosoft software. The results of RTP calculation were analyzed and gridded to interpolate the point data to produce an RTP grid map. All the filters for magnetic data were applied to RTP. Reduction to pole operator can be defined as (Geosoft Inc,1996):

$$L(\theta) = \frac{1}{\left[\sin(I_a) + i\cos(I)\cos(D-\theta)\right]} \tag{3.1}$$

With:

I geomagnetic inclination

I_a Inclination for amplitude correction (I_a>I)

D geomagnetic declination

3.4.2 Vertical derivative (VD)

First order vertical derivative filter applied to gravity and magnetic data sharpen the local features, edge or contact detection, trends and improve source resolution. This derivative technique suppresses signal from deep seated features or sources. Vertical derivative maps of both Bouguer and RTP greatly enhances shallow structures, improves edge or contact detection. Edge or contacts mapping is achieved by placing anomaly maxima at the point of the maximum or highest amplitudes of gravity and magnetic anomalies. Transformation of gravity and magnetic data using derivatives is based on two key assumptions that, the potential field is vertical and that lithological contacts causing anomalies are abrupt. The first vertical derivative of the gravity field g in the space domain is defined as:

$$FVD = \left(\frac{\partial g}{\partial z}\right) \tag{3.2}$$

Where ∂g/∂z is the derivative of the gravity field or magnetic field along the vertical direction.

3.4.3 Horizontal Derivative (HD)

The first order horizontal derivative is the value of gravity and magnetic anomaly horizontally (Fairfield, 2015). Horizontal derivative tends to have maximum values over the edges or contact of sources consequently, that can be used to determine locations of major basement structures or sedimentary structures. The only limitation about horizontal derivative is that it tends to offset boundaries if boundaries are not near-vertical and close to each other which in this case was not visible. The amplitude of the total horizontal gradient (Cordell and Grauch, 1985) is expressed as:

$$THD(x,y) = \sqrt{\left(\frac{\partial g}{\partial x}\right)^2 + \left(\frac{\partial g}{\partial y}\right)^2} \qquad (3.3)$$

With: THD-first order horizontal derivative
Where ∂g/∂x and ∂g/∂z are the horizontal derivatives of the gravity field in the x and y directions.

3.4.4 Tilt Derivative (TDR)

The tilt derivative was applied to Bouguer and RTP anomaly map for this study to improve edge or contact detection of structures in the study area. Tilt derivative is mostly applied to gravity and magnetic data to enhance source boundary determination because this filter is not sensitive to depth thus can enable identification of both deep and shallow structures in the study area (Marson and Klingele, 1993; Blakley and Simpson, 1986). It is also a proven technique to help resolve anomalies over individual structures from the gravity field because the vertical gradient is more sensitive than gravity itself to structural features (Marson and Klingele, 1993; Blakley and Simpson, 1986). This filter is based on a theory that, TDR produces a zero value over or very close to the source edges or contact, therefore can be used to map faults and or contact of geological sources (Selim, 2016; Mekkawi et al., 2017). Positive values are directly located above the sources while negative values are located away from the sources. The equation that represents the TDR filter can be expressed as:

$$TDR = \tan^{-1} \frac{\partial g / \partial z}{\sqrt{\left(\frac{\partial g}{\partial x}\right)^2 + \left(\frac{\partial g}{\partial y}\right)^2}} \quad (3.4)$$

With: ∂g/∂x, ∂g/∂y and ∂g/∂z are the first derivatives of the field g along the x, y, and z directions (Verdusco et al., 2004).

The tilt derivative transformation is the angle between the total horizontal derivative (x and y directions) and the first vertical derivative (for gravity or magnetic anomaly). The operator produces a zero value over the source edges, which therefore can be used to trace the outline of the edges (Pilkington and Keating, 2004).

3.4.5 Power spectrum

For this study, depth estimation of subsurface features using gravity and magnetic anomalies was achieved by the use of radially averaged power spectrum. Power spectrum is a Fourier analysis of data where, spectral analysis is represented as log power versus wavelength graph. According to Spector and Grant (1970), different sources can be defined as linear sections on the power spectrum. The Power spectrum graph's gradient of linear section is twice the depth to the top of subsurface source. Power spectrum technique enabled identification of long wavelength associated with deep or regional sources and short wavelength associated with shallow features. For this study power spectrum was applied and derived from Bouguer and RTP gridded data.

Power spectrum of both Bouguer and RTP map is represented by two graphs: 1) Radially averaged graph of power log versus wavelength. 2) Depth estimation graph of depth versus wavelength. Depth estimation is calculated using the slope of the radially averaged curve by using a straight tangent line on the curve of graph slope (Figure 4.3). The tangent lines represent the subsurface layers at various depth ranging from deep to shallow with the tail of the curve as the noise (white noise) (Figure 4.3).

3.5 The 2D seismic data

The seismic data for this study consisted of twenty-nine (29) 2D seismic lines data covering the whole Basin (Figures 3.2). The data set covered an area of about 10,000 km² with an average spacing between 2D seismic lines of 60 km. The seismic data used were collected and processed i.e. from SEGD (raw field data) to SEGY (processed data) by CGG for the period 2013 and 2014 (Figure 3.2). The 2D seismic data was provided as full stacked migrated SEGY sections, 2D seismic lines were shot in S-N and E-W directions. Seismic lines were acquired perpendicular to each other covering the study area to provide a 3D view of the subsurface geology during interpretation process (Figure 3.2). Table 3.1 shows the acquisition parameters used during the data collection.

Table 3.1 2D seismic data acquisition configuration

Survey	2D Durban and Zululand Basin
Contractor	CGG
Vessel	M/V Princess
Recording dates	01 March-26 May 2013
Energy source:	
Array type	Airgun – single array
Number of guns	24 (4 subarrays)
SP interval (m)	37.5
Volume (cu in)	5080
Depth (m)	6
Air pressure (psi)	2000
Streamer configuration:	
Acquisition system	Sercel SEAL
No. cables	1
No. of channels per cable	804
Group spacing (m)	12.5
Depth (m)	5 – 50 (BroadSeis™)
Nominal first offset (m)	150
Streamer length (m)	10050

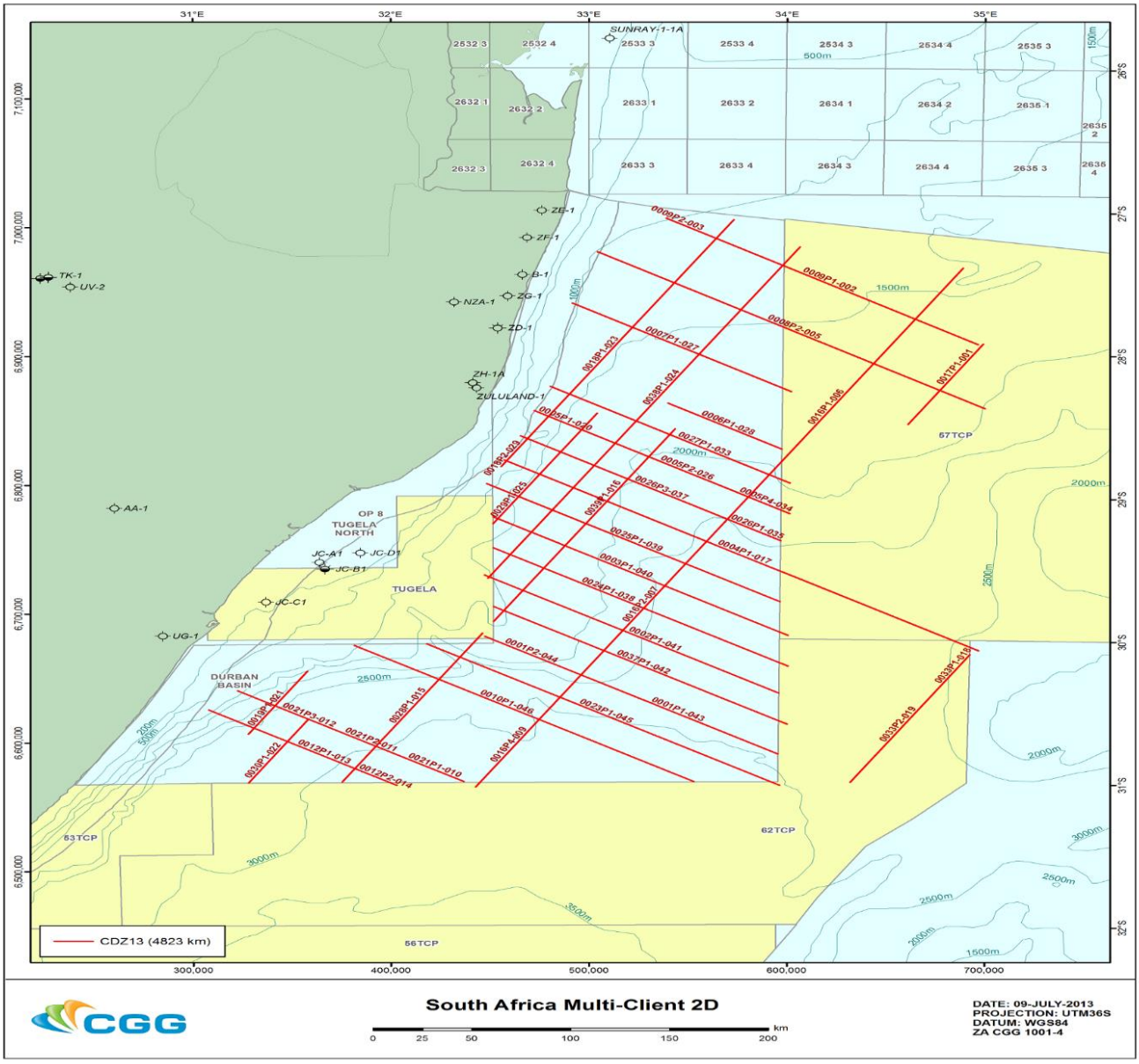

Figure 3.2 Map showing acquired and processed line data (seismic 2D, gravity and magnetic) in red, by CGG in the study area.

3.6 Well data

Well data (well Jc-C1) used for this study was supplied by PASA. Jc-C1 well was spuded in 1983 by Soekor with a total depth of 3169 m and was drilled on the continental shelf located on the adjacent block to the study area within the Durban Basin (Figure 3.2). Well data for Jc-C1 included well logs provided in LAS file, checkshots, and well tops. The well logs used for this study are sonic log and density log. Table 3.2 below displays detail information about the Jc-C1 well.

Table 3.2 Jc-C1 well checkshots, location and well tops information.

CHECKSHOTS

WELL NAME	CHECKSHOT	MD	TIME	CHEC
Jc-C1	2	1524	2196	MSL
Jc-C1	2	1884	2262	MSL
Jc-C1	2	2164	2327	MSL
Jc-C1	2	2474	2406	MSL
Jc-C1	2	2774	2490	MSL
Jc-C1	2	3074	2576	MSL

LOCATION

WELL NAME	X-Coord	Y-Coord	KB	TopDepth	BottomDep	Well Status
Jc-C1	29° 44' 8.1" S	31° 18' 35.3" E	26	311,2	3169	Dry

WELL TOPS

WELL NAME	KB	FORMATION TOP	DEPTH (m below KB)	TWT (msec)	TOTAL MD (m)	Age
JC-C1	26	Sea floor	123,7		3169	
		OLIG/ MIOC	530	445		Late Eocene/Late Miocene
		22At1	1740	1500		Late Maastrichtian/ Paleocene
		TOP OF SONIC	1900	1636		Campanian
		17AT1	1965	1694		Santonian
		13At1	2114	1812		Late Aptian/Albian
		15At1	2114	1812		Late Aptian/Albian
		1At1	2257	1902		Barremian-Early Aptian
		TOP-VOLCANIC	3104	2381		Undef.
		6At1	3115	2391		Undef.
		BOTTOM OF SONIC	3150	2409		Undef.

3.7 Seismic data analysis and interpretation methods

2D Seismic and well data was analyzed and interpreted using Schlumberger's Petrel 2015 software. Figure 3.3 is flow chart showing seismic data processing and interpretation procedure employed in this study. Processing and interpretation of seismic 2D data included: 1) Seismic well tie for establishing time depth relationship seismic data and well data and; 2) velocity model using the seismic stacking velocities to convert time surface to depth.

3.7.1 Well data

LAS log data for Jc-C1 well was imported into Petrel 2015 creating a new well folder; this included location coordinates (29°44'8.1'' S and 31°18'35.3'' E) of the well, sonic log and density log stored in the global logs folder. Six checkshots of Jc-C1 were imported thus creating a checkshot folder in Petrel. Well top for Jc-C1 well was imported into Petrel project stored in a new well tops folder. These data was used for seismic well tie process and formation picking after well tie. The sonic log (DT) and density log (RHOB) of Jc-C1 ran from depth of 1500 m to 3150 m.

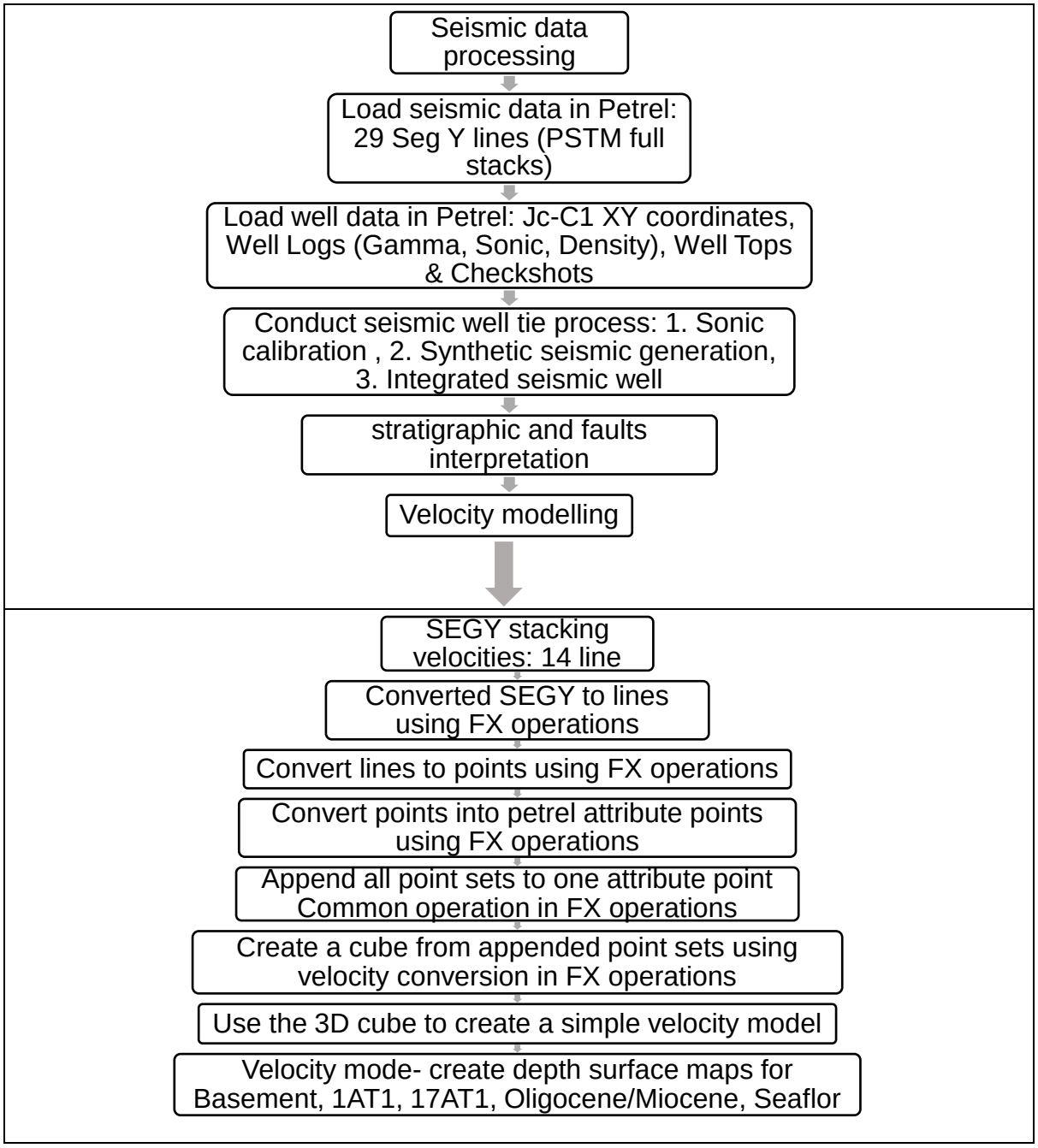

Figure 3.3 Detail seismic data processing and interpretation workflow.

3.7.2 Seismic dataset

A set of 29 seismic lines were imported into Petrel 2015 software in the SEG-Y format. For importing, the “SEG-Y preset parameters format into single 2D seismic survey” format was used for the line detection method. A new 2D survey folder was created and named TB132D-01 in Petrel 2015 to store the lines. A number was assigned to each line and they were sorted and organized. To get a 2D view of the 2D seismic lines the 2D window was used (Figure 3.4). In Petrel 2015, a unique interpretation

window was assigned to each seismic profile. 2D windows were used in combination with the interpretation window for seismic interpretation. Horizons delimiting the upper and lower margins of the lithologies were generated by use of the horizon management tool palette whereas faults were generated by use of the fault management tool palette. Other features such as the unconformity and pinch-outs were generated by use of the annotations tab. Figure 3.4 shows the base map of the seismic lines when they were uploaded to Petrel 2015 in a 2D window.

Seismic attribute datasets were extracted from the 2D surface seismic data. Well-log and core data are localized measurements that only represent a small volume of the reservoir. Seismically extracted attribute volumes describe heterogeneities away from the 1D well log data and core data and define structural and stratigraphic complexity (Raeesi et al., 2012). A seismic attribute is any quantitative measurement of seismic waveform data that quantifies or enhances geometric, kinematic, dynamic, or statistical features for interpretation (Chopra and Marfurt, 2007; Chen and Sidney, 1997; Chopra and Marfurt, 2005). Seismic attributes are interpretation aids that visually enhance features not resolvable in the seismic reflections, like a fault extraction algorithm. They are also mathematical transforms (Hampson et al., 2001) that extract information from the wavelet to output, or predict, well log properties, such as an acoustic impedance inversion.

3.7.1.1 Seismic-well tie

Seismic-well tie is an important procedure for seismic data interpretation process and is defined as forward modelling of a synthetic seismogram from sonic and density logs (White and Simm, 2003). The synthetic seismogram is matched to the seismic reflection data to create relationship well log in depth (m) and seismic in travel time. This process allows the interpreter to accurately map horizons and estimate wavelet for inverting seismic data to impedance (White and Simm, 2003). For this study, to accurately map the horizon or formation on seismic 2D lines, seismic well tie was applied using well data of Jc-C1 and seismic line IMP1188P1001. The following steps for seismic-well tie were followed:

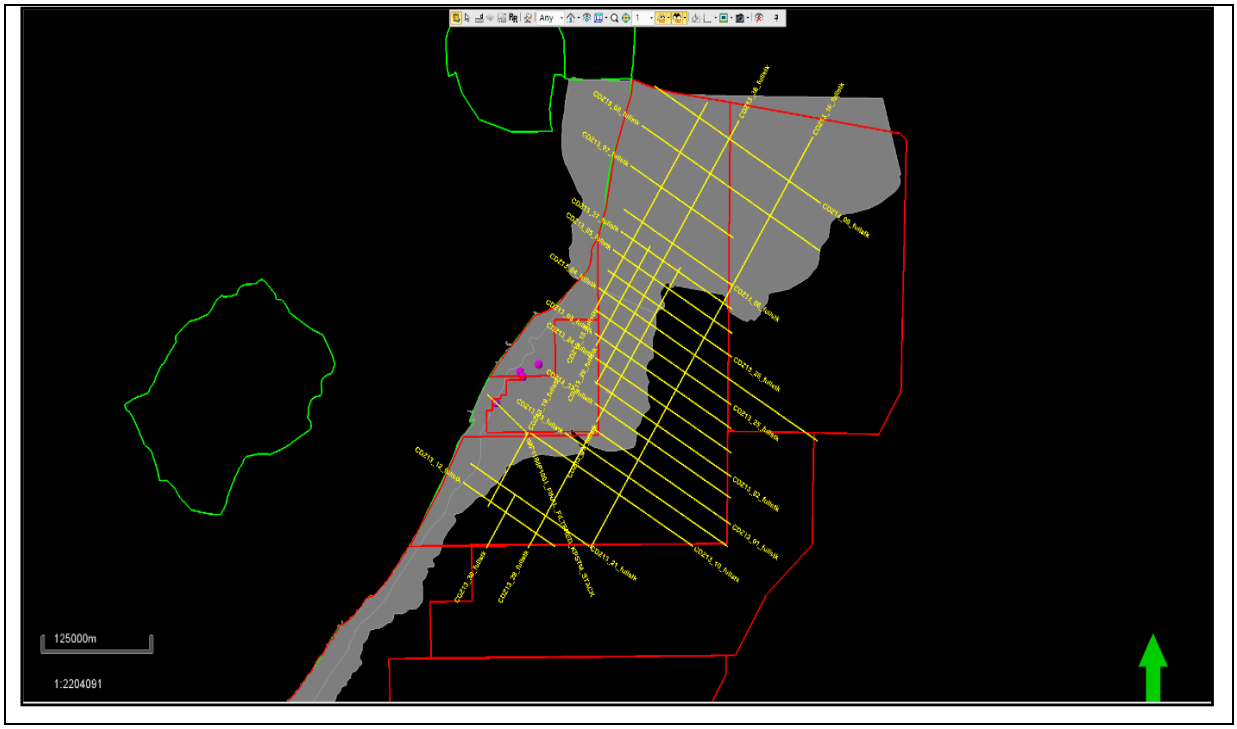

Figure 3.4 Basemap for the imported seismic data in Petrel software 2015 in 2D window; seismic profiles (yellow lines); onshore blocks (green lines), Durban Basin (red line L shaped) and other PASA license blocks (red lines) and well data points (pink dots).

3.7.1.2 Sonic calibration

Compressional sonic log data and check shot surveys are an accurate measure of vertical interval velocity (Luton and Prieto, 2000), and it provides a means to convert time to depth from well data. Sonic logs measure a travel time Δt, from which slowness Δt/Δz is calculated (Robein, 2003). This provides a sonic time-depth relationship. However, sonic logs are not typically measured from the surface and only measure interval velocities (Robein, 2003; Luton and Prieto, 2000; White and Simm, 2003), so vertical time and average velocities from the surface cannot be calculated (Robein, 2003). This results in generating synthetic seismograms with significant timing errors, which are more detrimental than errors in amplitude (White and Simm, 2003).

Checkshots are thought to measure times that are closer to surface seismic data (Robein, 2003) at the correct seismic scale (Simm and Bacon, 2014). Calibrating the sonic log data by a checkshot survey, or a Vertical Seismic Profile (VSP) provides a sequence of control depths corresponding to vertical time (Robein, 2003; White and Simm, 2003). For this study Jc-C1 checkshots were used as the initial input time-depth

relationships to conduct sonic calibration i.e. Sonic log, density log, checkshots (Table 3.2).

The sonic times are typically lower than the checkshot times due to the sonic tool's limitations, processing effects, and environmental factors (Robein, 2003; Box and Lowrey, 2003). A sonic drift curve, or calibration curve, is calculated by subtracting the sonic times from the checkshot times (Figure 4.7). The drift curve illustrates the effect of velocity dispersion between log and seismic frequencies (Simm and Bacon, 2014). Knee points, as denoted by the "blue dots" on Track 1 of Figure 4.7, connect straight line segments of the drift curve at each checkshot. The calibration log will suddenly bend at unconformities or changes in log character (White and Simm, 2003; Simm and Bacon, 2014). The application of knee points allows direct control of the calibration (White and Simm, 2003). Once knees are created, the drift curve is then applied to the sonic log (White and Simm, 2003) for calibration. This results in a calibrated sonic log, the input and output interval velocity curves, checkshot interval velocities, an average velocity curve, and a picked two-way time (TWT) curve (Figure 4.7). The calibration outputs a new time-depth relationship that relates vertical time and depth domains.

3.7.1.3 Synthetic seismic generation

To directly correlate the well log data to the seismic data, synthetic seismic traces are generated from the calibrated well log data. Synthetic seismic generation outputs a time-depth relationship that is used to estimate interval velocities at the well point (Viloria et al., 2009). Synthetic seismograms are generated following the convolutional model. The seismic wavelet is a function of acoustic impedance. An acoustic impedance log is obtained by multiplying a density log and the inverted calibrated sonic log (Figure 4.8).

Reflection coefficients are the fractions of incident energy reflected from some interface and is calculated as:

$$RC = \frac{AI_2 - AI_1}{AI_2 + AI_1} \tag{3.5}$$

where RC is the reflection coefficient and AI is an acoustic impedance value. The result is a series of delta functions (Figure 4.8) describing the acoustic impedance contrast at a reflective interface. To produce the synthetic seismic wavelet, the delta function series is convolved with a 25 Hz Ricker wavelet, which is about the same frequency of the seismic signal. It is important that the input wavelet frequency approximates the frequency of the wavelet for the seismic data so the convolution returns a synthetic seismogram that contains the same vertical resolution of the seismic data in order to accurately match reflection events during the well tie.

3.7.1.4 Well tie

Seismic well ties are crucial to seismic data interpretation. A seismic well tie allows the interpreter to accurately pick horizons (White and Simm, 2003) and map the depth domain into the time domain. A well tie involves matching events from the synthetic seismogram to events in the adjacent 2D seismic data (Figure 4.8). First, a bulk time shift is applied to shift the entire synthetic to a good-fit, wherein reflection events in the seismic match reflection events in the synthetic for a given time/depth. Next, stretching and squeezing may be applied to aesthetically enhance the tie, however anything but a static shift is not recommended (White and Simm, 2003). Stretching and squeezing were not applied to this well tie. The time-depth relationship was updated by bulk shifting the synthetic seismogram in depth and time 12 ms to closer match reflections and correct for refraction static effects, which were a large component of the time difference. Refraction statics are attributed to weathered layer effects. Relatively loose or uncompacted material overlying denser, compacted material produces a slow, variable velocity layer that distorts temporal measurements. It should be noted that refraction statics are not uncommon in seismic data.

3.7.1.5 Velocity modeling by seismic stacking velocity

Velocity modeling is important for domain-converting seismic data. Seismic profiles are displayed in two-way time, i.e. the length of time for a seismic wave generated at the Earth's surface to reflect off a subsurface acoustic reflector and travel to a receiver on the surface. For characterization purposes, it is useful to convert the vertical axis

from two-way time in milliseconds (ms) to total depth in meters (m) or kilometres (km). This allows the interpreter to correlate the seismic data to other datasets in the depth-domain, such as wireline log and core data, and it allows formation thickness to be measured. Time-to-depth velocity models integrate several datasets, including well logs, well top picks, checkshot data, seismic reflection data, and horizon interpretations. Seismic stacking velocities was used to create a velocity model to achieve time-depth relationship of time-domain seismic data. Formation top horizons were interpreted from the well tie, which are used to build the structural foundation for the velocity model. Figure 3.3 shows the detailed processes followed in creating a velocity model in Petrel 2015 using stacking velocity in a study without a drilled well i.e. seismic stacking velocities lines are converted to points to create a cube that is used to build a velocity model for the study area.

The FX operations features in Petrel 2015 is used to convert and generate line layout for 2D seismic stacking velocities. The generated lines layout are converted to points using FX operations to generate set of points. The generated set of points for 29 SEGY stacking velocity lines were converted into Petrel points with attributes using; Time: Min -12002.00, Max 2.00, Delta 12004.00 and a sampling interval of 4 to obtain average velocity. All the converted points sets were appended onto single selected point set to create a single set of points in one file. The appended points set was used to create a 3D cube using FX operations-velocity conversion (convert points to cube). The 3D seismic velocity cube was used to create a velocity model using simple model technique in Petrel 2015 seismic interpretation tools.

3.7.1.6 Depth Conversion by the velocity model

Depth conversion velocity models operate on simple velocity, time, and depth relationships. Instantaneous velocity V_{inst}, or the velocity as it relates to local elastic parameters that the seismic wave encounters, is the derivative of the vertical distance travelled with respect to the traveltime.

$$V_{inst}(z) = \frac{\partial z}{\partial t} \tag{3.6}$$

where z is vertical depth and t is traveltime (Robein, 2003). For the purposes of designing a velocity model, interval velocities are needed. Interval velocities describe the average velocity of some finite, horizontal geologic layer or formation in which instantaneous velocities may be similar. For some layer thickness (Z_2-Z_1), the vertical traveltime $T_{1\text{-}2}$ is expressed as:

$$T_{1-2} = \int_{z_1}^{z_2} \frac{\partial z}{V_{inst}(z)} \quad (3.7)$$

which is also known as the integrated sonic between some depth interval (Robein, 2003). Therefore, the interval velocity is expressed as (Robein, 2003):

$$V_{inst} = \frac{z_2 - z_1}{\int_{z_1}^{z_2} \frac{\partial z}{V_{inst}(z)}} \quad (3.8)$$

Seismic data is measured in two-way time, and in order to convert to the depth domain, a relationship between time and depth must be established. The best way to do this is to use sonic well logs and checkshot surveys. A continuous time-depth function $T=f(z)$ describes the vertical propagation time as a function of depth (Simm and Bacon, 2014; Robein, 2003). The time-depth function is inverted using a simple transformation:

$$T_z = f(z) \leftrightarrow Z(T) = f^{-1}(T) \quad (3.9)$$

And thus,

$$V_{inst}(T) = V_{inst}Z(T) \quad (3.10)$$

(Robein, 2003). The transformation allows the depth-domain well data to map into the time-domain (Figure 3.5). By fitting the well data into the depth domain, a new time depth relationship is calculated that provides the initial parameters for the velocity model. The velocity model generated for depth-conversion is a Linvel “layer cake” model. It is built from a structural framework made up of time-domain surfaces, which were derived from the seismic horizon picks (Figure 3.5).

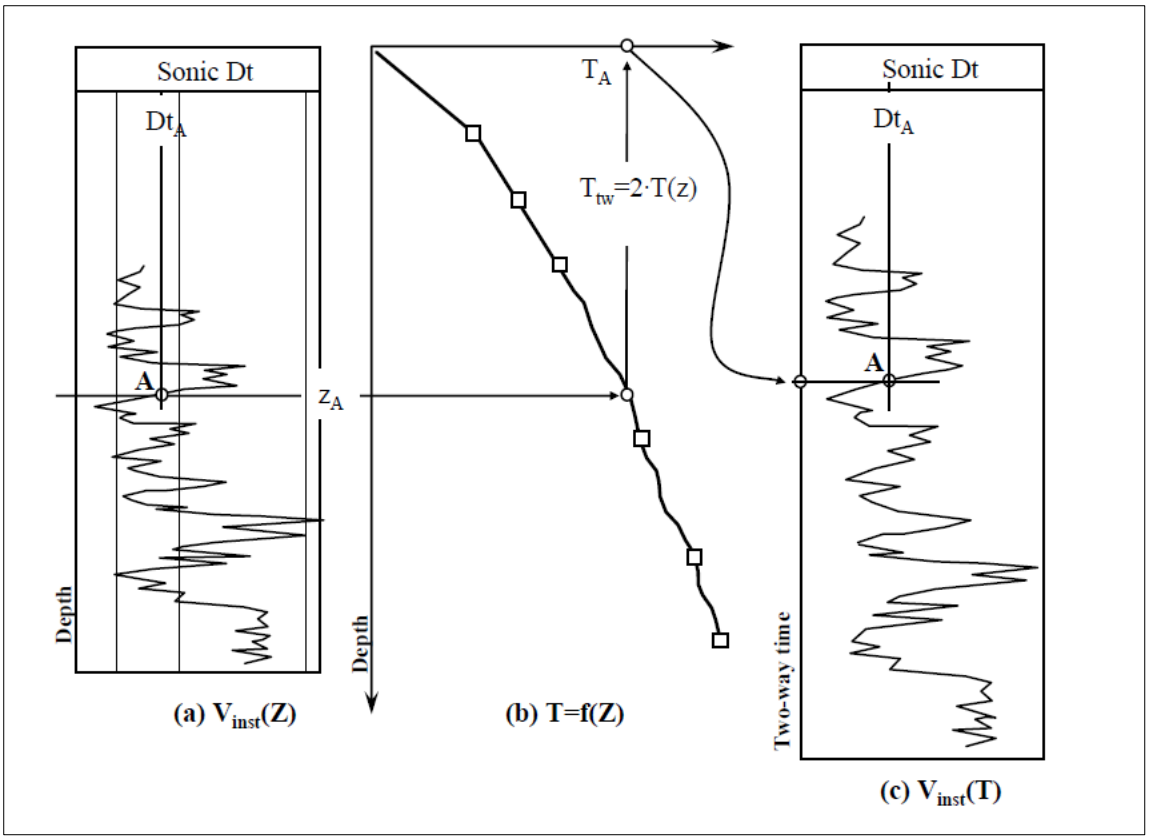

Figure 3.5 Well log data acquired in the depth domain can be mapped into the time domain by application of $T=f(z)$. A is some point in on the sonic curve in depth, denoted by ZA. DtA is the sonic value at point A. In part b), depth and time are related on a plot of depth on the y-axis and time on the x-axis. TA refers to the point in two-way traveltime in which point A plots according to the time-depth function (line with square points), or $T=f(z)$. (From Robein (2003).

3.7.1.7 Seismic stratigraphic and fault interpretation

Once the depth-domain well data was mapped into the time-domain using the transformation described by Equation 3.5, the well and its well top picks were superimposed onto a time-domain seismic intersection (Figure 3.5). Points corresponding to well top picks at the well provided a starting point for horizon picking across the seismic volume. The horizons were picked using a 3D autotracker for a single reflection event followed by manual editing. Table 3.3 display a summary of steps followed to interpret seismic stratigraphic horizons and faults for this study.

Five horizons namely: Seafloor, Oligocene/Miocece, 17AT1, 1AT1 and basement were picked in this study (Table 3.3).

Table 3.3 Detailed steps followed during seismic stratigraphic and fault interpretation.

1 Seismic data processing	• Petrel 2015 software was used to import 29 SEGY 2D seismic lines. • The shapefile of the study area was imported into Petrel 2015 software • Coordinate system is UTM Zone 36S (WGS84) • The X and Y coordinates, shot points interval, CDP as per byte numbers on the SEGY header of the 2D seismic lines was set in Petrel using “SEGY preset parameters”
2. Identification of reflectors	• Reflectors were picked in Petrel 2015 by inspecting seismic sections passing through Jc-C1 well. Reflectors are identified through tying the seismic sections to the well data (Figure 3.7A). • Five strong reflectors were identified and picked in Petrel 2015 representing seafloor, Oligocene/Miocece, 17AT1, 1AT1 and basement. These were distributed at various depths throughout the area. Correlating with the well lithologic information.
3. Picking and correlation of reflectors	• Studied horizons were picked up across seismic lines after the reflector identification. • When reflectors are either displaced vertically or disappear, this interruption may be due to faulting or pinch-out, respectively. • The horizons were picked along all seismic grids by correlating the seismic events, tying their times. • The picked horizons are correlated to the chronostratigraphical events in the Durban Basin (Figure 2.1)
4 Fault location detection	• Faults must be vertical continuous within a seismic section • Faults of large vertical displacements were easily recognized, especially from the sudden stepping-out of reflections across their planes.

	• Faults with small displacements were traced on the bases of identification of reflection gaps
5 Horizon surfaces	•Picked horizons were gridded into time surfaces of seafloor, Oligocene/Miocece, 17AT1, 1AT1 and basement • The time surfaces were converted into depth domain surfaces using velocity model

4. CHAPTER FOUR: RESULTS AND DISCUSSION

4.0 Introduction

This chapter presents the data analysis, results and discussions of gravity, magnetic and 2D seismic data. Petrel 2015 software was used to analyse and interpreted twenty-nine (29) 2D seismic lines while Geosoft software was used to analyse, process and interpret gravity and magnetic data. The results include Bouguer anomaly map, TMI anomaly map, RTP anomaly map, tilt derivative anomaly map (TDR), horizontal derivative anomaly map (HD), vertical derivative anomaly map (VD), and power spectrum of gravity and magnetic data. Seismic results include velocity model, Seismic well tie, delineated horizons (seafloor, Oligocene/Miocene, 17AT1, 1AT1 and Basement), surface depth horizon maps, and seismic sections displaying horizons and faults. The gravity, magnetic and seismic data (seismic sections) were used to interpret the faults and horizons and estimate the depth and thickness of sedimentary cover in the Durban Basin. TDR, HD and VD anomaly maps were more useful in mapping structures dissecting the study area. All maps were projected to WGS84, UTM zone 36S. The uninterpreted Bouguer, TMI, RTP, VD, HD, TDR, and power spectrum maps are placed in the appendix A (Figures A-1.1, A-1.2 and A-1.3).

4.1 Gravity and magnetic data interpretation

4.1.1 Gravity data

Figures 4.1A, 4.1B, 4.1C and 4.1D displays complete Bouguer gravity anomaly, 1st order vertical derivative (VD), 1st order horizontal derivative (HD) and tilt derivative (TDR) maps respectively. Figure 4.1A displays corrected Bouguer gravity anomaly map, with 20 mGal contour interval. A complete Bouguer anomaly map, in general is the gravity anomalies showing the lateral variation in the density of the subsurface geology and geological structures of different sizes and depth. The Bouguer anomalies of shallow features is characterized by shorter wavelengths while deep features have longer wavelengths.

In Figure 4.1A the contoured Bouguer anomaly map displays the gravity values ranging from 21.5 (blue-green) to 126.3 (orange-pink) mGal from NW to SE direction.

The variation in gravity anomaly represents the lateral geological variations from less dense sediments corresponding to the sediments rich to highly dense basement with gravity anomaly highs (Figure 4.1A).

The followings are the characteristics of the gravity anomalies amplitudes in the study area: Amplitudes ranging from 20 to 33.7 mGal representing very low anomalies covers the northwestern (NW) corner of the study area (Figure 4.1A). Amplitudes ranging from 33.7 to 68 mGal representing low anomalies is distributed in most parts of the study area, extending from SW to NE parts of the map. These anomalies are represented by blue to green colours of the histogram colour scheme. These anomalies represent the thickest sedimentary cover part of the study area, which could represent the area with sedimentary package of more than 4 km thickness in Tugela Cone as reported by Broad and Mills, (1993) and Broad et al., (2006) (Figure 2.1) (Figure 4.1A).

High gravity anomalies occupy most of the SW, SE and NW parts of the study area, with amplitudes ranging from 68 to 119 mGal and very high gravity anomalies occupy the NE corner of the study area with amplitudes ranging from 119 to 129 mGal. These gravity high and very high values are represented in orange to pink on the colour histogram. These anomalies represent shallow basement rocks, which could be related to the highly dense volcanic Naude Ridge and Tugela Ridge that divides the Durban Basin and Zululand Basin (Kitchin, 1995, Ben-Avraham et al., 1997 and Broad et al, 2006).

The computed first order vertical derivative (VD), using a fast Fourier transformation (FFT) (Figure 4.1B), is a high-pass filter designed to accentuate the more detailed features and structures in the subsurface (Copper and Cowan, 2004; Marson and Klingele, 1993). It is also a proven technique to help resolve anomalies over individual structures from the gravity field because the vertical gradient is more sensitive than gravity itself to structural features (Marson and Klingele, 1993; Blakley and Simpson, 1986). It should be noted that this transformation technique also amplifies the short wavelength thus enhancing shallow features. Transformation of gravity data using vertical derivatives is based on two key assumptions that: the potential field is vertical and that lithological contacts causing anomalies are abrupt (Marson and Klingele,

1993; Blakley and Simpson, 1986).The vertical derivative map (Figure 4.1B) greatly enhanced shallow structures, improved the visibility of the edge or contacts.

The contoured 1st order Total Horizontal Derivative (THD) of Bouguer anomaly and the Total Horizontal Derivative of the Tilt angle (TDR-THDR) of Bouguer anomaly maps show high anomalies in the central parts and the SE regions of the study area (Figures 4.1C and 4.1D). It is observed that 1st order horizontal derivative and tilt derivative filters of the Bouguer anomaly data sharpens the local features, edge or contact zones, the trends of the features and improves the source resolution (Figures 4.1C and 4.1D). Clear distinctive boundaries are observed in Figures 4.1C and 4.1D. These derivatives are known to suppress signals from deep seated features or sources. The two derivatives are powerful techniques used to detect gravity discontinuities. The (THD) and the (TDR-THDR) behave like an automatic gain control filter which tend to equalize the amplitude of the transformed total field of the gravity anomalies (Fedi and Florios, 2009). Only the horizontal derivatives were used to obtain the THD (Blakley and Simpson, 1986; Cordell and Grauch, 1985) and then applied for computing the TDR-THDR (Pilkington and Keating, 2004) as discussed in sections 3.4.3 and 3.4.4. The zero crossing of TDR-HTDR locates the boundaries of the causative sources, whereas they are detected by the high amplitude of the THD method (Ardestani, 2010).

From Figures 4.1B, the Bouguer maps derivative were able to delineate the less dense shallow linear structure cutting through the study area, trending in the SW-NE direction (represented by low gravity anomaly values in green to blue) which was not clear in comparison to CBA in figure 4.1A. This less dense linear geological structure correlates to the Tugela Cone, which is characterised by thick sedimentary package (Broad et al., 2006).

The first order horizontal derivative and tilt derivative filter enhanced four gravity high amplitudes (pink) with closed elongate shaped contours. Consequently, using the maxima principle technique, four major structures or lineaments represented by enhanced high gravity anomalies were delineated which could be faults dissecting the study area trending in S-N, W-E and NE-SW direction.

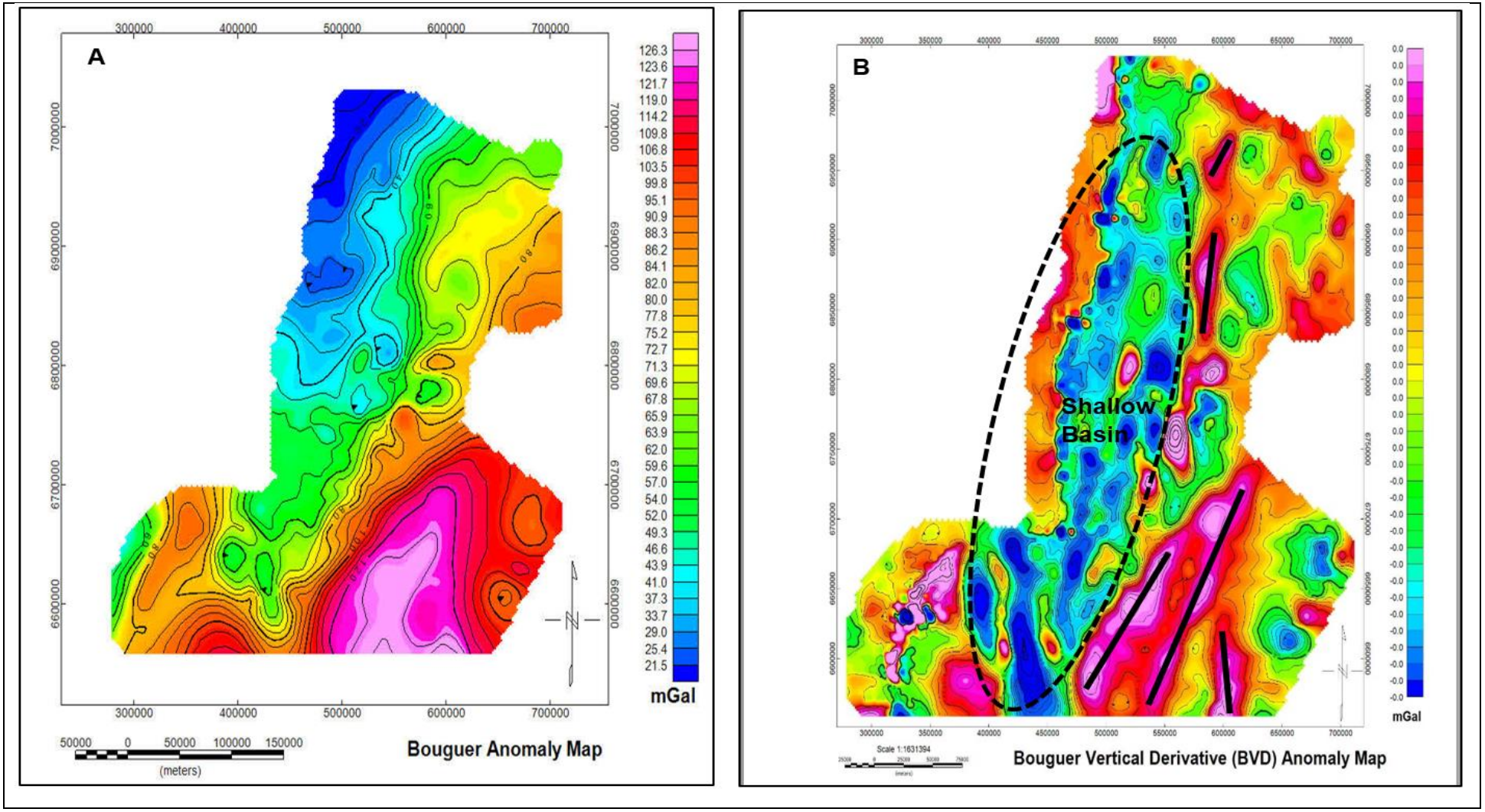

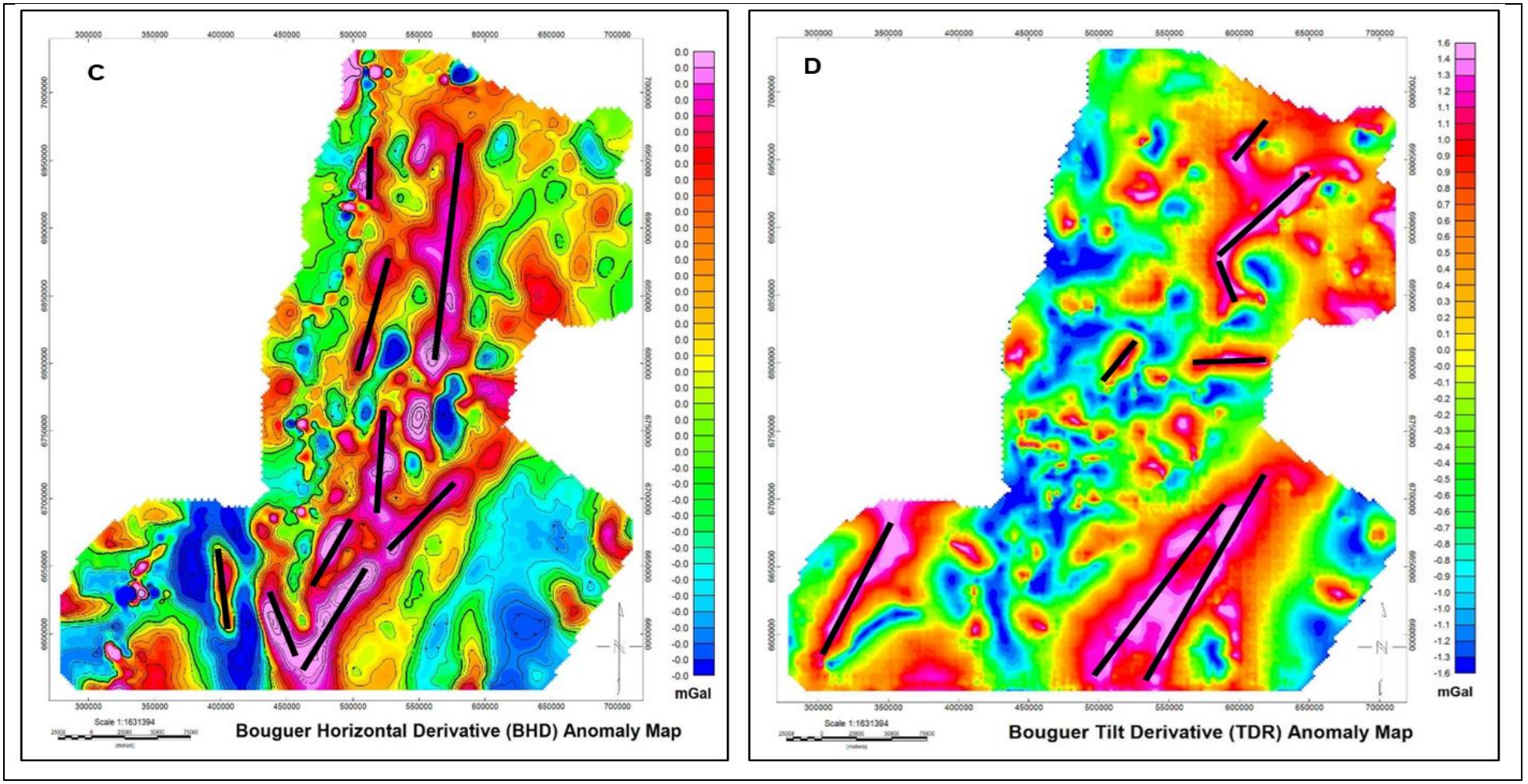

Figure 4.1 (A) Bouguer anomaly map of the Durban Basin with a 20 mGal contour interval. Interpreted (B) Contoured 1st order VD anomaly map of Bouguer. (C) Contoured 1st order HD anomaly map of Bouguer. (D) TDR anomaly map of Bouguer. 4.1C and D shows the first order horizontal derivative and tilt derivatives Bouguer anomaly maps.

4.1.2 Magnetic data

Figures 4.2A shows the corrected total magnetic intensity (TMI) anomaly map of the study area with a 100 nT contour interval. Figure 4.1B, C, D and E. display the RTP, VD, TDR, and HD maps. The red and blue colours represent high and low magnetic anomalies respectively (Figures 4.2 A, B, C D and E). The Magnetic intensity in the study area ranges from -388.8 nT to 789.1 nanotesla (nT). A comparison of the gravity and magnetic data, show two major differences. First, the magnetic anomalies do not show gradually increase like the gravity anomalies (Figures 4.1A and Figures 4.2A), rather there are low and highs magnetic variations scattered across the study area. This is indicative of different lithological composition and possibly at different depths and trends. Second, the high magnetic anomalies are concentrated in the NE and central part of the study area (these high anomalies shown by closed contours lines, mostly as ball shaped or elongated in shape in some instances) unlike the gravity where the high gravity anomalies are concentrated in the SE section of the study area.

The high magnetic anomalies range between 149.3 and 789.1 nT. These high anomalies indicate shallow subsurface structures in the basin which are rich in ferromagnetic material related to the basement. Their linearity is indicative of the trend of these rocks. The low magnetic anomalies range from -388.8 to -7.4 nT. These low magnetic anomalies represent non-magnetic sedimentary cover of the Durban Basin (Figures 4.2A, B, C, D, and E).

Figure 4.2 B shows the RTP map. The RTP transformation aligns the anomalies directly above the sources, which makes corrections of the effects from latitude variation (Fairfield, 2015). However, comparing the RTP and TMI maps, the RTP map does not significantly differ from the TMI map (Figures 4.2 A and B). Like the TMI map, the RTP map shows both the low and high anomalies scattered across the study area. The high anomalies range from 175.6 to 894.1 nT (in pink color). These high anomalies occupy the central, south western and north eastern parts of the study area (Figures 4.2 A and B). These high magnetic anomalies clearly correlate with basement high Tugela Ridge and Naude Ridge mapped by Goodlad, (1986), Kitchin, 1995, Ben-Avraham et al., (1997) and Broad et al, (2006) (Figures 4.2A and B). This basement

high ridges seems to divide the basin into shallow and deep basin as recorded by Goodlad, (1986) and Broad et al., (2006). The shallow basin is represented by low magnetic anomalies (Blue) occupying the south western and northern section of the study area. The deep basin occupies the south eastern corner of the study area represented by large low magnetic anomaly (Figure 4.2B). The magnetic lows indicate the presence of shallow thick sedimentary cover in the study area which could be related to the Tugela Cone characterised by thick sediments of more than 4000 m thickness as reported by Broad and Mills, (1993) and Broad et., (2006) (Figure 2.1).

Figures 4.2C, D and E shows first order vertical derivative, tilt derivatives and horizontal derivatives of RTP map. When using derivatives edge or contacts mapping is achieved by placing anomaly maxima at the point of the maximum or highest amplitudes of gravity and magnetic anomalies (Selim, 2016; Mekkawi et al., 2017). The magnetic anomaly values from these maps are enhanced and distributed across the study area. Their distributions and shapes suggest that the study area is dissected by shallow structures or faults because vertical derivative is known to enhance shallow or localized structures. Most of these structures are trending in the S-N, NE-SW and W-E directions. The structures dissecting southwest part of the study could be related to AFFZ that affected the Durban Basin and resulted into listric faults (Bhattacharya and Duval, 2016). The NE-SW trending structures correlates with multiple fault systems and graben structures recorded by PASA (2016), related to initial rifting and movements of the AFFZ.

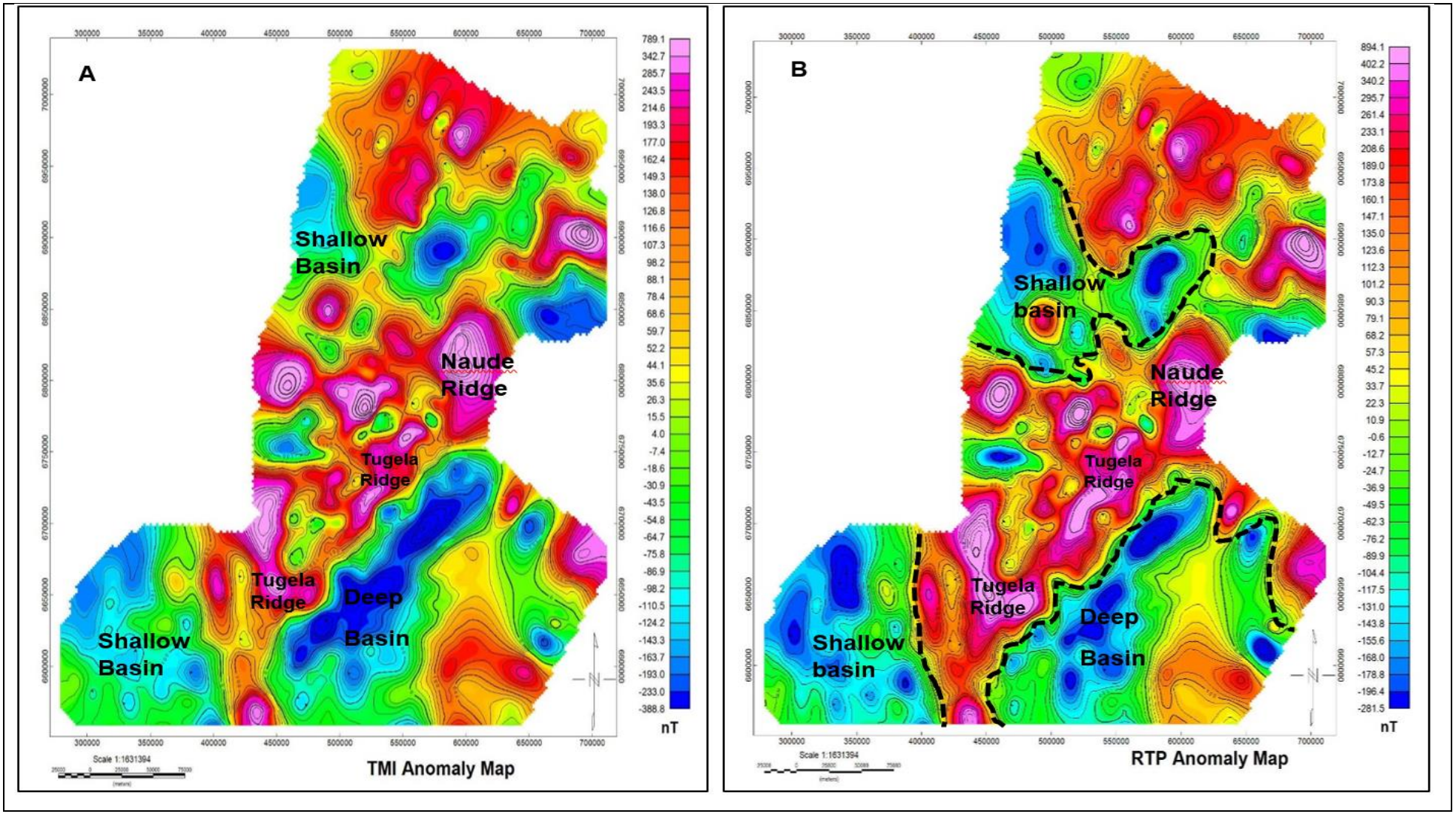

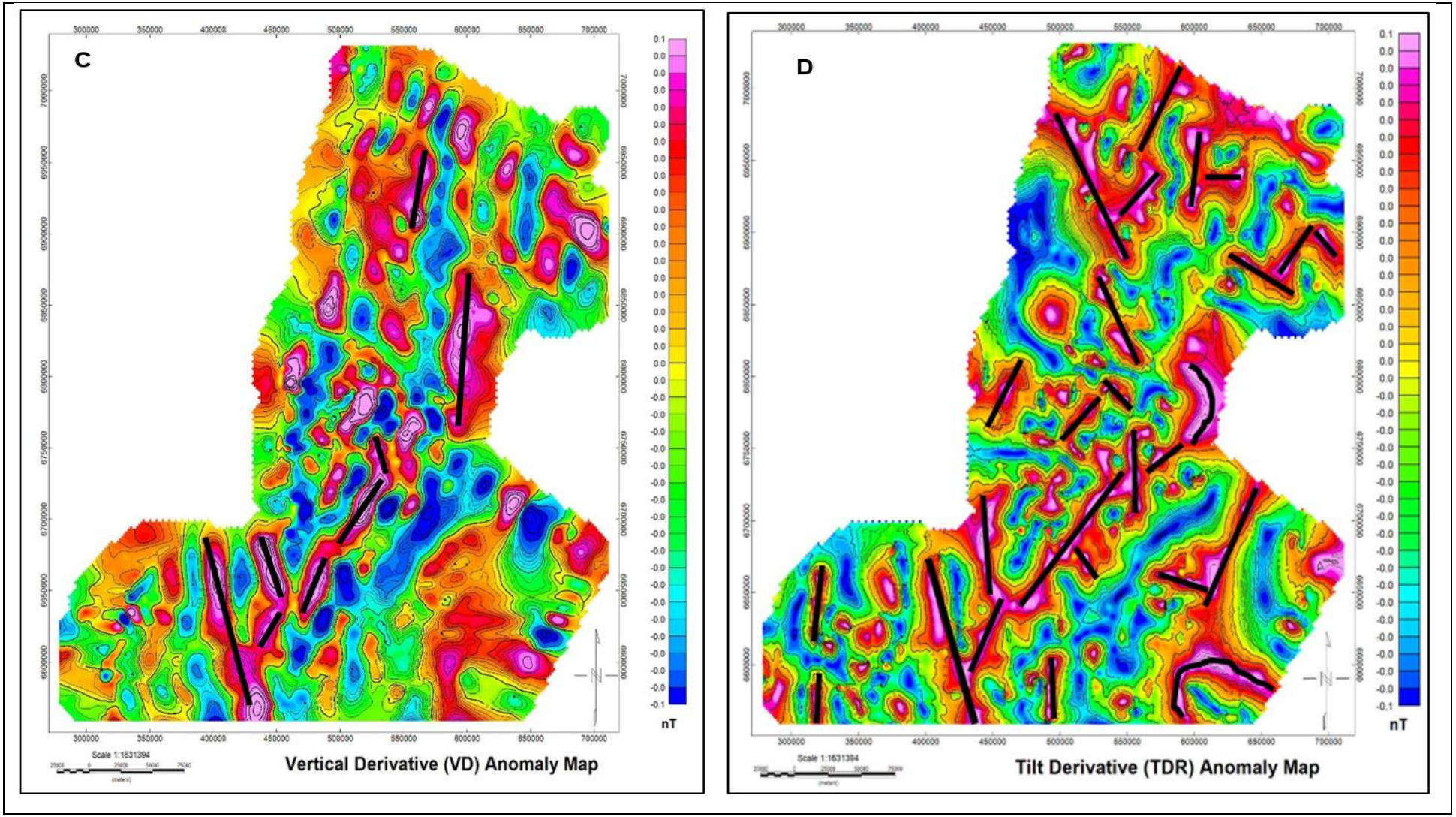

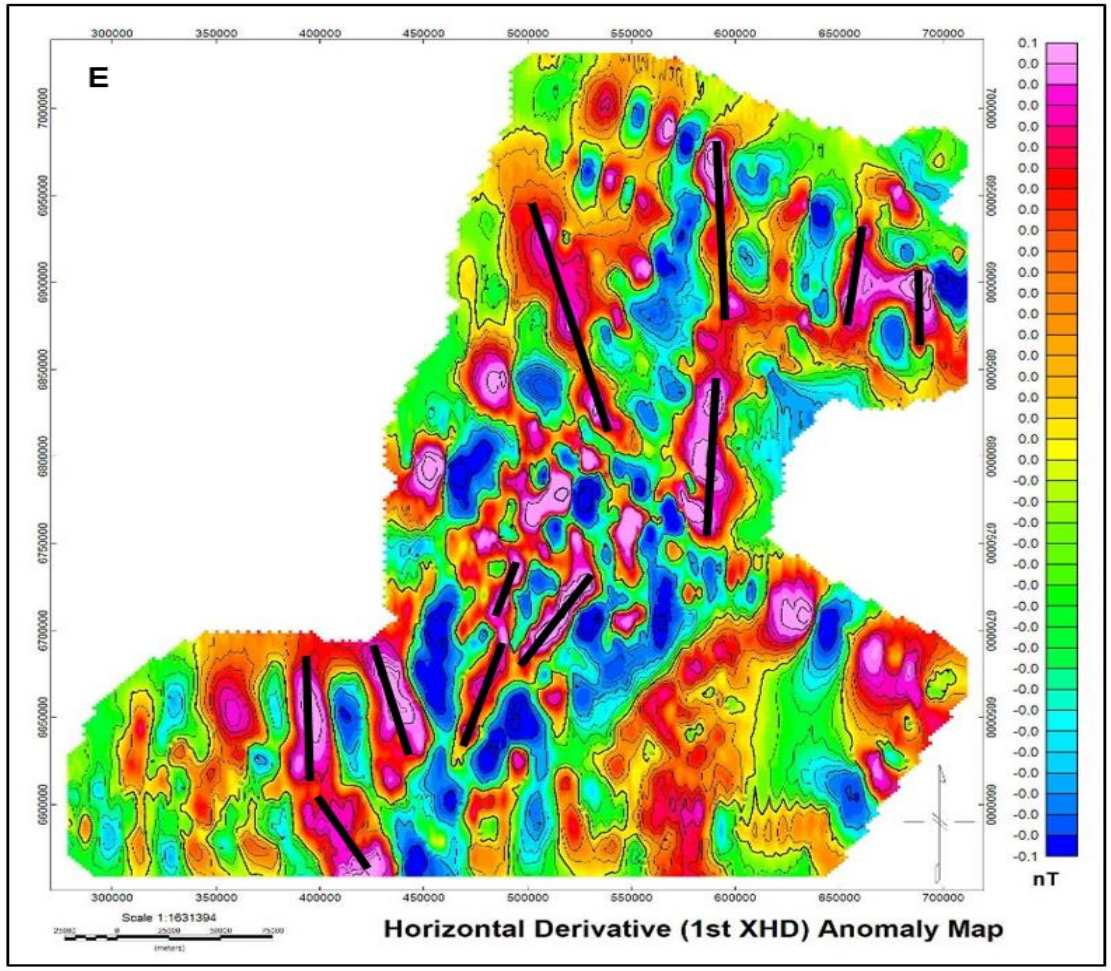

Figure 4.2 Interpreted (A) Total magnetic intensity (TMI) anomaly map of the Durban Basin with 100 nT contour interval. (B) contoured RTP magnetic anomaly map. (C) Contoured 1st order VD anomaly map of RTP. (D) Contoured TDR anomaly map of RTP. (E) Contoured 1st order HD anomaly map of RTP.

4.1.3 Depth estimation by power spectrum

Radially averaged power spectrum of gravity and magnetic anomalies was used for depth estimation in this study (Figure 4.3). Power spectrum technique is a powerful method for depth estimation of subsurface geological features in gravity and magnetic surveys. This technique enables the interpreter to gain important information about the relationship between subsurface features depth from either magnetic or gravity anomalies using spectral analysis of gridded data. This method can also assist in determining the number of layers or horizons and estimating top of basement depth.

The power spectrum was obtained from Fast Fourier Transform (FFT) analysis on gridded data represented by a graph of log power versus wavelength number (1/km unit) and Depth (km) versus wavelength number (1/km unit) (Figures 4.3A and B). Sources at different depths are then defined as linear sections on the power spectrum. The gradients of each linear section of the power spectrum graph is twice the depth to the subsurface source. The long wavelengths are associated with deep or regional sources while the short wavelength is associated with shallow features.

Four slopes are identified on both Bouguer and RTP power spectrum curve assuming that sources are statistically independent (Figures 4.3A and B). The first slope is in low frequency range of 0.01-0.02 (1/km unit), represents deep sources; the second slope is in average frequencies of 0.05-0.07 (1/km unit), represents intermediate-shallow sources; the third slope in high frequencies of 0.12-0.19 (1/km unit), represents shallow sources and the last slope in the very high frequencies, represents white noise.

Using both Bouguer and RTP derived radial average power spectrum three horizons at different depths within the crust were identified (Figure 4.3A and B). The three horizons can be classified as from top of basement as shallow, intermediate and deep-seated layers at various depth. The tail of the power spectrum curve at very high frequencies is the recorded white noise.

The following are the top to basement depths identified from radially averaged power spectrum of Bouguer (Figure 4.3A):

- The deepest basement to at about 30 km;
- The intermediate-shallow basement depth at about 12 km; and
- The shallow top of basement at about 3 km.

The RTP radially averaged power spectrum also identified three top to basement depths (Figure 4.3B), namely;

- The deepest top of basement at about 18 km.
- Intermediate basement at about 10 km; and
- The shallow basement at about 5 km.

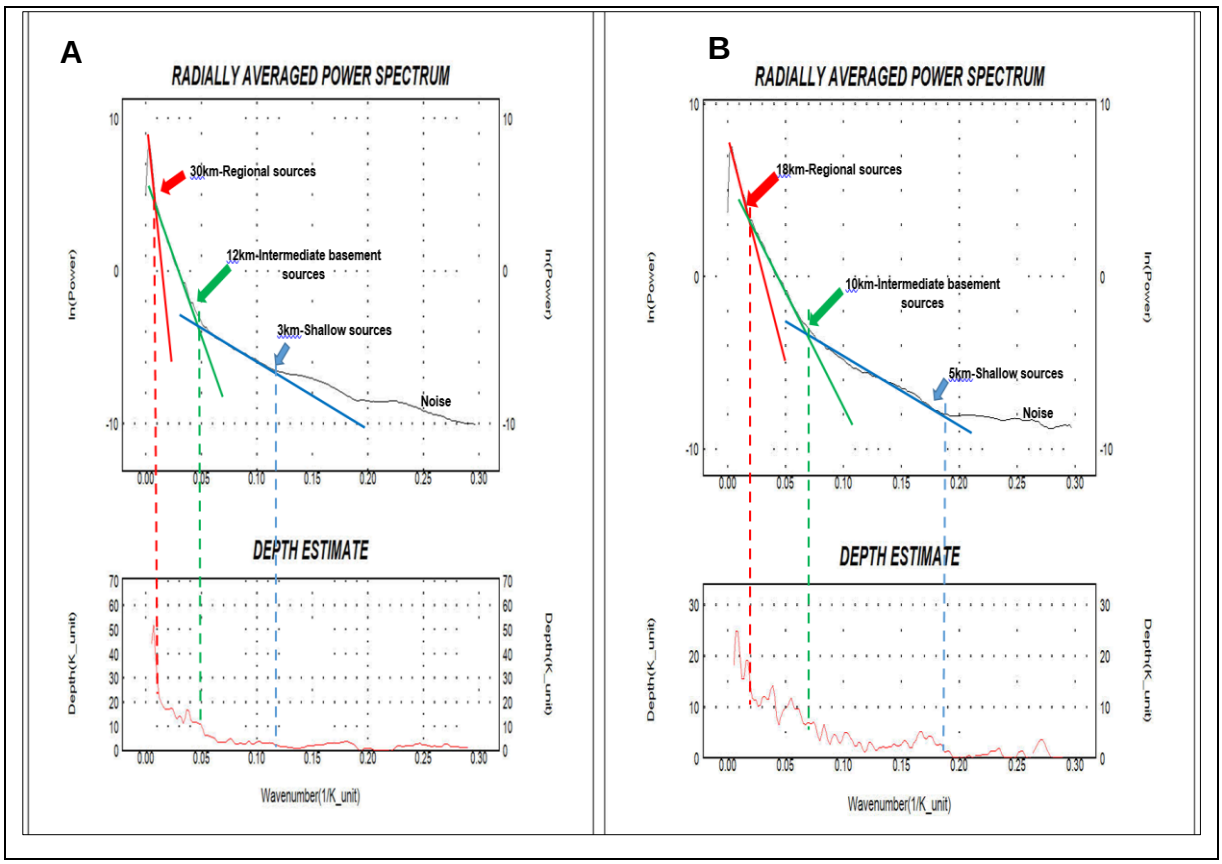

Figure 4.3 (A) Interpreted radially averaged power spectrum of Bouguer map. (B) Interpreted radially averaged power spectrum of RTP map. Red slope represents deep basin, green represents intermediate to shallow basin, blue slope represents shallow basin and last tail slope represents noise.

4.1.4 Basin extent map

Figure 4.4 shows the basin extent map of the study area. The basin extent in the study area was digitized in ArcGIS 10.6 by integrating the RTP and Bouguer HD anomaly map in ArcGIS 10.6. The dominant structural features of the Durban Basin are the AFFZ, Tugela Cone, basement high Tugela Ridge, Tugela Canyon and basement high Naude Ridge (Goodlad, 1986, Dingle et al., 1983, Wiles et al., 2013, 2003, McMillian, 2003, and PASA, 2016). Based on integration of RTP (Figure 4.2B) and Bouguer HD (Figure 4.1C) anomaly map the Durban Basin extent was delineated and classified into shallow and deep basins based on distribution of low versus high magnetic and gravity anomalies in the study area (Figure 4.4).

The shallow basin occupied the SW and central-northern part of the study area while the deep basin occupied the SE part of the study area. On the RTP anomaly map (Figure 4.2B), the shallow basin was represented two low magnetic anomalies occupying the SW and northern part of the study area while on Bouguer HD map (Figure 4.2C), the shallow basin was delineated by linearly gravity low feature cutting through the study area with enhanced contact from low (blue) to high (pink) gravity values. The enhanced contact on Bouguer HD map was used to delineate the shallow basin occupying the central-northern part of the study area. The SW and central part of the shallow basin represents the thick sedimentary package of the Tugela Cone while the northern part represents the thin sedimentary cover of the Durban Basin.

According to Broad et al., (2006), Bhattacharya and Duval, (2016) and PASA (2016), the Durban Basin is thin on the north-north part towards the Zululand Basin and thickest on the Tugela Cone within >4000 m which occupies most SW part of the basin. The Durban Basin deepens seaward from the continental shelf into the oceanic crust, the boundary between the continental and oceanic crust was marked by the basement highs of Tugela Ridge and Naude Ridge (Goodlad, 1986; Broad et al., 2006). The low anomaly that represents deep basin occupies the SE part of the study area (Figure 4.4). The shallow and deep basin are separated by visible magnetic high anomalies that correlates to basement high Tugela Ridge and Naude Ridge (Figure 4.4 and 4.2B).

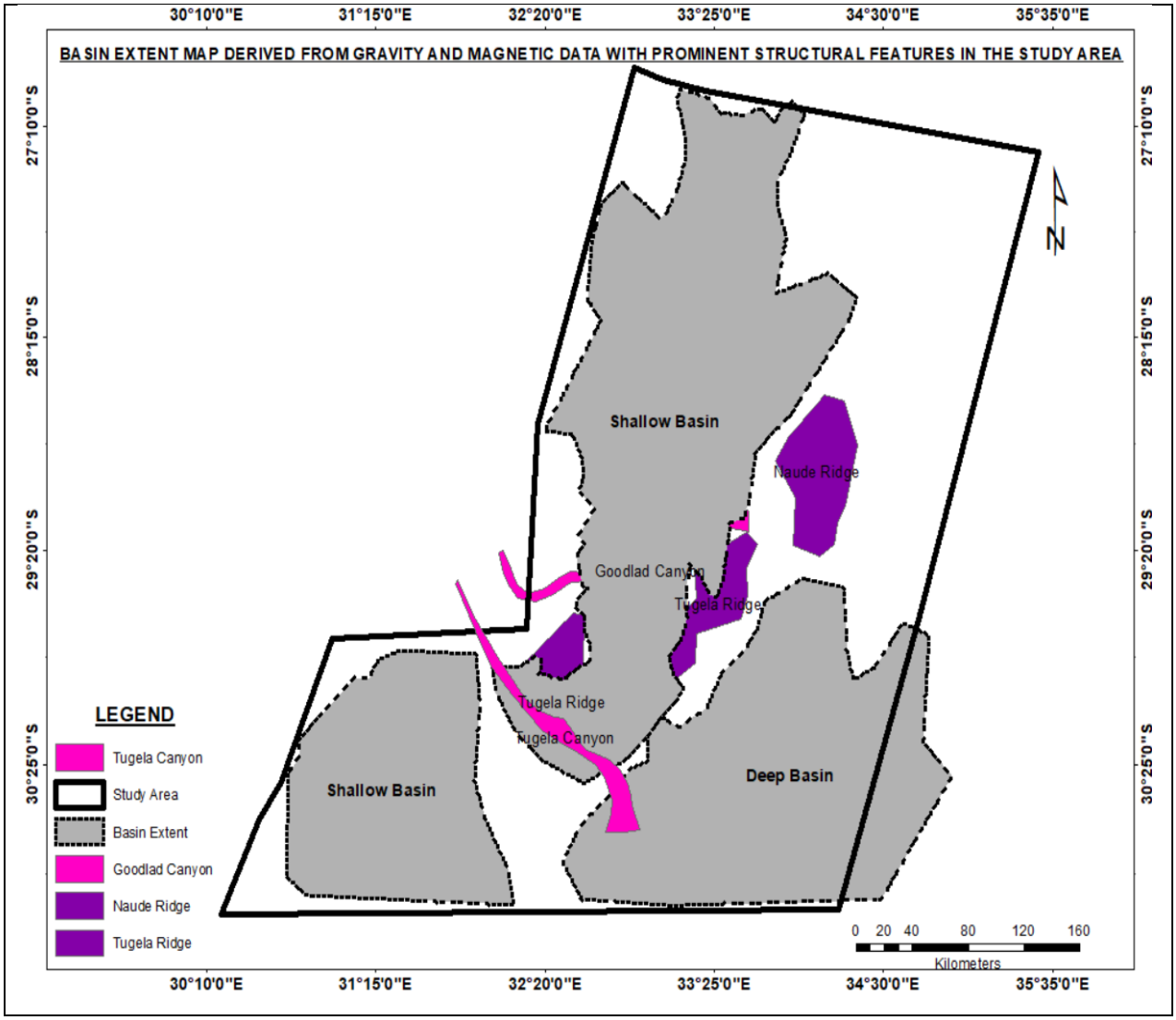

Figure 4.4 Basin extent map derived from gravity and magnetic data, showing the shallowest and deepest parts of the basin separated by basement high Naude Ridge and Tugela Ridge.

4.1.5 Structural map

Broad et al., (2006) defined the Durban Basin as a rift Mesozoic basin which is structurally complex. The Durban Basin is characterised by multiple fault systems related to initial drift, Godwana break-up, and initial activation of the AFFZ. General directional trends of fault structures within the basin are NE-SW, E-W and NW-SE (Dingle et al., 1983, Goodlad, 1986, McMillian, 2003, Broad et al, 2006, and PASA, 2016). Figure 4.5 displays the structural map of the study area derived from integration of gravity and magnetic data i.e. mainly the 1st VD, 1st HD and TDR. For this study, structural interpretation was achieved by integrating the first order vertical derivative of gravity and magnetic data (Figures 4.1B and Figure 4.2C), first order horizontal

derivative data (Figures 4.1C and Figure 4.2E) and tilt derivative data (Figures 4.1D and Figure 4.2D). These derivative maps were integrated in ArcMap 10.6 to digitized the visible structures based on the maxima principle derivatives that, derivatives tend to enhance structures by placing the maximum or zero value (pink) above the subsurface structures (Figure 4.1B, C D and Figure 4.2C, D and E). Consequently, the structures were placed or digitized above the gravity and magnetic highs (pink) represented by solid black lines. Structural interpretation using the integration of VD, HD and TDR of gravity and magnetic is based on three reasons: 1) VD tends to edge or contacts mapping by placing anomaly maxima at the point of the maximum or highest amplitudes of gravity and magnetic anomalies; 2) HD tends to have maximum values over the edges or contact of sources consequently, that can be used to determine locations of major basement structures or sedimentary structures; and 3) TDR produces a zero value over or very close to the source edges or contact, therefore can be used to map faults and or contact of geological sources.

The results from gravity and magnetic derivatives revealed a highly fractured study area, intersected or dissected by fault structures. The fault structures dissecting the study area are characterized by elongate and closed contours of high gravity amplitude (pink) and positive magnetic anomalies (pink). The mapped fault structures dissecting the study area are characterized by four directional trends; S-N, W-E, SW-NE, and NW-SE directional trend (Figure 4.5). According to Broad et al., (2006) the structures with W-E directional trend are as a result of pre-rift tectonic events and the structures that occupy the southwest part of the study area are related to AFFZ movements which resulted into faults (Bhattacharya and Duval, 2016).

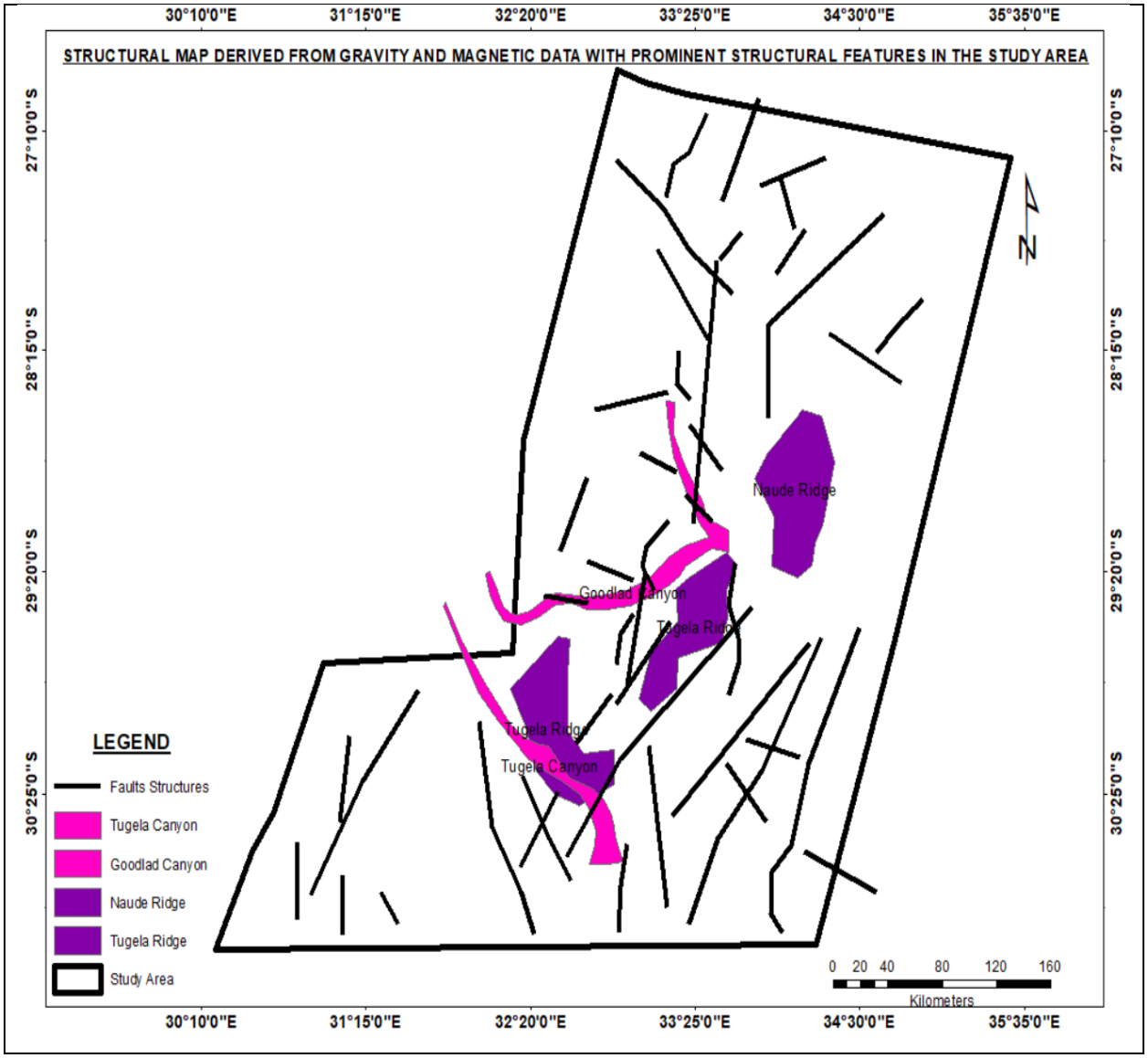

Figure 4.5 Structural map of the Durban Basin obtained from interpretation of gravity and magnetic maps. The faults structures are in four different trends (directions): (1) SW-NE directional trend, (2) SE-NW directional trend, (3) W-E directional trend and (4) S-W directional trend.

4.2 Seismic data

In this study a total of twenty-nine (29) seismic 2D data were processed and out this total, there were 10 strike lines and 19 dip lines (Figure 3.2). One dry well drilled on the continental shelf and far outside the study area was used for seismic well tie process i.e. Jc-C1 (TD 3169m). This well did not penetrate the basement, the Jc-C1 well tops were used to pick horizons or formations in the study area. For this study, five horizons were picked, namely, from older to younger Basement, 1AT1, 17AT1, Oligocene/Miocene and seafloor.

4.2.1 Depth conversion by velocity model

Figure 4.6A, B, and C displays merged stacking velocities point set, stacking velocities cube and final velocity model. Time-depth conversions is an important step in seismic data interpretation for exploration study. Generally, time-depth conversion i.e. velocity modelling is achieved using well data (checkshots, well tops, sonic and density logs) using the using V0-K method but it is difficult to build a velocity model in an area with no well drilled (Eichkitz and Amtmann, (2010). The study area does not have a well drilled consequently; velocity model for this study is achieved using stacking velocities. The workflow in Figure 3.3 was used to create a velocity model in the study area, by converting stacked velocities into distance interval and average velocities using the Dix equation. Seismic stacking velocities are also known as normal moveout (NMO) defined as a value of seismic velocity resulting from best fit of the traveltime curve. Stacking velocity are used for processing of seismic data by correcting the arrival times of events in the trace to improve the signal-to-noise ratio of seismic data (Schlumberger, 2020).

The FX operations for seismic stacking velocity conversion (convert points to cube) in Petrel 2015 were used to convert and generate line layout for 2D seismic stacking velocities. The generated lines layout are converted to points using FX operations to generate set of points. The generated set of points for 29 SEGY stacking velocity lines were converted into Petrel points with attributes using; Time: Min -12002.00, Max 2.00, Delta 12004.00 and a sampling interval of 4 to obtain an average velocity. All the converted points were appended together to create a single set points (Figure 4.6A). The appended points set were used to create a 3D cube using FX operations-velocity conversion (convert points to cube) (Figure 4.6B). The 3D seismic velocity cube is used to create a velocity model using a simple model technique in Petrel 2015 seismic interpretation tools (Figure 4.6C). This velocity model was used to conduct time-depth conversion relationship to estimate sedimentary cover thickness. The depth maps of the horizon: basement, 17AT1, 1AT1, Oligocene/Miocene and seafloor presented below in section 4.4 (Figure 4.17, 4.18, 4.19, 4.20 and 4.21).

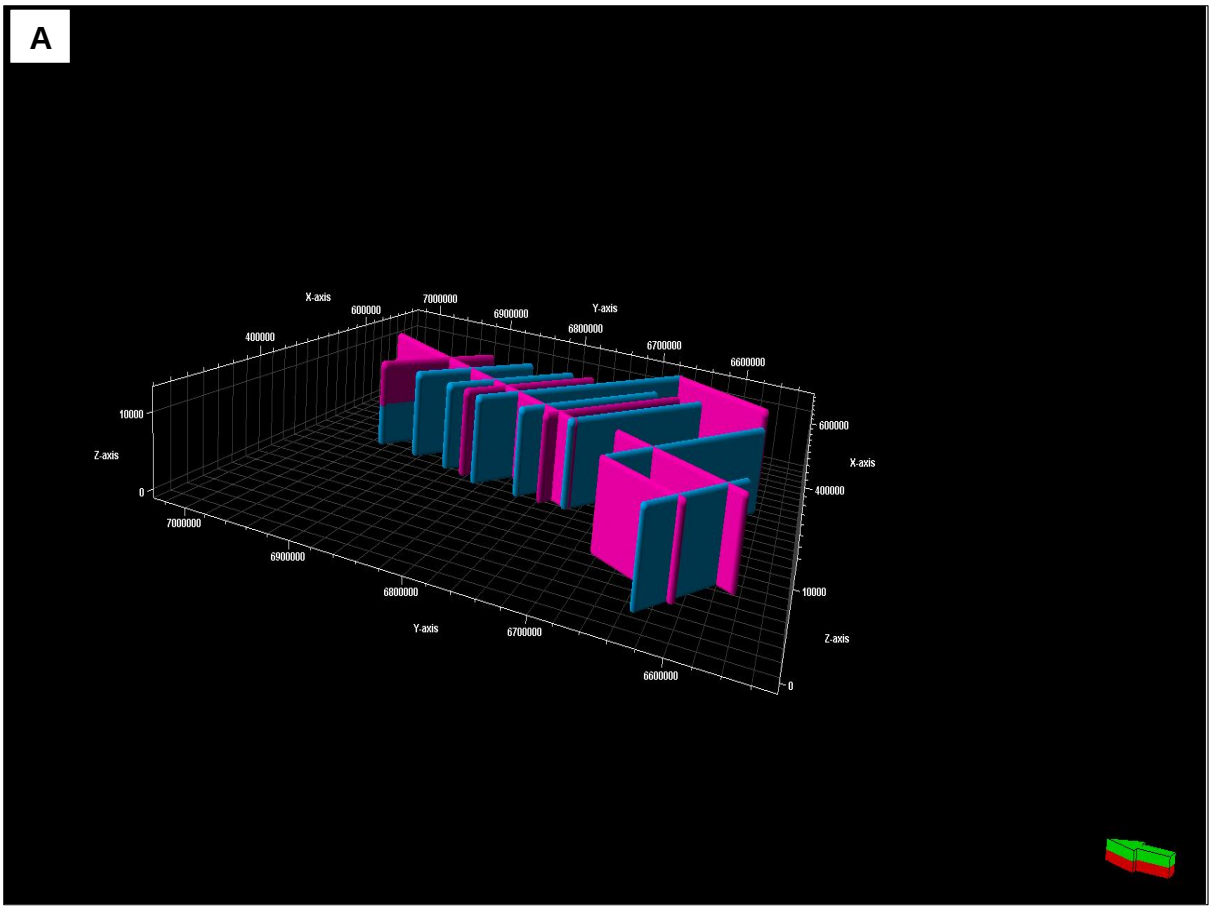

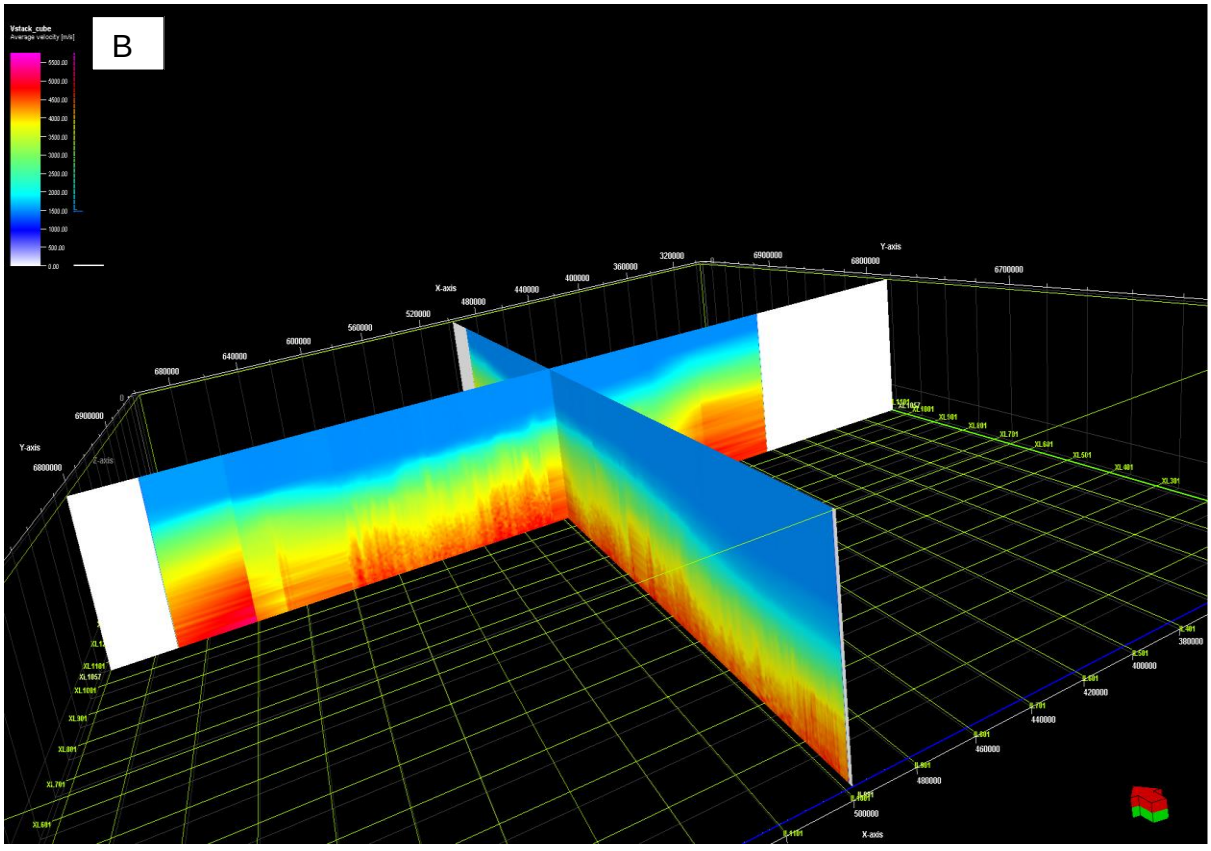

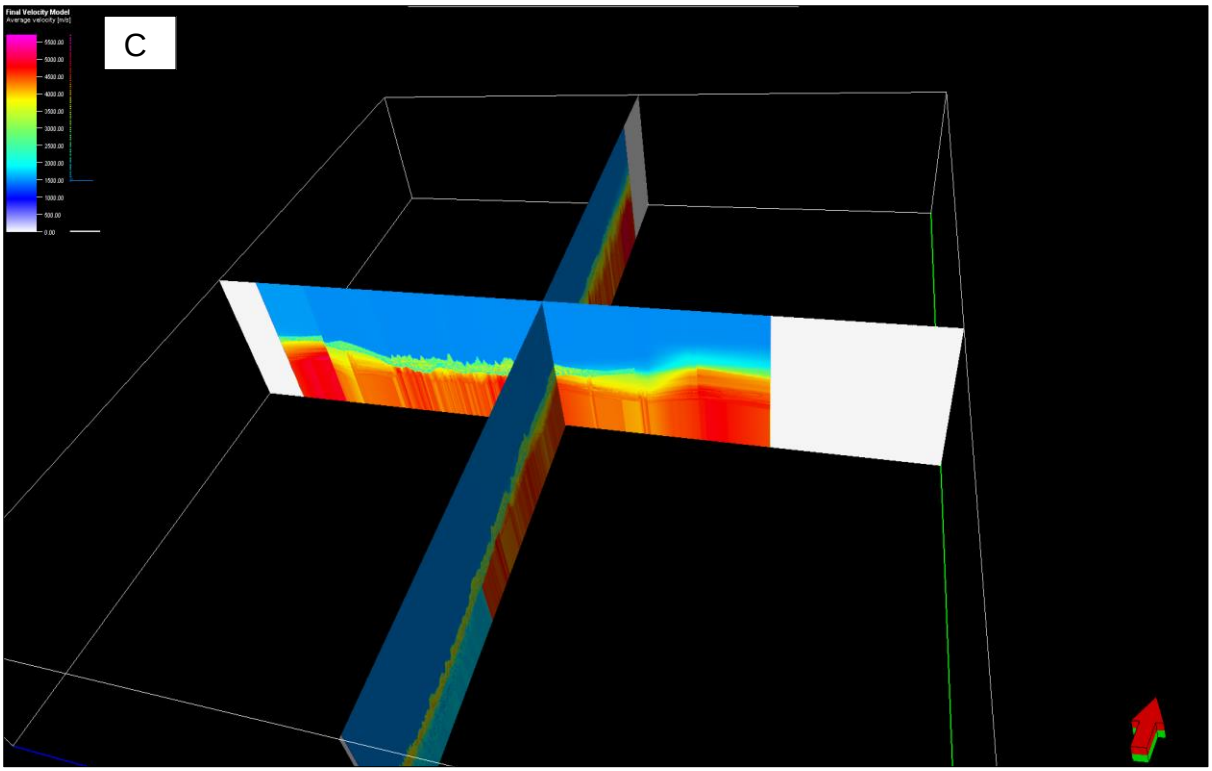

Figure 4.6 (A) 3D Seismic stacking velocities points derived from 14 stacking velocities line of the study area. (B) 3D seismic velocity cube derived from seismic stacking velocities points set conversion with average velocities ranging from 1500-5500 m/s. (C) velocity model created from the average velocity cube with average velocities ranging from 1500-5500 m/s. the velocities are displayed by color histogram in purple, green, blue and red.

4.2.2 Seismic well tie

Seismic-well tie is an important procedure for seismic data interpretation process and is defined as forward modelling of a synthetic seismogram from sonic and density logs (White and Simm, 2003). This involved sonic calibration, synthetic seismogram and seismic well tie.

Figure 4.7 shows the calibrated sonic log in red color, which indicate sand and shale ratios. The straight-line segments “red dotted line” between knee points were used in the calibration, knee points in “blue dots” were chosen at major jumps in the sonic log to avoid introducing artificial or abnormal reflection coefficients. Calibration points often show sudden bend at unconformities, and changes in character of the logs. Knee points allow direct control of calibration (White et al., 1998) and was interpreted as “red curve” (Figure 4.7). For this study, six checkshots for Jc-C1 well at various depths (meters) of the well with various times were used (Figure 4.7). According to Robein (2003) and Simm and Bacon (2004) checkshots measure times that are nearer to

seismic data at surface at an accurate seismic scale thus calibrating sonic log using checkshots enables conversion of depth to vertical time. Sonic log calibration using checkshots resulted into sonic drift curve, which is calculated by subtracting the sonic times from checkshot time (Figure 4.7). Simm and Bacon (2014) defines the drift curve as a curve that shows the effect of velocity distribution between the seismic and log frequencies.

Track 1 of Figure 4.7 shows the knee points illustrated by “blue dots” connecting the drift curve at each checkshot. The drift curve is applied to the sonic log for calibration to create a calibrated sonic log, input and output interval velocity curves, checkshot interval velocities, average velocity and a picked TWT (two-way traveltime) curve (Figure 4.7). A drift curve was applied to the sonic log and then integrated to give time-depth relationship that fits the check point, as a result five formations were encountered, namely; Basement, 1AT1,17At1, Oligocene/Miocene and seafloor (represented in different colours in Figure 4.9 (details in section 4.3.1).

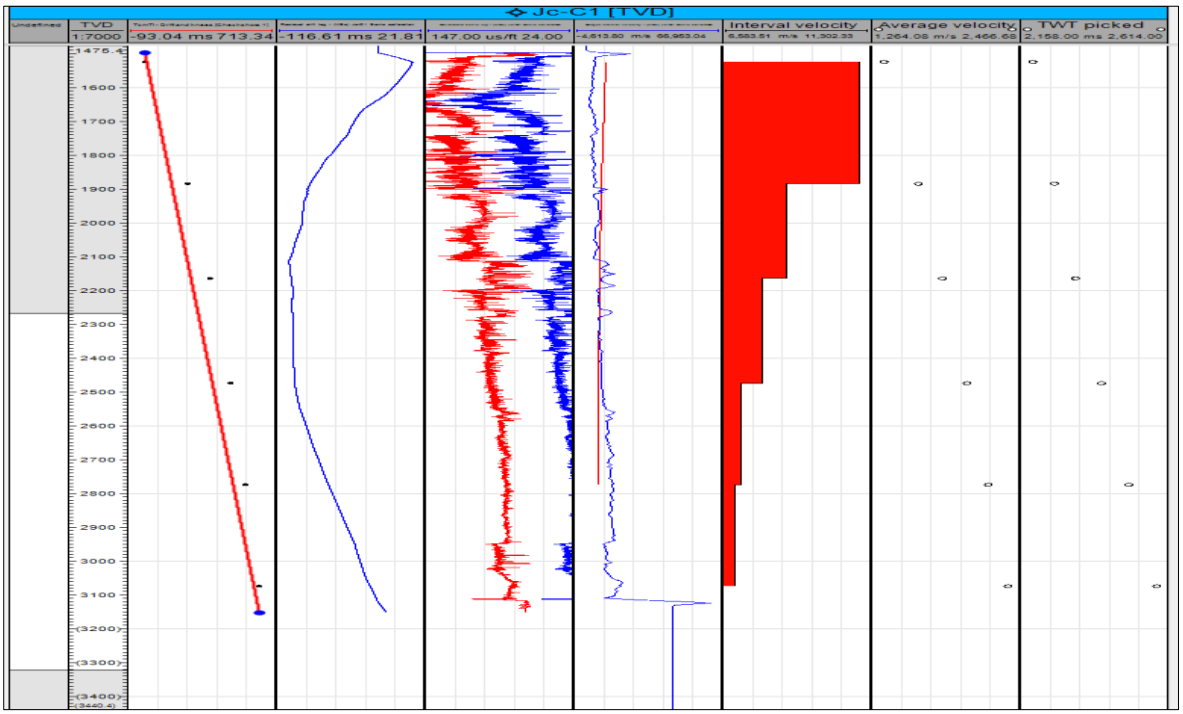

Figure 4.7 Sonic log calibration for Jc-C1 well with track 1, representing time of the checkshots minus time of the sonic log (knees represented by blue dots). Track 2 is drift curve, track 3 is the original sonic log (red) and calibrated sonic log (blue). Track 4 is the output interval velocity (blue) and the input interval velocity (red). Track 5 is interval velocity, track 6 is average velocity curve and track 7 is the TWT curve.

For this study, the seismic line that intersects Jc-C1 well is IMP1188P1001 from TB122D-01 survey acquired by CGG. Figure 4.8 represents a synthetic seismogram based on convolutional model wherein seismic wavelet is a function of acoustic impedance which is a product of the multiplication of the density log and the calibrated sonic log. Reflection coefficients are proportions of incident energy reflected from interface. The synthetic seismic wavelet was created using a 25 Hz Ricker wavelet, which similar to seismic signal frequency. Extended white wavelet was created to correct the phase mismatches between the final processed seismic data and synthetic seismogram. The sonic and density from Jc-C1 well were used as inputs for generation of synthetic seismograms.

4.3 Interpretation of structures on 2D seismic lines

Durban Basin is structurally complex thus consist of multiple faults systems and graben structures (Broad et al., 2006; Khattacharya and Duval 2016). Initial rifting and AFFZ movements resulted into graben structure and steep vertical faults (PASA, 2016). Structures and horizons are key features responsible for understanding the tectonic history and basin evolution of any prospects. Structures are also useful in recognising hydrocarbon processes. The structures and horizons interpretations were manually extracted using Petrel 2015 software.

4.3.1 Stratigraphic and fault interpretation

After sonic calibration and synthetic waveform generation, an integrated seismic well tie was accomplished and a good fit relationship between depth and time match was established (Figures 4.9 and 4.10). From the seismic section five horizons were determined: basement (pink); 1At1 (orange; Oligocene/Miocene (green); and seafloor (dark blue) (Figures 4.9 and 4.10). These selected horizons represent major events that occurred in the Durban Basin thus will assist understanding the structural development of the basin. Basement represent Archean age, 1At1 represent rift-synrift process, 17At1 represent drift process, and Miocene/Oligocene horizon represents the Tertiary sediments deposition (Figure 2.3). To interpolate the selected horizons in the study area, a composite image was created in Petrel 2015 using “select a composite

section" in the seismic interpretation tool palette (Figure 4.10). Below is the summary of the five mapped horizons from oldest to youngest i.e. Basement, 1AT1, 17AT1, Oligocene/Miocene, and seafloor) based on seismic interpretation and chronostratigraphy of the Durban Basin:

4.3.1.1 Basement

The basement flooring the Durban Basin is characterized by rugged and eroded appearance (Bhattacharya and Duval, 2016). According to Kitchin (1995) and Ben-Avraham et al. (1997) the geometry of the basement is highly affected by normal faults and right lateral strike slip faults. The basement (pink line) represents the oldest Archaean rocks of Durban basin i.e. Archaean period (Figure 2.3). The basement is composed of Archaean granites, gneiss and Schists (Broad et al, 2006) (Figure 2.3). The basement is marked on the seismic section with a last very bright red reflectance with the absence of internal reflectors that are commonly associated with sedimentary horizons (Figures 4.9 and 10). The basement is highly faulted or fractured, dominated by normal faults extending from the basement through the sedimentary package (Figures 4.16). The highly faulted or fractured basement could be due to rifting and drifting during the Gondwana break-up. Seismic interpretation revealed volcanic pipes on the flanks of the Naude Ridge (Figure 4.15). The observed two most visible basement highs in the area are correlated to the volcanic Naude Ridge and Tugela Ridge. The Tugela Ridge is deeply buried underneath younger sediments (Figure 4.11). These basement highs of Naude Ridge and Tugela Ridge are consistent with the magnetic highs in the study area (Figures 4.2A and B).

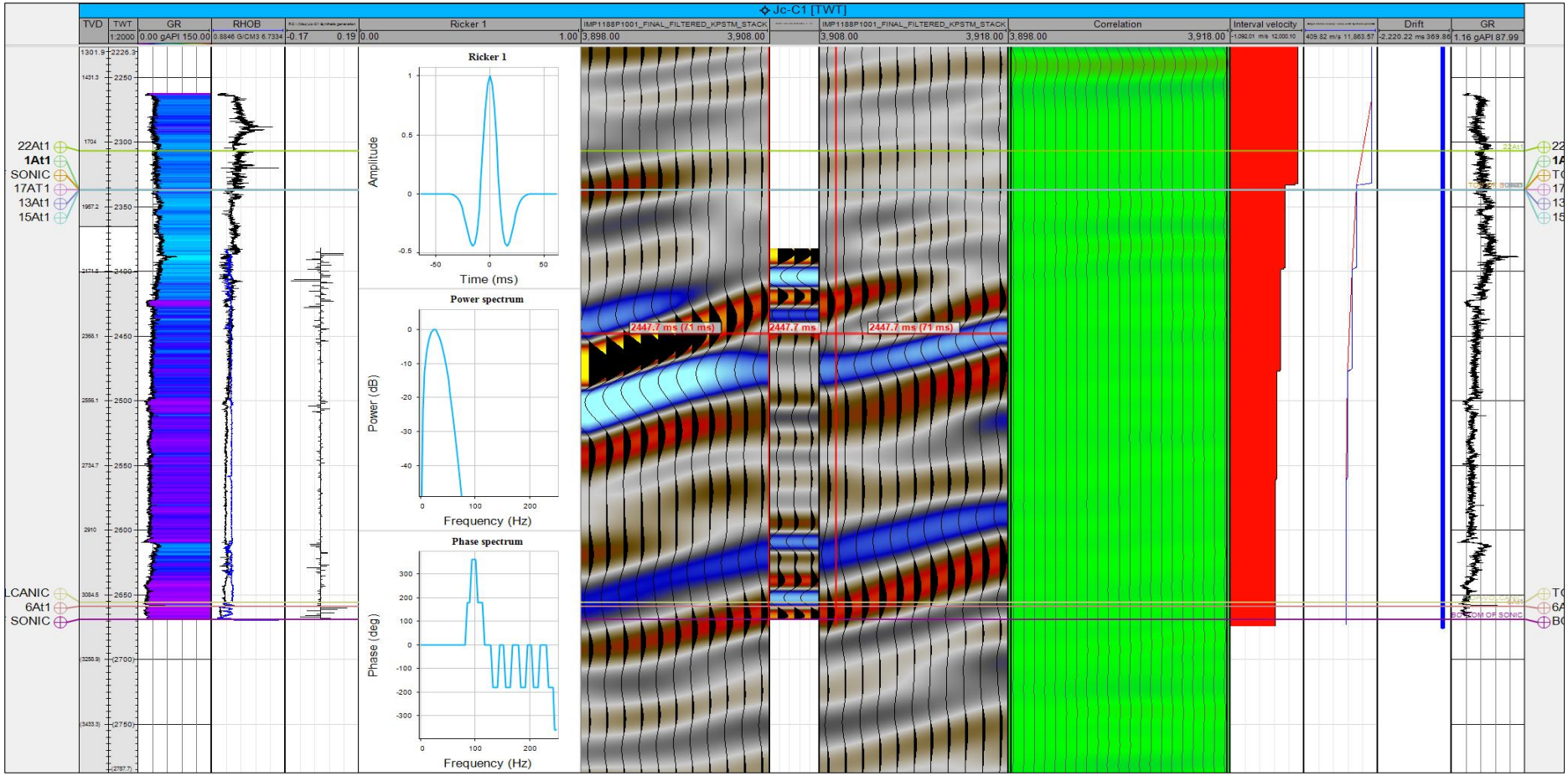

Figure 4.8 Synthetic seismic generation for Jc-C1 well. Track 1 is density log (blue) and calibrated sonic log (red). Track 2 is the reflection coefficient (RC), Track 3 is the acoustic impedance (AI). Track 4 is the zero-phase 25 Hz Ricker wavelet with its power spectrum and phase spectrum below it. Track 4-6 displays the synthetic seismogram in-between the seismic data (IMP1188P1001) near to the well.

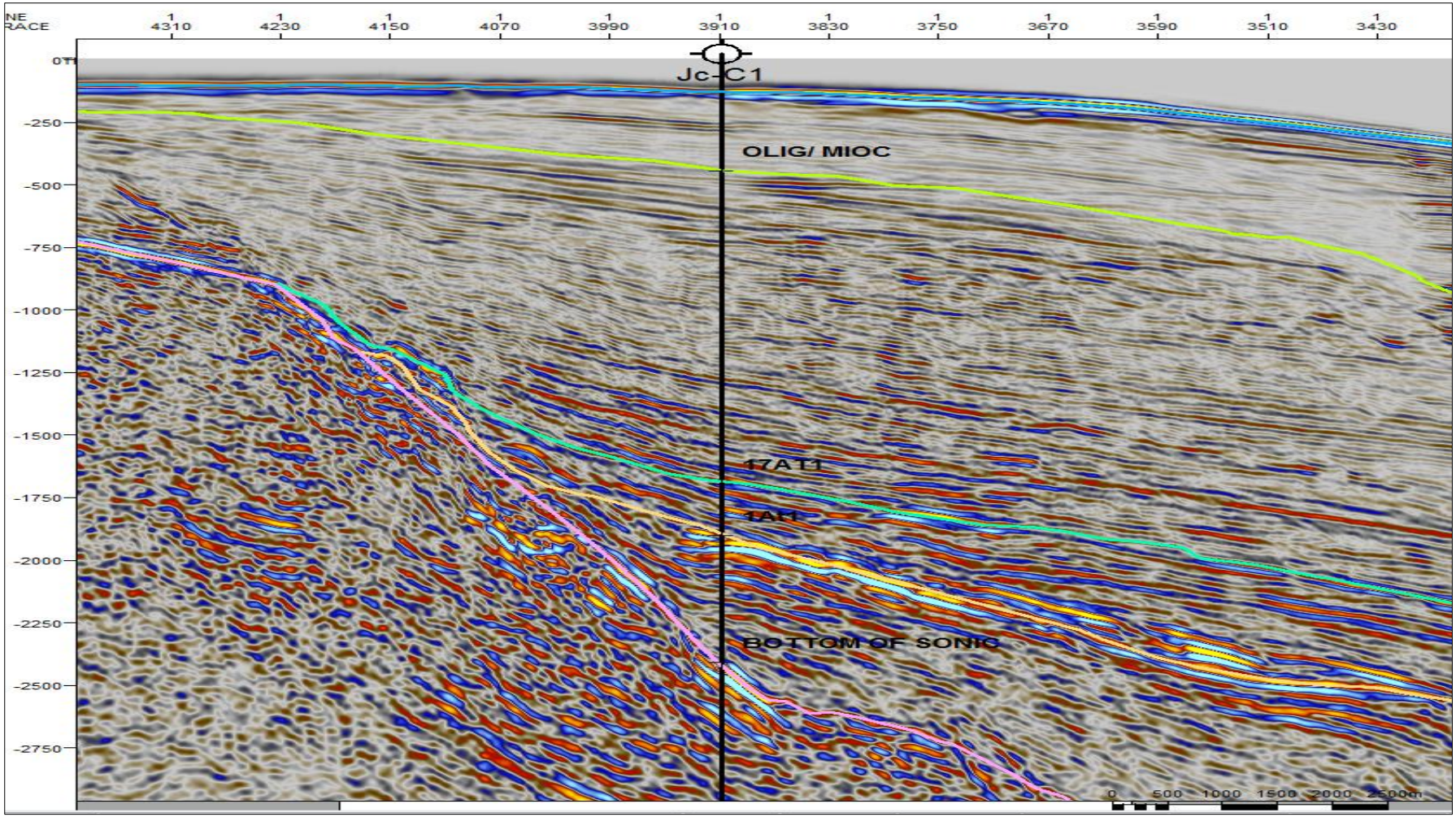

Figure 4.9 Jc-C1 well displayed on seismic cross section, line IMP1188P1001 with horizons matched after seismic well tie.

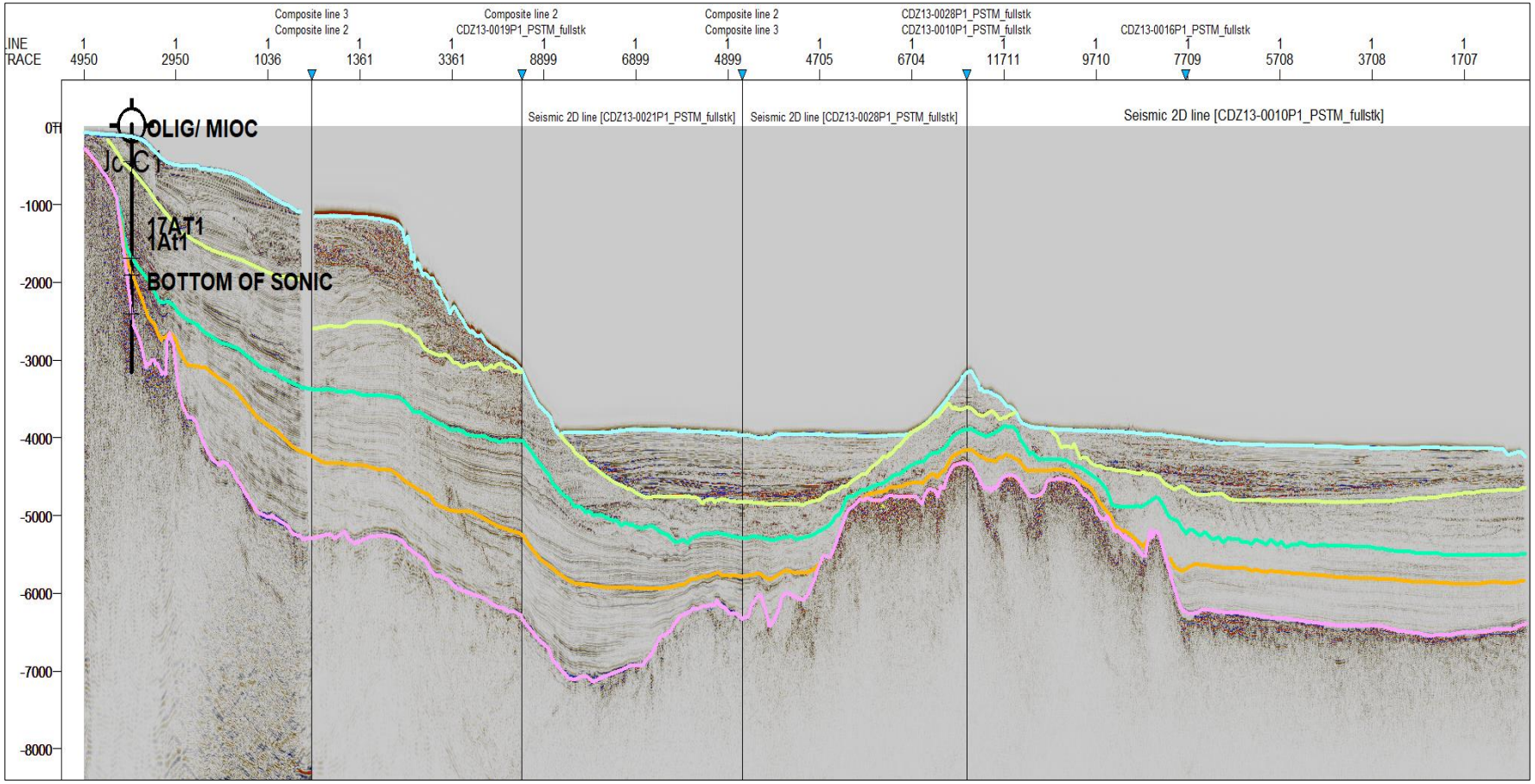

Figure 4.10 A composite line for interpolation of Line IMP1188P1001, CDZ13-0019, CDZ13-0021, CDZ13-0028 and CDZ13-0010. The z-axis is vertical travel time in milliseconds; each black line corresponds to a well top pick formation/surface. Five horizons picked on seismic data representing major geological events in the study area i.e. Basement (pink), 1AT1 (orange), 17AT1 (green), Oligocene/Miocene (yellow) and seafloor (blue).

4.3.1.2 1At1 Horizon

The Durban Basin is consisted of thick sedimentary package of more than 4000 m thickness (Broad et al., 2006). The 1At1 horizon (Orange colour) is dominated by grabens structures bounded by normal faults that resulted due to tension and rifting process during the separation or breakup of Gondwana (Figures 4.16). The 1At1 horizon overlay the basement representing the rifting and synrift event in the basin during the lower Cretaceous period (Figure 2.3). This horizon consists of synrift sediments represented by red bright and low reflectors corresponding to sands and clays respectively, these sediments are variable in thickness ranging from thin to thick (Figure 16). Normal faults within this horizon resulted into horst graben structures. The graben structures are filled with thick synrift sediments of Lower Cretaceous age (2.3). According to Singh and McLachlan (2003), these sediments filled graben structures overlying the basement could be targets for petroleum exploration and exploitation especially if formed during Cretaceous to Upper Cretaceous period and (Singh and McLachlan, 2003) (Figure 2.3). This horizon is consisting of turbidites sands and shales with the main source of sediments as the Tugela River that could were derived from the Karoo Supergroup sediments such as the tillites, shales and sandstones (Goodlad, 1986).

4.3.1.3 17At1 Horizon

The 17AT1 horizon sediments are deposited during the Upper Cretaceous period (Figure 2.3). The 17At1 horizon (light blue colour) overlays the 1At1 and represents the drift process during the formation of the Durban Basin (Figures 2.3, 4.9 4.10 and 4.14). Like the 1At1 horizon, 17At1 is dissected by normal faulting extending from the basement related to regional tectonic processes (rifting and drifting) and compaction during the late formation of Durban Basin. These normal faulting structures resulted into horst and grabens structures (Figures 4.16). The grabens are filled with thick Upper Cretaceous sediments which consists of mainly deltaic submarine fan sands and clays represented by low reflectors in bright colours. The main source of sediments is the Tugela River deriving the sediments from Karoo Supergroup sediments that includes the tillites, sandstones and shales (Goodlad, 1986). At some

instances intrusives derived from the Lebombo Mountains (Broad et al, 2006). These deltaic submarine sediments dominated by shales and sands could be potential sources for petroleum exploration because according Singh and McLachlan (2003) potential petroleum prospects are sediments formed during upper Cretaceous-Turonian period.

4.3.1.4 Miocene/Oligocene horizon

The Oligocene/Miocene horizon is a result of three upliftment tectonic events during the Oligocene, Miocene and Pliocene period (Cartwright, 2014). This upliftment processes in the development of the Durban Basin resulted into channel structures (Wiles, 2003; Broad et al, 2006; Cartwright, 2014). The Oligocene/Miocene horizon (green colour) overlay the 17AT1 and represents the Tertiary-Cenozoic sediments consisting of shelf sediments of fluvial and fan type (Broad et al., 2006) (Figure 2.5). These sediments, based on the chronostratigraphy of the Durban Basin were deposited in the Cenozoic period (Figure 2.3). This horizon is consisting of aeolian, fan and fluvial sediments mainly shales and sandstones (Goodlad, 1986). Seismic interpretation for this study revealed channel structures filled with thick sands within this horizon (Figures 4.12). According to Singh and McLachlan (2003), this channel sands could be targets for petroleum exploration in the study area. This channel structures that incised the Miocene/Oligocene are related to three upliftment events in the basin and they further represents prolonged margin fluvial incision and eustatic sea level variations (Wiles et al, 2013).

4.3.1.5 Seafloor topography

Generally, the seafloor topography is characterized by smooth and rugged topography. Smooth seafloor topography is represented by a bright blue continuous reflector while the rugged is characterized bright blue discontinuous reflector (Figures 4.9, 4.10,4.11,4.12, 4.13, 4.14 and 4.15). Prominent features that enhance the ruggedness of the seafloor topography are the Tugela Canyons, Tugela Ridge and Naude Ridge that are visible on seismic sections (Figures 4.14 and 4.15). The Tugela Canyon incised the seafloor from W-E direction with 13000 m and 3915 m width and

height respectively (Goodlad, 1986). The deeply buried Tugela Ridge with a dome-like shape underneath the Tugela Canyon (Figures 4.14).

4.3.1.6 Structural interpretation

Structurally, the rift Mesozoic Durban Basin is affected by multiple faults systems which includes normal faults, listric faults, right lateral strike-slip faults, folds, graben structures local volcanoes, sills and dykes intrusions related to pre-rift, initial rifting, AFFZ movements and upliftment (Broad et al., 2006; Wiles, 2003;Cartwright, 2014; Bhattacharya and Duval, 2016; PASA, 2016). Seismic data interpretation revealed that the study area is dissected by normal faults that affected the geometry of the basement and sedimentary package (1AT1, 17AT1 and Oligocene/Miocene horizon), creating horst and graben structures (Figures 4.13, 4.14, 4.15 and 4.16).

Most prominent geological features in the study area confirmed by seismic interpretation are Tugela Canyon, Tugela Ridge (Figure 4.11) and Naude Ridge (Figures 4.15), supporting the assertion of Broad et al., (2006) that the Tugela Cone, Tugela Canyon, Tugela Ridge and Naude Ridge are the most dominant geological features in the Durban Basin.

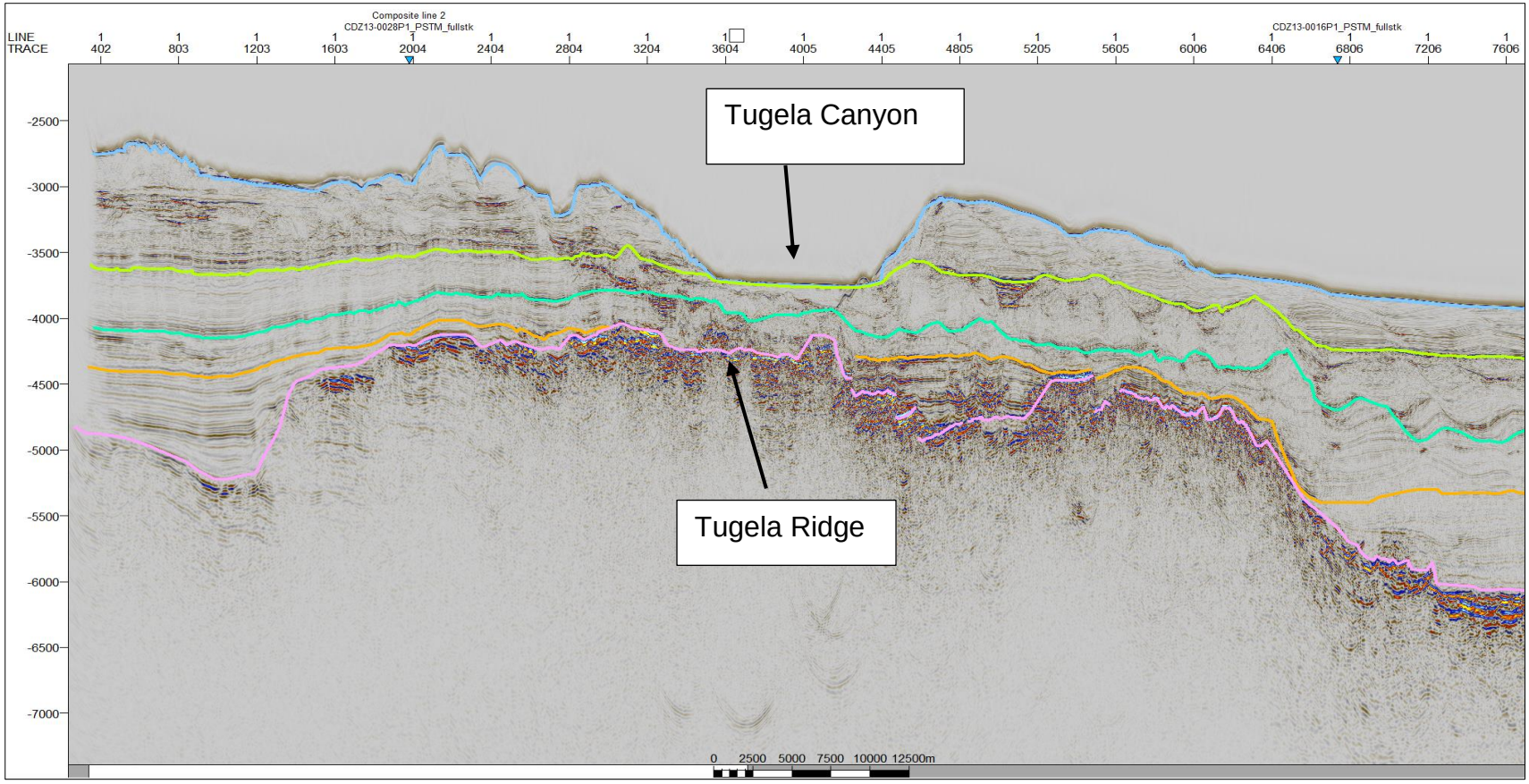

Figure 4.11 Rugged seafloor (blue) displaying the Tugela Canyon underlain by a basement high of Tugela Ridge.

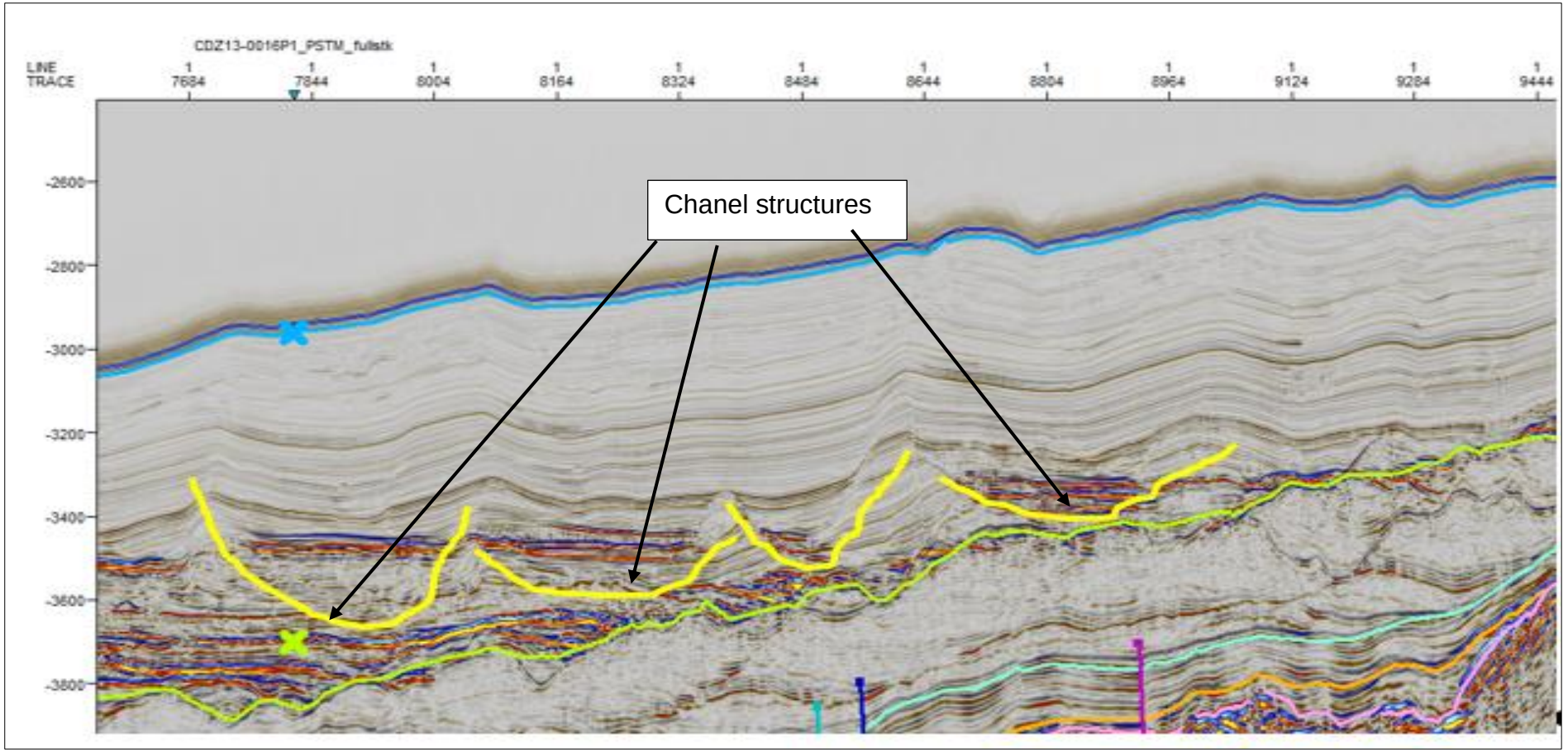

Figure 4.12 Chanel structures filled with thick sands (bright reflectors) marked by yellow arcs within the Miocene/Oligocene horizon.

Seismic interpretation further revealed gas chimneys extending from 1AT1 through to 17AT1, which may be a sign of an active petroleum system in the area (Figure 4.13 and 4.14). Studies in the Durban Basin revealed the presence of a mature petroleum system based on core logging, seismic data interpretation and satellite gas seepage (Singh et al., 2005, Singh and McLachlan, 2003; Broad et, al. 2006; and PASA, 2016). The core logging of Jc-D1 well intersected sandstone with hydrocarbon extracts at 1550m and bitumen stained shale related to dry gas anomaly intersected at 2720 m. Seismic interpretation by Singh et al., (2005) and Singh and McLachlan (2003) recorded gas escape features while satellite seepage slick studies identified second and third order gas seepage slicks which proves the expulsions of hydrocarbons in the Durban Basin.

Bhattacharya and Duval (2016) based on seismic data interpretation noted two volcanic events in the Durban Basin. Furthermore, local volcanoes, sills and dykes intrusions were mapped on seismic sections (Bhattacharya and Duval, 2016). There is evidence of late volcanism in the study area because seismic data interpretation revealed and mapped volcanic pipes on the flank of the Naude Ridge (Figure 4.15). These mapped volcanic pipes support the work by Broad et al., (2006) which recorded intrusive rocks during core logging of the Jc-series wells related to Tertiary volcanism in the Durban Basin.

In Figure 4.14, 4.15 and 4.16, it is observed that the study area is dissected by normal faulting. The faults are classified into Type I and Type II normal faulting. Type I normal fault structures extend from the basement through the sedimentary package (1AT1 and 17AT1 until the Oligocene/Miocene horizon) and these faults are related to regional development of the basin during the breakup and separation of the Gondwana (Kitchin, 1995; Ben-Avraham et al., 1997). Generally, the Type I normal faults resulted into horst and graben structures and have small throws and are vertically steep (Figure 4.16) thus agreeing with Cartwright (2014) and PASA (2016), that the Durban Basin is dissected by steep vertical faults due to tectonic events that occurred during the formation of the basin such as pre-rift, rifting, AFZZ movements.

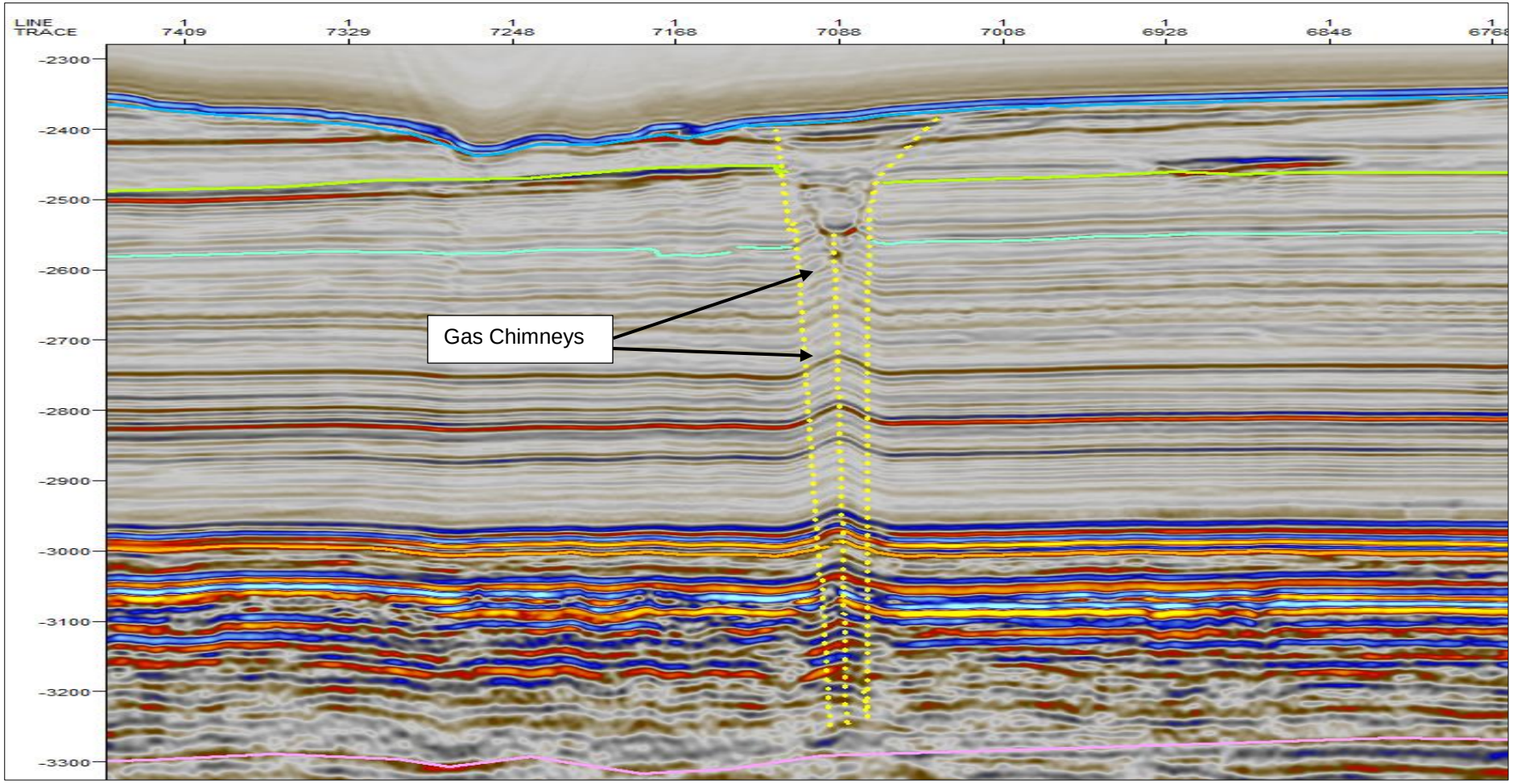

Figure 4.13 Shows mapped gas chimneys (yellow dotted lines) that could be signaling an active petroleum system in the study area from dip line cutting through the sedimentary package.

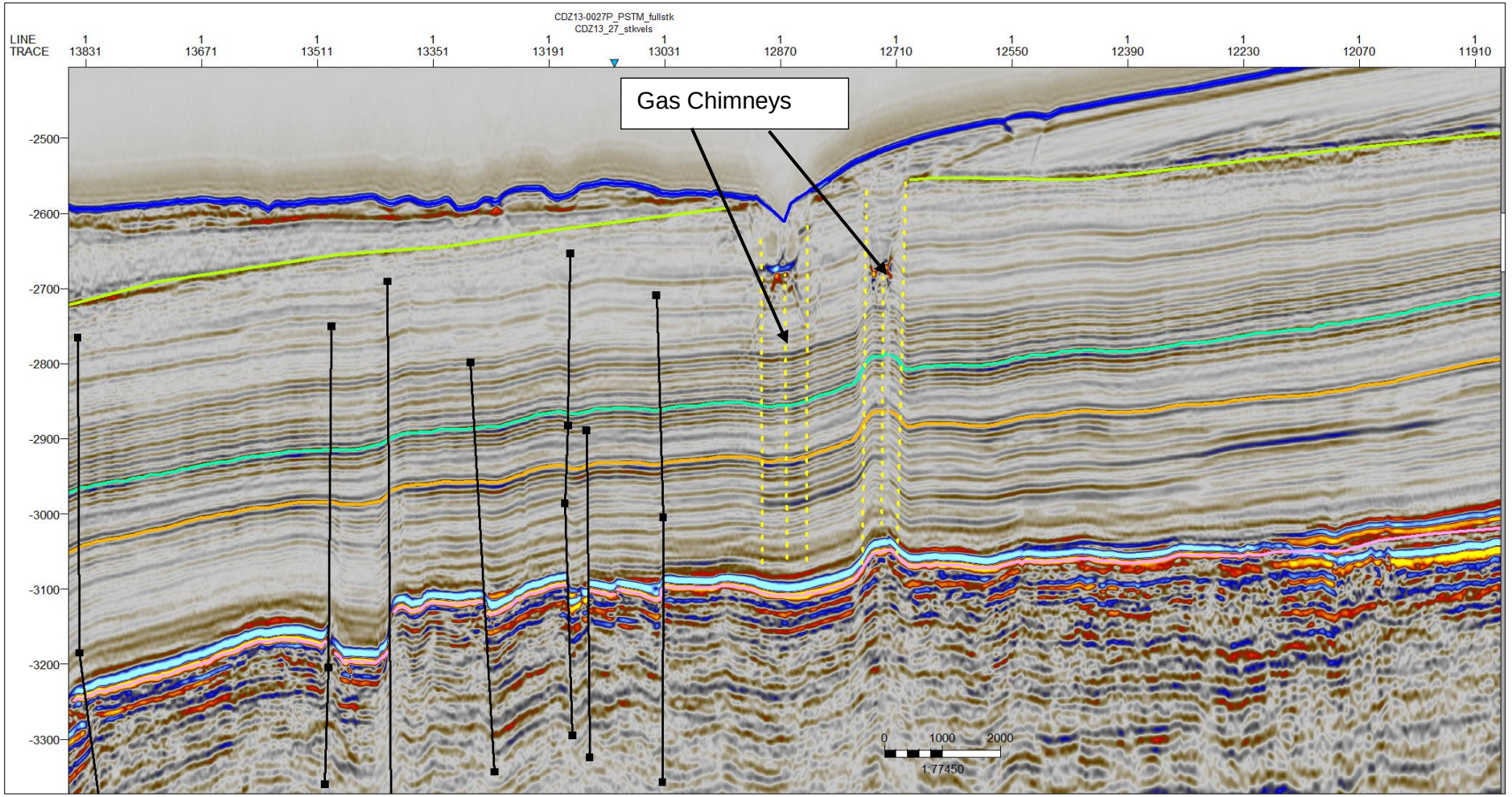

Figure 4.14 Shows mapped gas chimneys (yellow dotted lines) that could be signaling an active petroleum system in the study area from dip line cutting through the sedimentary package. Normal faults extending from the basement trhough sedimentary package.

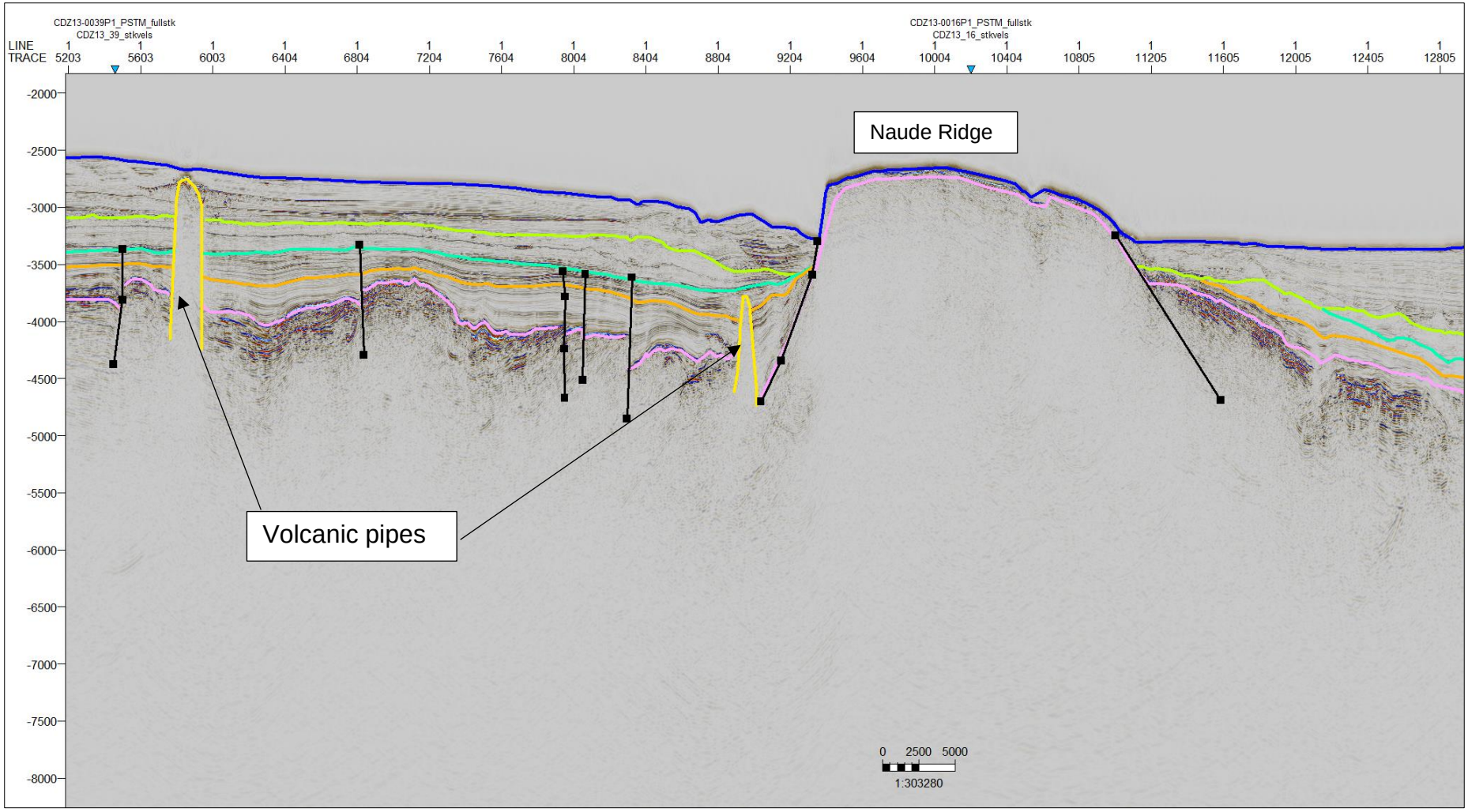

Figure 4.15 Strike line showing the prominent Naude Ridge with volcanic pipes (yellow solid polylines) and normal faults (black lines).

The Type II normal faults are within the sedimentary package and do not start from the basement and horst graben structures as Type I normal faults, these faults are due to compaction in the basin (Figure 4.16). Type II normal faults according to PASA (2016) and Cartwright (2014) developed during the Cretaceous period due to compaction, shallow overpressure development, abnormal gravitational load, fluvial expulsion, diagenesis and contraction. Furthermore, this normal fault type is generally characterized by low throws (Cartwright, 2014).

4.4 Depth conversions by velocity model

Depth conversion for this study was employed to convert time-domain surfaces (ms) to depth-domain surfaces (km) for basement, 1AT1, 17AT1, Oligocene/Miocene and seafloor. This conversion aided the depth and sedimentary cover thickness estimation. The deepest and thickest part of basement in the Durban Basin is the southmost part of the basin while the shallowest part is the north-north east part of the Durban Basin (Bhattacharya and Duval, 2016). All the depth maps i.e. Basement, 1AT1, 17AT1 and Oligocene/Miocene agree with the above assertion in that, the study area within the Durban Basin is deeper in the central to SW and SE parts represented by pink colour with contour depth values of ~2000-6000 m. the shallow parts are northern parts of the study area represented by blue-green-yellow and red colour with contour depth values of ~2000-600 m (Figure 4.17, 4.18, 4.19, 4.20 and 4.21).

Figure 4.17 shows depth map of the basement in the study area. The deepest part of the basemen is >4000 m, represented by the purple colour covering most of the study area. The intermediate depth ranges from 2000 m-2250 m, these values are represented by light blue to dark blue colour. The shallow depth of the basement covers the northern part of the study area with values ranging from 1500 m -1800 m, represented by green to yellow colour (Figure 4.17). The seafloor depth map shown by figure 4.18 indicates an increase in depth from 1000 m to >4000 m. Both the seafloor depth visibly shows the basement high Naude Ridge located in the central part of the map, represented by light blue colour with a 2200 m circular closed contour. The Tugela Canyon is visibly displayed by seafloor depth map located western part of the map with elongate contour lines of 2000 m to 1500 m values (Figure 4.18).

Figure 4.21 displays the 1AT1 depth map of the study area. It is dominated by synrift sediments consisting of turbidites sands and shales. deposited during the lower Cretaceous period. The depth in this horizon ranges from 3000 m to 6000 m forming the deep and thick part of the study area. The deep and thick part of the 1AT1 horizon is represented by the purple colour and it covers most of the study area. The light blue to orange colour covering the northern part of the study area represents the shallow and thin part (Figure 4.21).

The 17AT1 horizon depth map of the study area is depicted by Figure 4.20. The 17AT1 consists of syrift sediments deposited during the upper Cretaceous period mailnly the sands and shales. The depth variation of this horizon ranges from deep to shallow represented by purple and light blue to red colour of the histogram. The purple colour represents the deep part of the study area at >2500 m depth covering most of the study area. The light blue to red represents the shallow part ranging from 1600 m-600 m depth covering far western and northern part of the study area (Figure 4.20). The thickness estimation of the 17AT1 is >2000 m and <1400 m for thickest and thinnest areas respectively.

The Oligocene/Miocene horizon depth map of the study area is represented by Figure 4.19. The Oligocene/Miocene horizon geologically, consists of Aeolian, channel, fan and fluvial sediments mainly shales and sandstones. These sediments were deposited during Oligocene, Miocene and Cenozoic upliftment period (Wiles et al., 2013). The deepest and thickest part of the Oligocene/Miocene horizon is represented by the dark blue to purple colour of the histogram covering most of the study area i.e. central to SW and SE, ranging from 3000 m to 5000 m in depth. The thinnest and shallowest parts of this horizon is represented by light blue to orange colour that covers the northern part of the study area with values ranging from 2000 m to 600 m (Figure 4.19). The overall sedimentary cover thickness of the Durban Basin within the study area is ~2000-6000 m for most the study area i.e. central to SW and SE parts. The thinnest part of the study area is 2000-600 m occupying the northern part of the study area. These findings are consistent with work of Broad et al., (2006) that the Durban Basin has a sedimentary thickness of more than 4000 m based on core logging of Jc series wells and seismic data interpretation

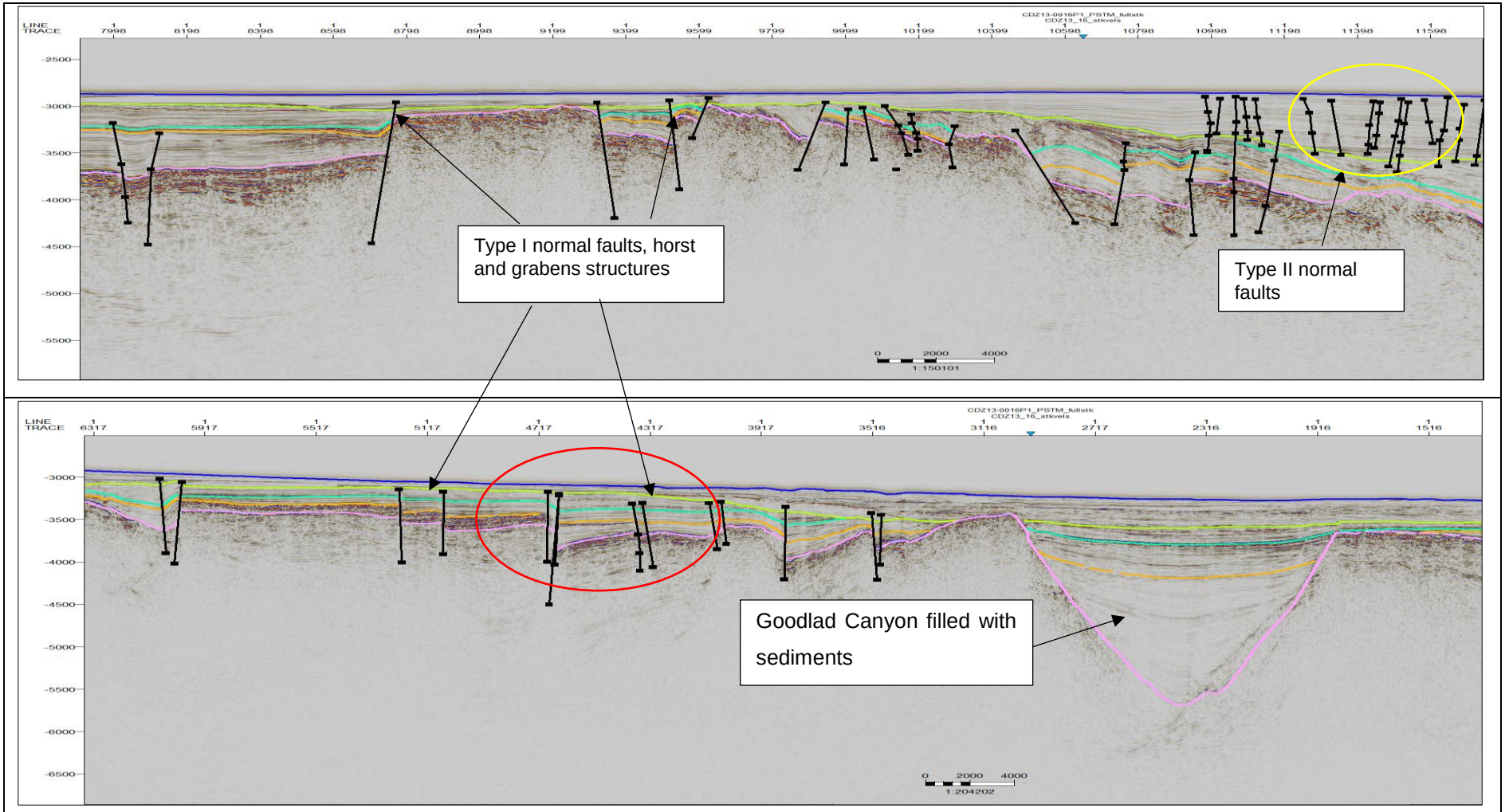

Figure 4.16 Shows Type I,Type II, horst and grabens structures, and Goodlad Canyon. Type I normal faults (black lines) extends from basement through sedimentary package (1AT1, 17AT1 and Miocece/Oligocene) due to separation of the Gondwana. Type II normal faults (yellow circle) is within the sedimentary package and does not extend from the basement and could be due to compaction in the basin. Grabens are filled with thick synrift sediments.

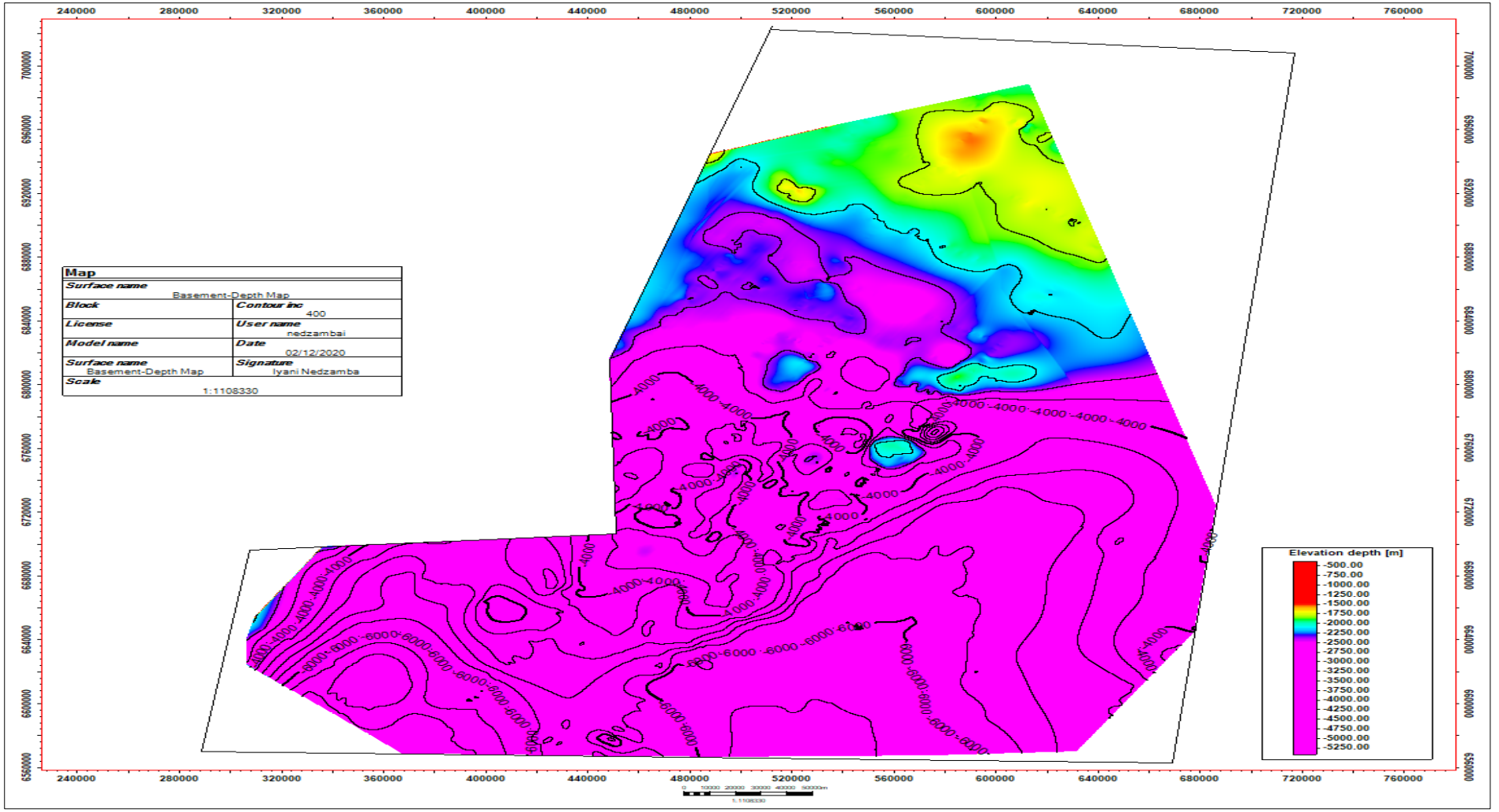

Figure 4.17 A basement depth map of the study area. The colours; purple, green, blue, and red on the colour histogram represent depth values.

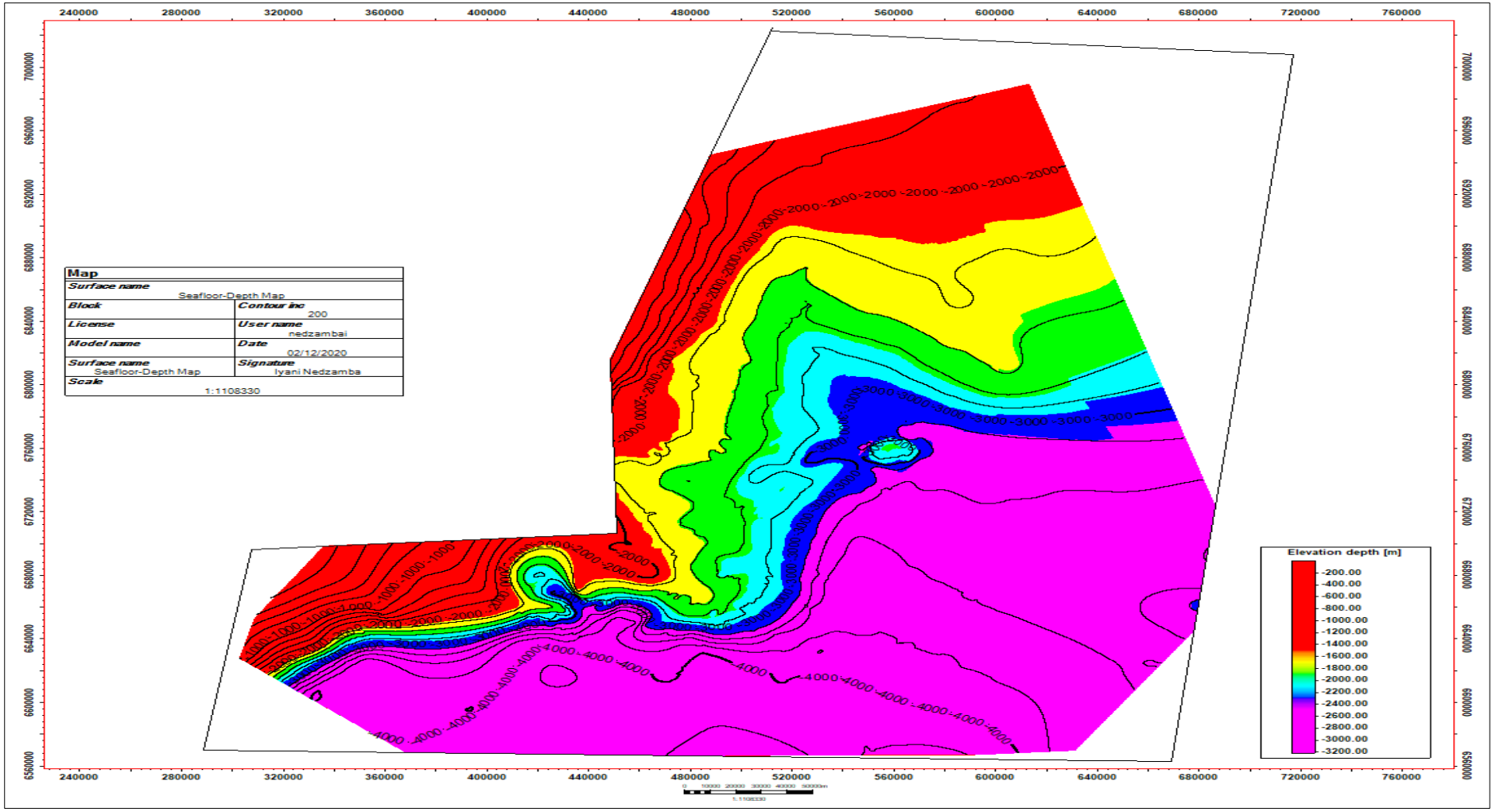

Figure 4.18 A seafloor depth map of the study area. The colours; purple, green, blue, and red on the colour histogram represent depth values i.e. from shallow (Red-green) to deep (Blue-purple).

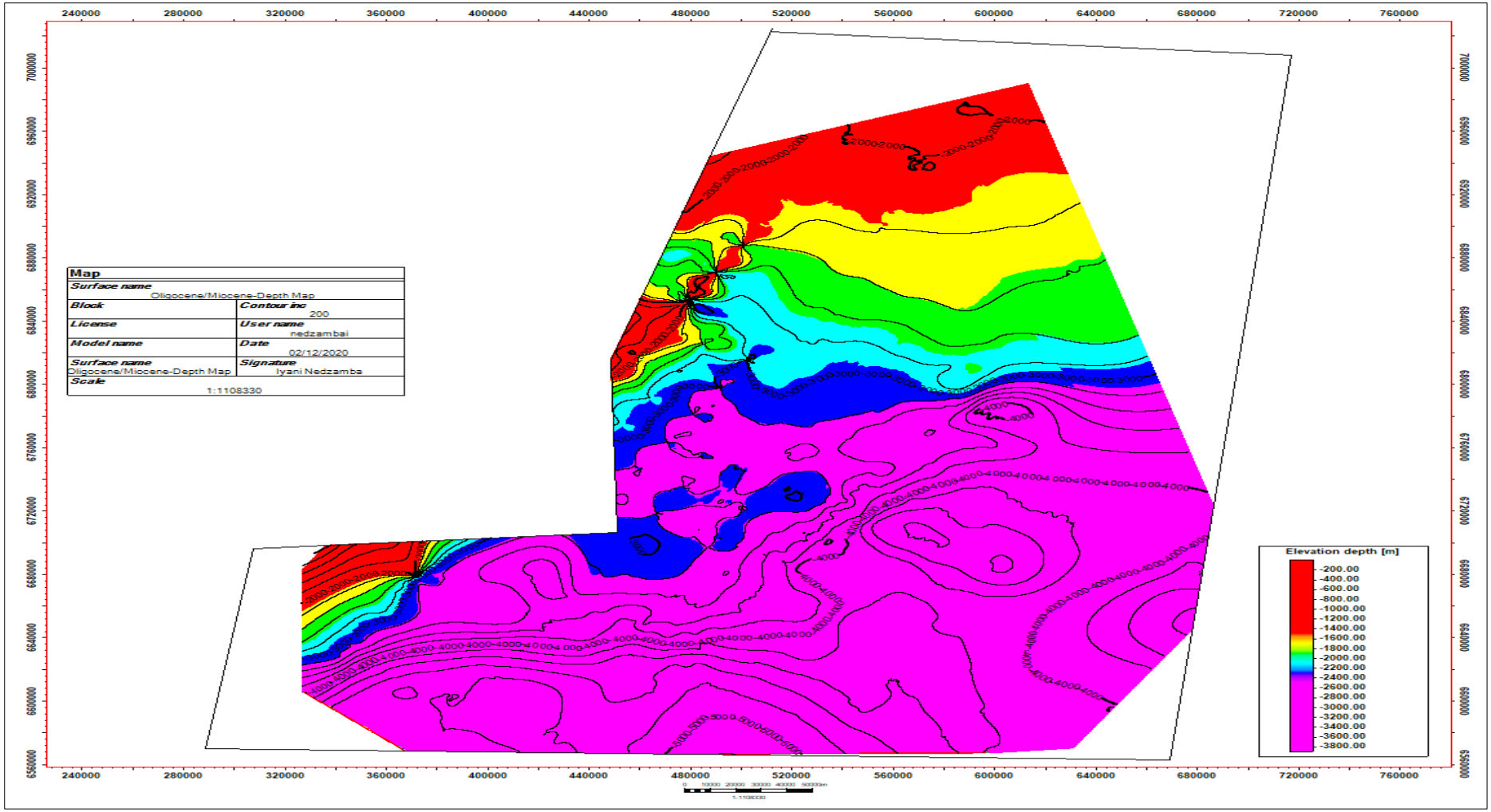

Figure 4.19 Depth map of Oligocene/Miocene horizon. The colours; purple, green, blue, and red on the colour histogram represent depth values.

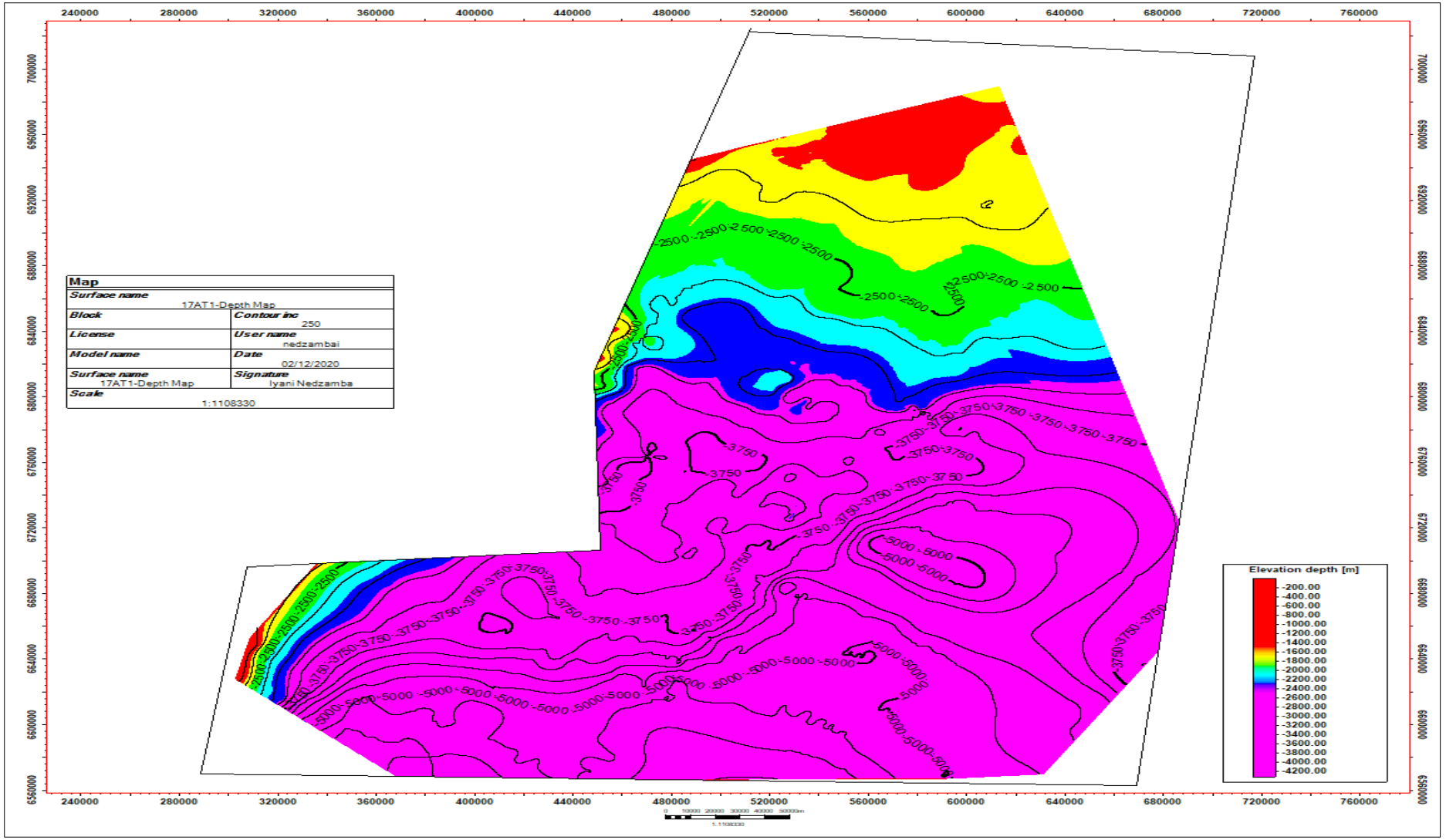

Figure 4.20 Depth map of 17AT1 horizon. The colours; purple, green, blue, and red on the colour histogram represent depth values.

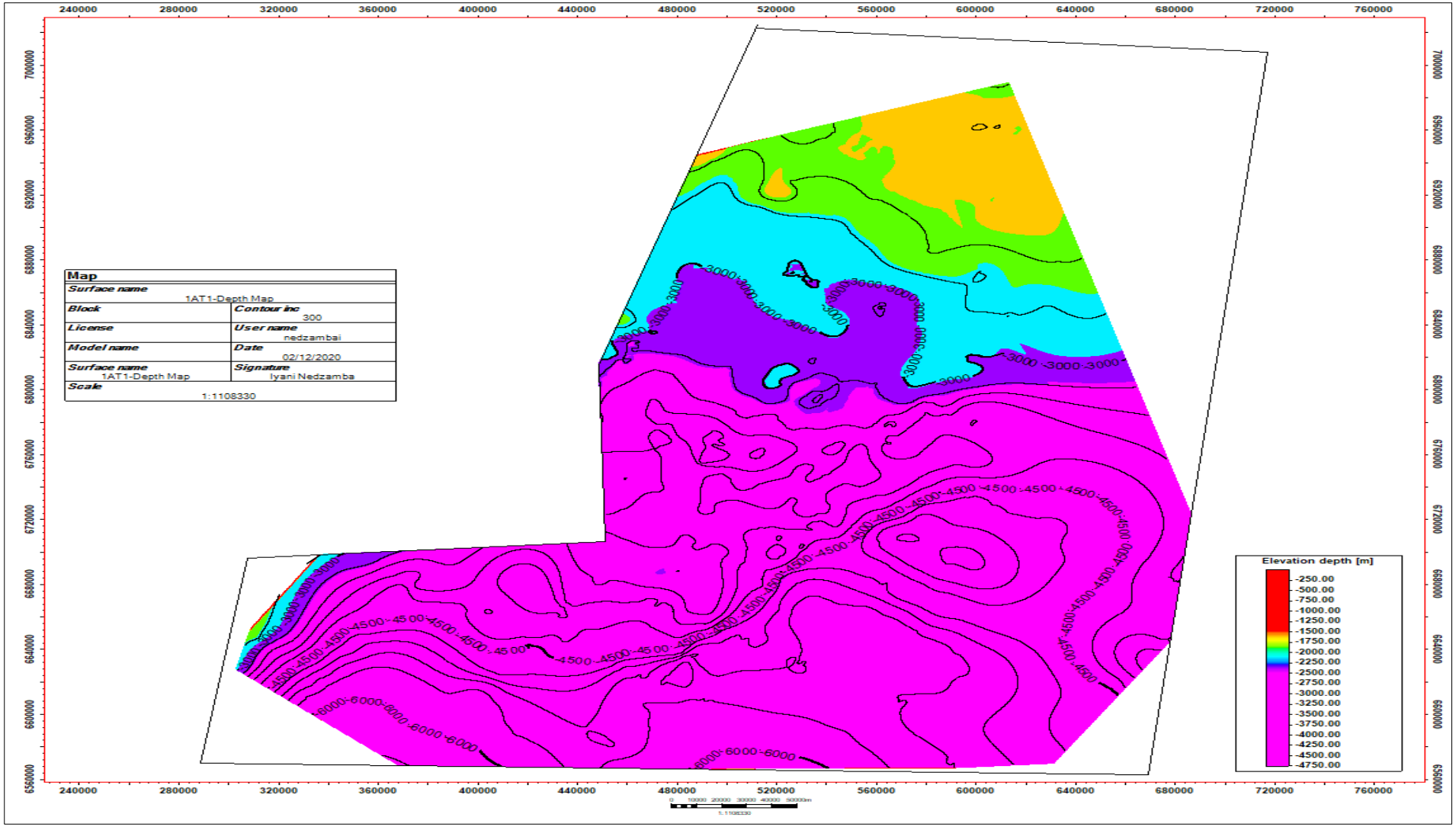

Figure 4.21 Depth map of 1AT1 horizon. The colours; purple, green, blue, and red on the colour histogram represent depth values.

4.5 Discussion

The Durban Basin is rift Mesozoic basin which formed due early extension of the East African continental plate that occurred before the Gondwana break-up and transformation which resulted in the formation of the new oceanic crust along the Agulhas Falkland Fracture Zone (AFFZ) (Broad et al., 2006). It is structurally complex and consist of multiple fault systems with a stratigraphic sedimentary thickness of > 4000 m based on core logging and seismic interpretation (Broad and Mills, 1993, Broad et al., 2006, McMillian, 2003).The investigation of the structural setting of the Durban Basin was used to establish: Durban Basin extent in the study area, structural settings and estimation of sedimentary and depth of subsurface structures. This was achieved using an integrated approach thickness cover of gravity, magnetic and seismic data. The interpretation process of gravity anomalies, magnetic anomalies and seismic data in the study area provided a better understanding of the subsurface geology and structural controls of the Durban Basin.

Stratigraiphic and fault interpretation was achieved using well top data (Jc-C1) after successful seismic well tie process. Seismic interpretation of 29 2D seismic lines using well tops of Jc-D1 picked the following horizons; basement, 1AT1, 17AT1 and Oligoce/Miocene representing major events during the development of the Durban Basin i.e. Early Archaean tectonism (basement), rifting (1AT1), drift (17AT1) and Cenozoic sediments deposition (Oligoce/Miocene) and seafloor represents current day sediments. Depth conversion for this study estimated that the sedimentary cover thickness ranges from ~2000-600 m to 2000-6000 m for the thinnest and thickest parts of the study area respectively (Figures 4.19, 4.20 and 4.21).

Depths estimation for basement of the study area based on depth map of basement versus power spectrum indicates the following; Basement depth map indicates that the deepest top of basement is >6000 m covering the SW and SE part, intermediate is ~3000 m occupying mostly the central part and shallow is <2000 m occupying the northern part (Figure 4.17). Radially averaged calculated power spectrum of Bouguer and RTP estimated top to basement depth into; 18-30 km as deepest, 10-12 km as intermediate and 3-5 km as shallow basement (Figure 4.3A and B). Power spectrum

is grid-based and estimates depth based on spectral analysis using the FFT algorithm calculation thus cannot specify the deepest and shallowest part of the study area as such depth maps are more reliable. Comparing the two-depth estimation methods the following remarks can be made about the study area; deepest top of basement is >4000 m and shallowest as <2000 m covering the central to SW and SE parts and northern part of the study area. The above-mentioned depth estimates agree with the findings of Bhattacharya and Duval (2016), the deepest and shallow parts of the Durban Basin is the SW and NNE.

The interpretation of gravity, magnetic and seismic data agrees with the work of Broad et al., (2006) who noted that Tugela Canyon, Tugela Canyon, basement high Naude Ridge and Tugela Ridge are the most prominent structures in the Durban Basin. The seismic data visibly mapped these basement features (Tugela Ridge and Naude Ridge) in Figures 4.13 and Figures 4.17 and 4.19 respectively. This interpretation is complimented by interpreted RTP anomaly map which distinctively mapped the Tugela Ridge and Naude Ridge represented by closed elongated and circular contour of magnetic high (pink) magnetic values (894 nT) located on the southwestern and northeastern part of the study area respectively (Figure 4.2B).

Based on seismic, gravity and magnetic data interpretation the basin extent was achieved by integrating magnetic and gravity maps in ArcGIS 10.6 and the basin was subdivided into shallow and deep basin (Figure 4.4). The shallow basin occupies the southwestern and central part of the study area. The deep basin occupied the southwestern part of the study area. The shallow and deep basin in the study area are separated by the basement high Tugela Ridge and Naude Ridge (Figure 4.4). This assertion agrees with Goodlad (1986) work, which identified the Tugela Ridge and Naude Ridge as the continental-oceanic boundary (COB) that separated the shallow and deep basin within the continental and oceanic crust respectively.

The Durban Basin is Mesozoic rift basin which is structurally complex, comprised of multiple fault system (McMillian 2003, Broad et al., 2006, PASA, 2016). The faults are vertically steep with a general directional trend of this fault system is NE-SW, NW-SE and W-E directional trend (McMillian 2003, Broad et al., 2006, PASA, 2016). Kitchin (1995), Ben-Avraham et al., (1997), Broad et al., (2006) and Bhattacharya and Duval

(2016) based on seismic data interpretation recorded normal faults that affected the geometry of the basement related to pre-rift and AFFZ movements. Seismic, gravity and magnetic data interpretation for this study revealed a highly fractured basement flooring the basin dissected by fault structures (Figure 4.5A). These fault structures dissecting the basin based on seismic interpretation revealed that they are normal faults which can be classified into Type I and Type II (Figure 4.18).

Type I normal faults extend from the basement through the sedimentary package and these faults type is related to the separation and breakup of Gondwana, this agrees with conclusions made by Broad et al., (2006), that the Durban basin is dominated by normal faults extending from the basement through the stratigraphic unit. Type I normal faults resulted into horsts and grabens structures. These grabens are within the 1AT1 and 17AT1 horizons, they are filled with synrift sediments consisting of turbidites, sandstone overlying the basement and this could be potential targets for petroleum exploration and exploration (Figure 4.18). This graben structures are related to initial rifting and initial movements of the AFFZ (Wiles et al., 2003, Broad et al., 2006 and PASA, 2016).

Type II normal faults are mostly within the sedimentary package and do not extend from the basement and the fault structures could be due to compaction in the Durban Basin. According to Cartwright (2014) and PASA (2016), this fault type (Type II normal faults) developed during the Cretaceous period due to both tectonic and non-tectonic events which includes compaction, shallow overpressure development, abnormal gravitational load, fluid expulsion, diagenesis and contraction within the basin.

The four drilled wells (Jc-A1, B1, C1 and D1) were not successful because they were not optimally positioned according to Singh and McLachlan (2003). Singh and McLachlan (2003), further suggested that petroleum targets are channel sands, distal fans, fourway closure and Turbidites sands overlying basement developed in upper Creataceous and Cenomanain-Turonian period respectively. The grabens within 1AT1 and 17AT1 horizon for this study overly the highly fractured basement and chronostratigraphically, they are of lower Cretaceous to upper Cretaceous period when the drift began and depocenter formed. This graben structures could be related to intial movements of AFFZ and initial rifting movements (PASA, 2016). Seismic data

interpretation for this study mapped channel structures filled with thick sands alternating with shales within the Oligocene/Miocene horizon, which could be potential targets for petroleum exploration. These channel structures represent three upliftment events, eustatic sea level changes and prolonged fluvial incision on the continental margin in the Durban Basin during the Oligocene, Miocene and Pliocene due to (Wiles, 2003).

Seismic interpretation revealed gas chimneys (Figure 4.15 and 4.16) thus agrees with the work of Broad et al., (2006) that; the petroleum system within the Durban Basin is active based on core logging of Jc-D1 that intersected sandstone with extracts of hydrocarbon and bitumen shales associated with dry gas. Seismic data interpretation for this study mapped volcanic pipes in the study area which could be evidence of volcanic intrusion in the Durban Basin. This assertion is supported by the two volcanic events recorded in the study based on seismic data interpretation that mapped local volcanoes, sills and dykes intrusion (Bhattacharya and Duval, 2016).

These structural trends of the study area were more visibly derived more on gravity and magnetic data interpretation using filtering techniques. The combination of horizontal, vertical and tilt derivative anomaly map identified four dominant structural trends; S-N, W-E, SW-NE and NW-SE directional trends (Figure 4.5). This interpretation fairly agrees with the work by Kitchin, (1995), Ben-Avraham et al., (1997) and PASA 2016) who identified the W-E, SW-NE and NW-SE as the dominant direction trends (Figure 4.5). It is worth noting that the scope of this study did not include detail lead and play investigation of petroleum system in the study area.

5. CHAPTER FIVE: CONCLUSIONS AND FUTURE WORK

5.1 Conclusions

The study area is part of the Mesozoic rift Durban Basin and this type of basin are regarded as source economic petroleum interest and highly favoured for oil and gas exploration. The Durban Basin is structurally complex consisted of multiple fault systems. Core logging information from JC series revealed an active petroleum system and the JC-D1 analysis identified traces of oil and bitumen. This research work employed an integrative approach to investigate the structural setting of Durban Basin using marine gravity, magnetic and seismic data complimented by well data. Listed below are accomplishments and observation of this study:

- Seismic well tie using well top data was achieved to pick the horizon in the study i.e. basement, 1AT1, 17AT1, Oligocene/Miocene and seafloor. Some of the mapped horizons have petroleum potential.
- The velocity model was achieved using the seismic stacking velocities (SEGY). The velocity model was used to convert surfaces from time to depth creating depth maps for basement, 1AT1, 17AT1, Oligocene/Miocene and seafloor.
- Based on seismic, gravity and magnetic; the basin is subdivided into the shallow and deep basin thus separated by the basement high Tugela Ridge and Naude Ridge. The shallow basin occupied the southeastern, and northern part of the study area. The deep basin occupies the southwestern part of the study area.
- Filtering techniques were successfully applied to corrected gravity (Bouguer) and magnetic (TMI) data using Geosoft to enhance anomaly interpretation. This includes reduced to the pole (RTP), first order vertical derivative (VD), first order horizontal derivative (HD), tilt derivative (TDR) and power spectrum.
- Based on depth to basement derived from power spectrum and basement depth map, the study area can be further characterised into shallow top of basement is at <2000 m, covering the northern part and the deepest top to basement depth at >2500 m, covering the central to SW and SE part.
- The estimated sedimentary cover thickness of the study area is < 2000 m-600 m for thinnest and 2000 m- >6000m for thickest part of the study area, based

depth maps derived from seismic data interpretation using velocity model and seismic well tie.

- The major geological structures in the study area are the Tugela Canyon, Tugela Ridge and the Naude Ridge with the latter two being the most visible on seismic data.
- Structurally based on seismic, gravity and magnetic data interpretation, the study area is dissected by faults. Seismic data interpretation revealed that, the faults dissecting the study area are normal faults.
- Normal faults in the study area can be classified into two types; Type I normal faults extending the basement through the sedimentary package which could be due to separation and breakup of the Gondwana, Type I normal faults resulted into horst and grabens structures. Type II normal faults that only existed within the sedimentary package and did not extend from the basement and this type could be due to compaction, shallow overpressure development, gravitational load in the basin, fluid expulsion and contraction. This graben structures within the study area could be due to initial rifting and movements of the AFFZ.
- The major structural trends in the study area are S-N, W-E, SW-NE and SE-NW structural trend directions.
- The study area consists of horst and grabens structures created by normal faulting. The graben structures are filled with thick sediments visible on seismic data. Sediments filling the grabens are marine deltaic sandstones and shales and based on Durban Basin chronostratigraphy, these sediments formed during the lower Cretaceous and upper Cretaceous. According to Singh and McLachlan (2003) sediments formed during the Lower and Upper Cretaceous-Turonian are source target for petroleum exploration in the Durban Basin especially those that overlay the basement rocks.
- The seismic data interpretation revealed gas chimneys in the study area and this could a sign of the presence of an active petroleum system in the study area. According to Broad et al., (2006), Singh and McLachlan (2003) and Bhattacharya and Duval, the Durban Basin has a mature petroleum system based recorded by core logging work of Jc series wells, seismic interpretation and satellite seepage slicks studies.

5.2 Suggestion for future work

The study area requires acquisition of 3D seismic data to improve fault interpretation and mapping, velocity model, detail lead, play, and trap investigation to improve the knowledge about the petroleum system in the area.

REFERENCES

Adagunodo, T.A., Adenji, A.A., and Sunmonu, L.A. 2015. *An overview of magnetic method in mineral exploration*. Akintola University of Technology, Ogbomoso, Nigeria. Journal of Global Ecology and Environment, p. 13-15.

Anderson, P., and Newrick, R. 2008, *Strange but true stories of synthetic seismograms*: CSEG Recorder, p. 51–56.

Ardestani, E.V. (2010). *Precise Edge detection of gravity anomalies by Tilt angle filters*. Journal of Earth Space Physics 36(2), p. 11–19.

Ben-Avraham, Z., Hartnady, C.J.H., and Kitchin, K.A. (1997). *Structure and tectonics of the Augulhas-Falkland Fracture Zone*. Tectonophysics, 282, p. 83-98.

Box, R. and Lowrey, P. 2003. *Reconciling sonic logs with check-shot surveys: Stretching synthetic seismograms*: The Leading Edge, Interpreter's Corner, p. 510-517.

Bhattacharya, M and Duval, G. (2016). *A snapshot of the geotectonics and petroleum geology of the Durban and Zululand Basins*, offshore South Africa.

Blakely, R. (1995). *Potential theory in gravity and magnetic applications*. Cambridge University Press, 461.

Blakely, R. and Simpson, R. (1996). *Approximating edges of sources bodies from magnetic or gravity anomalies*. Geophysics 51(7), p. 1494–1498.

Broad, D.S. and Mills, S.R. (1993). *South Africa offers exploratory potential in variety of basins*. Oil Gas Journal, p. 38-44.

Broad, D.S., Jungslager, E.H.A., Mclachlan, I.R, and Roux, J. (2006). *Offshore Mesozoic basin In: Johnson, M.R, Anhaeusser, C.R. and Thomas, R.J. (Eds.), The*

Geology of South Africa. Geological Society of South Africa, Council for Geoscience, Pretoria, p. 553-571.

Bronner, M., Barrere, C., Ebbing, J., Gernigon, L., Koziel, J., Olesen, O., and Roberts, D. 2009. Barents Sea aeromagnetic remapping BASAR-08: *Acquisition, processing and interpretation. Geological Survey of Norway*. NGU Report 2009.020.

Cartwright, J. 2014. *Are outcrop studies the key to understanding the origins of polygonal fault systems?* Department of Earth Sciences, University of Oxford, South Parks Road, Oxford OX1 3AN, UK.

Chen, Q. and Sidney, S. 1997. *Seismic attribute technology for reservoir forecasting and monitoring*: The Leading Edge.

Chopra, S. and Marfurt, K.J. (2007). Seismic attributes for prospect identification and *reservoir characterization*: SEG Geophysical Developments Series No. 11, Tulsa, OK.

Chopra, S. and Marfurt, K.J., (2005). Seismic attributes- A historical perspective: Geophysics, v. 70, p.3-28.

Cooper, G.R.J. and Cowan, D.R. (2006.) *Enhancing potential field data using filters based on the local phase. Computers and Geosciences* 32(10), p. 1585-1591

Cordell, L and Grauch, V.J.S. 1987. *Limitations of determining density or magnetic boundaries from horizontal gradient of gravity or pseudogravity data*. Short note, Geophysics 52(1), p.118-121.

Cordell, L.; and Grauch, V.J.S. (1985): *Mapping basement magnetization zones from aeromagnetic data in the San Juan basin,New Mexico. In the Utility of the regional Gravity map and Magnetic Anomaly Maps*, W.J. Hinze (ed.) p. 181–197.

Petroleum Agency South Africa (PASA). (2016). *East coast basin analysis. Petroleum Agency SA internal report*. (Unpublished paper).

Dingle, R.V., Siesser, W.G., Newton, A.R. 1983. *Mesozoic and Tertiary Geology of Southern Africa*. Balkema, Rotterdam, p. 375.

Dingle, R.V., Goodlad, S.W. and Martin, A.K. (1997). *Bathymetry and stratigraphy of the Northern Natal Valley (SW Indian Ocean)*: A preliminary account. Marine Geology, 28, p. 89-106.

Dobrin, M.B. and Savit, C.H. (1998). *Introduction to Geophysical Prospecting (4th Edition)*. McGraw Hill, New York.

Du Toit, S.R. and Leith, M.J., 1974. *The J(c)-I borehole on the continental shelf near Stanger*. Geological Society of South Africa, 77, p 247-252.

Eichkitz, C and Amtmann, J. (2010). *P103 enhanced velocity modeling for geothermal project in the southern Vienna Basin-A stacking velocity approach*. 72nd EAGE conference and exhibition incorporation SPE EUROPEC 2010. Barcelona, Spain.

Fairhead, J.D., Cooper, G.R.J., and Sander, S. (2017). *Advances in Airborne gravity and magnetic processing and interpretation.* In “Proceedings of Exploration 17: Sixth Decennial International Conference on Mineral Exploration” edited by V. Tschirhart and M.D. Thomas, p. 113–127.

Fedi, M.; and Florio, G. (2009). *Detection of potential fields source boundaries by enhanced horizontal derivative method*. Geophysics Prospect 49, p. 13–25.

Goodlad, S.W. (1986). *Tectonic and sedimentary history of the mid Natal Valley (S.W. Indian Ocean)*. University of Cape Town.

Gunn, P.J., (1997). *Application of aeromagnetic surveys to sedimentary basin studies*. Journal of Australian Geology and Geophysics 17, p. 133-144.

Haeskanen, W.A. and Moritz, H. 1967. *Physical geodesy*. San Francisco.

Kearey, P., Brooks, M, and Hill, I. (2002). *Geophysical exploration (third edition)*. Blackwell Sciences Ltd Editorial offices, Oxford, London.

Leinweber, V.T., and Jokat, W. 2011. *Is there continental crust underneath the Natal Valley and Mozambique coastal plains.* Geophysical research letters, v.38, p 1-7.

Hampson, D.P., Schuelke, J.S., and Quirein, J.A. (2001). Use of multi attribute transforms to predict log properties from seismic data: Geophysics, v. 60, p. 220-236.

Hicks, N., Davids, S., Beck, B., and Green, A. (2014). *Investigation of the potential for CO_2 storage of the offshore Durban Basin, KwaZulu-Natal*, South Africa. International Conference on Greenhouse Gas Technologies In Energy Procedia Volume: 63, p. 5201-5210.

Kitchin, K.A. 1995. *Tectonics related to the northern termination of the Agulhas-Falkland Fracture Zone offshore Southern Natal*. Geol. Soc. S. Aft., Centennial Geocongress Abstract, Rand Afrikaans University, Johannesburg, v. 1, p. 460-463.

Li, X., and Götze, H. (2001). *Ellipsoid, geoid, gravity, geodesy, and geophysics*. Geophysics journal, volume 66, issue 6, p. 1660-1959.

Luton, L.C. and Prieto, C. 2000. *Accurate depth conversions reduce risk: Gulf Coast* Association of Geological Societies Transactions, v. L, p. 243-246.

Marson,I and Klingele,E.E. (1993). *Advantages of using the vertical gradient of gravity for 3-D interpretation.* Geophysics 58(11), p. 1588– 1595.

McMillan, I.K., 2003. *Foraminiferally defined biostratigraphic episodes and sedimentation pattern of the Cretaceous drift succession (Early Barremian to Late Maastrichtian) in seven basins on the South African and southern Namibian continental margin*. South African Journal of Science 99, p. 537–576.

Mekkawi, M.M, Fergani, E.A and Abdella, K.A. (2017). *Seismic risk zones and faults characterization using geophysical data*. Department of Applied Geophysics Institute of Astronomy and Geophysics Geomagnetism and Geoelectricity, Egypt.

Miller, H.G and Singh, V. (1994). *Potential-Field Tilt – a New concept for location of potential field sources*. Journal of Applied Geophysics 32, p. 2-3.

NOAA/NGDC and CIRES. (2014). *Map reviewd by NGA and BGS*. http://ngdc.nooa.gov/geomag/WMM. Accessed on 20 October 2019.

Oasis Geosoft Montaj. 2014. *How to guide publication*. Geosoft Inc.

Pilkington, M.; and Keating, P. (2004): *Contact mapping from gridded magnetic data a comparison: extended abstracts*. ASEG17th Geophysical Conference and Exhibition, August 2004, Sydney

Raeesi, M., Moradzadeh, A., Ardejani, F.D., and Rahimi, M. (2012). Classification and identification of hydrocarbon reservoir lithofacies and their heterogeneity using seismic attributes, logs data and artificial neural networks: Journal of Petroleum Science and Engineering, v. 82-83, p. 151-165.

Robein, E. (2003). *Velocities, Time-imaging and depth-imaging in reflection seismics: Principles and methods*. EAG publications. Houten, Netherlands.

Rosid, M.S. and Siregar, H. (2017). *Determining Fault Structure using First Horizontal derivative (FHD) and Horizontal Vertical Diagonal Maxima (HVDM) Method: A Comparative Study*. Universitas Indonesia, Depok 16424, Indonensia.

Rivas, J. (2009). *Gravity and magnetic methods*. UNU geothermal training programme.

Selim, E.I. (2016). *The integration of gravity, magnetic and seismic data in delineating the sedimentary Basin of northern Sinai and deducing their structural controls*. Journal of Asian Earth Sciences. 11, p. 345-367.

Selley, R.C. (1998). *Elements of Petroleum Geology*. Academic Press, San Diego, CA, 470 p.

Schlumberger Limited. (2020). https://www.glossary.oilfield.slb.com/en/Terms/s/stacking_velocity.aspx. Accessed January 20 2020.

Simm, R and Bacon, M. (2014). *Seismic amplitude: An interpreter's Handbook*. Cambridge University press. Cambridge, UK.

Singh, V. and McLachlan, I. (2003). *South Africa's east coast frontier offers untested mid to deepwater potential.* Oil Gas J. 101 (22), p. 40–45.

Singh, V., Van der Spuy, D., and Cameron, N.K. (2005). *The South Africa East Coast: Evidence for an active petroleum system within the Tugela Fan, Durban Basin (part 2)*. Petroleum Agency SA. Unpublished report.

SOEKOR. 1994. *Licensing Round Information Brochure: Durban/Zululand Basin*. Stellenbosch, p. 24.

Spector, A. and Grant, F.S., 1970. Statistical models forinterpreting aeromagnetic data. Geophysics 35, 293-302.

Spector, A. and Grant, F.S. 1970. *Statistical models for interpreting aeromagnetic data*. Geophysics 35, p 293-302.

Uenzelmann-Neben, G. (2009). *Sedimentary deposits on the Southern African continental margin: Slumping versus non-deposition or oceanic currents?* Marine and Petroleum Geology Journal. 266, p 65-79.

Telford, W.M., Geldart, L.P., Sheriff, R.E, and Keys, D.A. (1986). *Applied geophysics (1st Edition)*. Cambridge University press. London.

Telford, W.M., Geldart, L.P., Sheriff, R.E, and Keys, D.A. (1990). *Applied geophysics (2nd Edition)*. Cambridge University press. London.

Verduzco, B.; Fairhead, J.D.; Green, C.M. and Mackenzie, C. (2004): *New ınsights into magnetic derivatives for structural mapping*. The Leading Edge 23, p. 116–119.

Viloria, R., Garcia, I., Caudron, A., Cariel, R., De Caires, F., Hernandez, J.G., and Bustos, A. (2009). *Using a fine-tuned interval velocity model for improving the quality of time-to-depth conversion*: The Leading Edge, p. 1430-1434.

White, R.E. (1980). *Partial coherence of matching synthetic seismogram with seismic traces*. Geophysical Prospecting 28, p 333-358.

White, R.E and Simm, R. (2003). *Tutorial: Good practice in well ties*. School of Earth Sciences, University of London.

Wiles, E., Green, A., Watkeys. M., Jokat, W., and Krocker, R. (2013). *The evolution of the Tugela canyon and submarine fan: A complex interaction between margin erosion and bottom current sweeping, southwest Indian Ocean*, South Africa. Marine and Petroleum Geology 44, p. 60-70.

APPENDIX: A

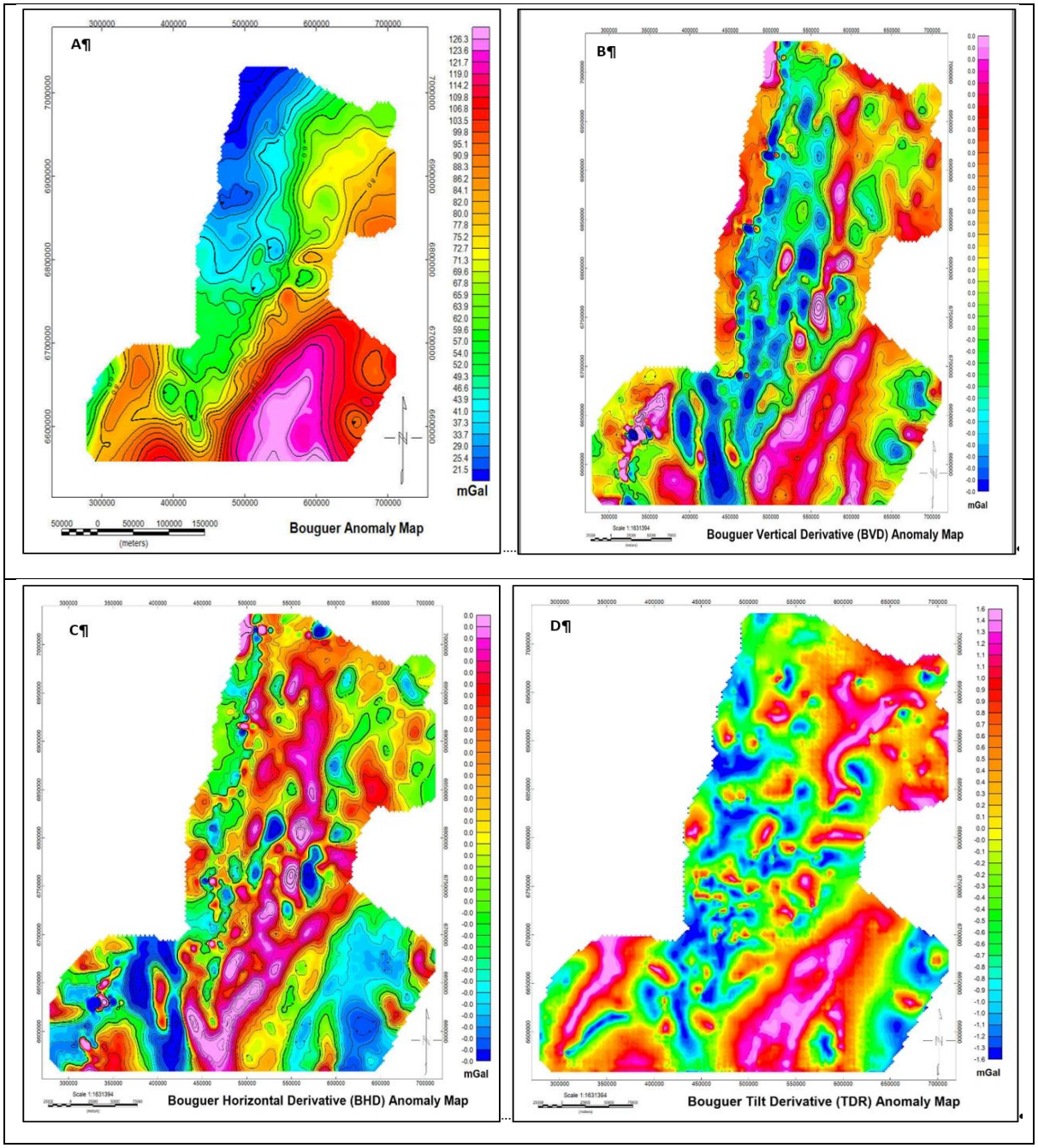

Figure A-1.1. uninterpreted (A) Bouguer anomaly map of the Durban Basin with a 20 mGal contour interval. (B) Contoured 1st order VD anomaly map of Bouguer. (C) Contoured 1st order HD anomaly map of Bouguer. (D) TDR anomaly map of Bouguer.

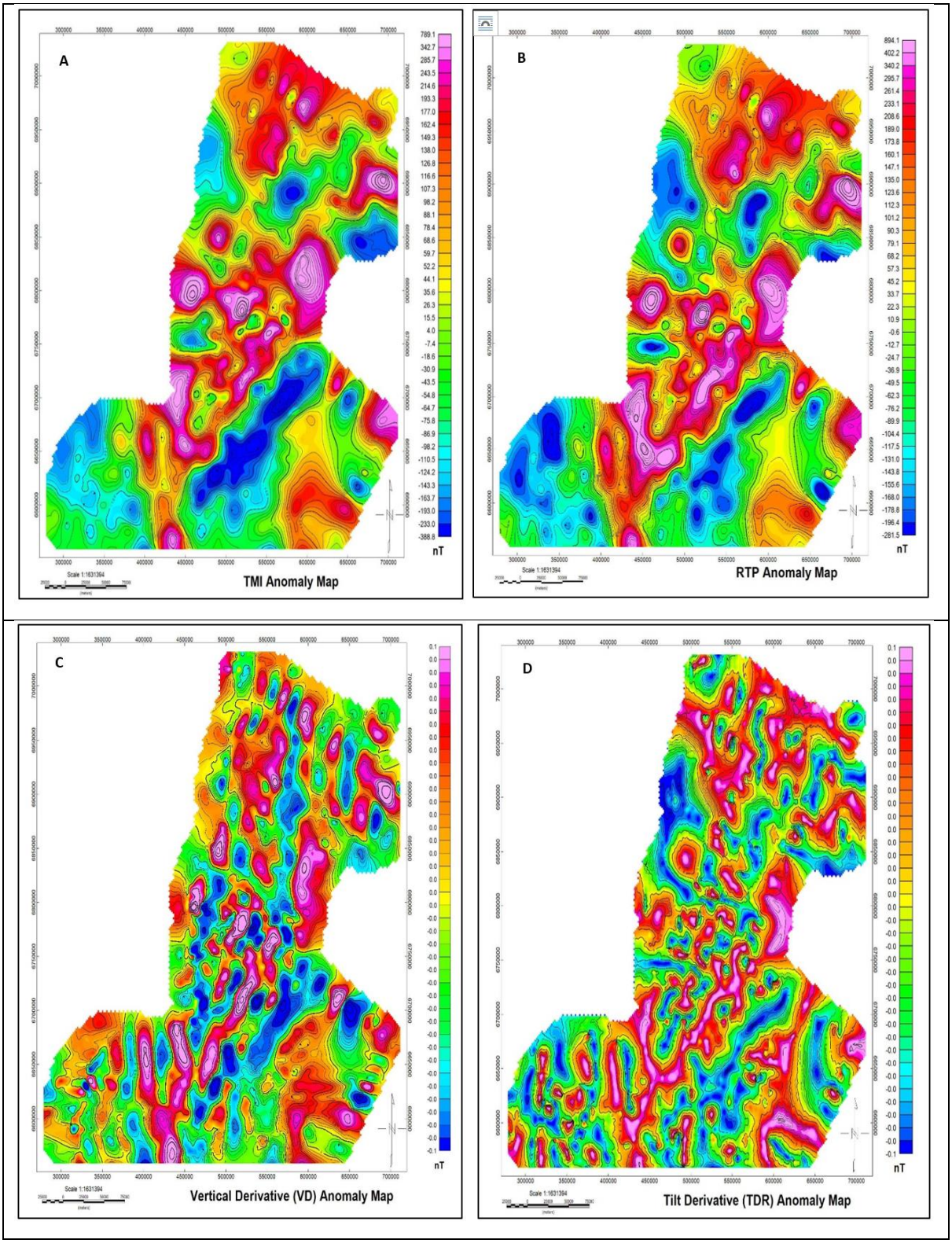

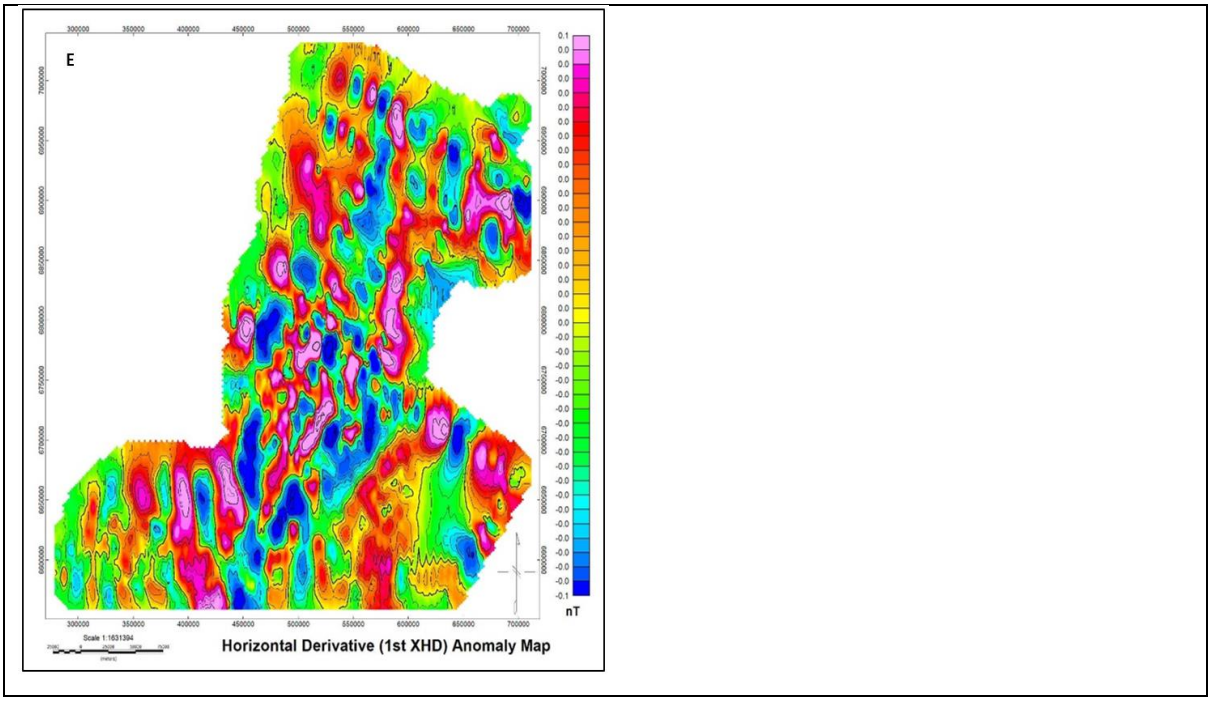

Figure A-1.2. Uninterpreted (A) Total magnetic intensity (TMI) anomaly map of the Durban Basin with 100 nT contour interval. (B) contoured RTP magnetic anomaly map. (C) Contoured 1st order VD anomaly map of RTP. (D) Contoured TDR anomaly map of RTP. (E) Contoured 1st order HD anomaly map of RTP.

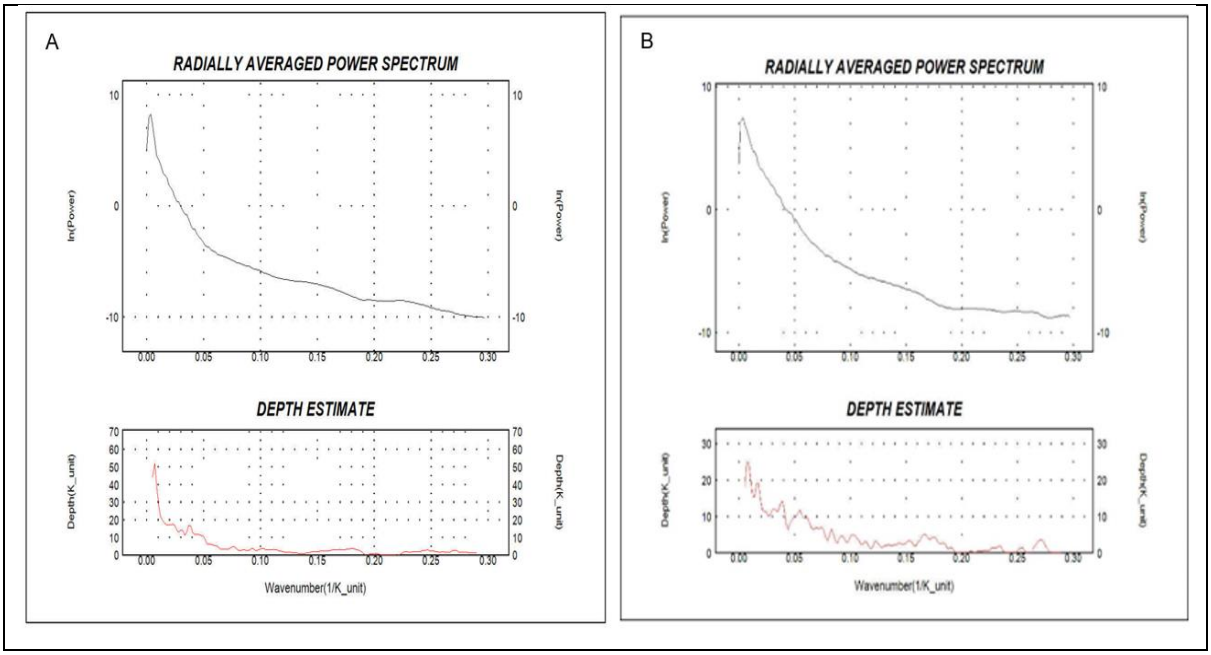

Figure A-1.3. Uninterpreted (A) radially averaged power spectrum of Bouguer map. (B) Interpreted radially averaged power spectrum of RTP map.